National Library of Canada
Bibliothèque nationale du Canada

Canadian Theses Service
Service des thèses canadiennes

Ottawa, Canada
K1A 0N4

NOTICE

The quality of this microform is heavily dependent upon the quality of the original thesis submitted for microfilming. Every effort has been made to ensure the highest quality of reproduction possible.

If pages are missing, contact the university which granted the degree.

Some pages may have indistinct print especially if the original pages were typed with a poor typewriter ribbon or if the university sent us an inferior photocopy.

Reproduction in full or in part of this microform is governed by the Canadian Copyright Act, R.S.C. 1970, c. C-30, and subsequent amendments.

AVIS

La qualité de cette microforme dépend grandement de la qualité de la thèse soumise au microfilmage. Nous avons tout fait pour assurer une qualité supérieure de reproduction.

S'il manque des pages, veuillez communiquer avec l'université qui a conféré le grade.

La qualité d'impression de certaines pages peut laisser à désirer, surtout si les pages originales ont été dactylographiées à l'aide d'un ruban usé ou si l'université nous a fait parvenir une photocopie de qualité inférieure.

La reproduction, même partielle, de cette microforme est soumise à la Loi canadienne sur le droit d'auteur, SRC 1970, c. C-30, et ses amendements subséquents.

NL-339 (r. 88/04) c

Canada

UNIVERSITY OF ALBERTA

Techniques of Microwave Noise Measurement on Cooled Transistors

by

Eric C. Valk

A THESIS
SUBMITTED TO THE FACULTY OF GRADUATE STUDIES AND RESEARCH
IN PARTIAL FULFILMENT OF THE REQUIREMENTS FOR THE DEGREE
OF Doctor of Philosophy

Department of Electrical Engineering

EDMONTON, ALBERTA
FALL 1990

National Library
of Canada

Bibliothèque nationale
du Canada

Canadian Theses Service

Service des thèses canadiennes

Ottawa, Canada
K1A 0N4

C

The author has granted an irrevocable non-exclusive licence allowing the National Library of Canada to reproduce, loan, distribute or sell copies of his/her thesis by any means and in any form or format, making this thesis available to interested persons.

The author retains ownership of the copyright in his/her thesis. Neither the thesis nor substantial extracts from it may be printed or otherwise reproduced without his/her permission.

L'auteur a accordé une licence irrévocable et non exclusive permettant à la Bibliothèque nationale du Canada de reproduire, prêter, distribuer ou vendre des copies de sa thèse de quelque manière et sous quelque forme que ce soit pour mettre des exemplaires de cette thèse à la disposition des personnes intéressées.

L'auteur conserve la propriété du droit d'auteur qui protège sa thèse. Ni la thèse ni des extraits substantiels de celle-ci ne doivent être imprimés ou autrement reproduits sans son autorisation.

ISBN 0-315-65025-7

UNIVERSITY OF ALBERTA

RELEASE FORM

NAME OF AUTHOR Eric C. Valk

TITLE OF THESIS Techniques of Microwave Noise Measurement on Cooled Transistors

DEGREE FOR WHICH THESIS WAS PRESENTED Doctor of Philosophy

YEAR THIS DEGREE GRANTED FALL 1990

Permission is hereby granted to THE UNIVERSITY OF ALBERTA LIBRARY to reproduce single copies of this thesis and to lend or sell such copies for private, scholarly or scientific research purposes only.

The author reserves other publication rights, and neither the thesis nor extensive extracts from it may be printed or otherwise reproduced without the author's written permission.

(SIGNED) Eric Valk

PERMANENT ADDRESS:
#201 7835 157 ST
Edmonton, Alberta

DATED Oct 12 1990

UNIVERSITY OF ALBERTA

FACULTY OF GRADUATE STUDIES AND RESEARCH

The undersigned certify that they have read, and recommend to the Faculty of Graduate Studies and Research, for acceptance, a thesis entitled Techniques of Microwave Noise Measurement on Cooled Transistors submitted by Eric C. Valk in partial fulfilment of the requirements for the degree of Doctor of Philosophy.

....
Dr. R.H. Johnston
External Examiner

D. Routledge
....
Dr. D. Routledge
Supervisor

....
Dr. J.F. Vaneldik
Co-supervisor

A. Craggs
....
Dr. A. Craggs

C. G. Englefield
....
Dr. C. Englefield

T. Landecker
....
Dr. T.L. Landecker

....
Dr. R.P.W. Lawson

Date......28 Sept 1990......

Abstract

Cooled low noise microwave FET amplifiers are used extensively in radio telescopes, satellite earth stations, and radar systems to minimize noise added to the signal by the receiver. When designing these amplifiers it is essential to know the noise parameters of the component transistors. However, because of their high input reflection coefficients, it is difficult to accurately measure the noise parameters of the GaAs FET and HEMT transistors often used in these amplifiers. It is even more difficult to obtain the noise parameters of these transistors when they are cooled to cryogenic temperatures. At cryogenic temperatures it is difficult to adjust the mechanical tuners which are often used to measure noise parameters. It is also difficult to estimate the small signal and noise behavior of the connections between equipment at room temperature and the equipment at cryogenic temperatures.

In the research described in this thesis, a load having an electronically controlled reflection coefficient and noise temperature was constructed, and was used to measure the noise parameters of a Mitsibushi MGF1412 GaAs FET at 12K at frequencies from 1.2 GHz to 1.6 GHz. This device had an input reflection coefficient near 0.98 and a minimum noise temperature of 10K. The electronic load simplified the measurement of noise parameters at cryogenic temperatures because its reflection coefficient was adjusted from outside the cooling apparatus, and the reflection coefficients were

repeatable.

The author developed and tested a number of novel noise measurement techniques. New techniques of estimating the noise parameters of a noise measurement receiver and of the device under test were introduced. The use of the singular value decomposition to improve and analyze noise parameter estimation by least squares fitting was introduced. An analysis was made of the measurement errors due to frequency errors and non-zero noise power measurement bandwidth.

A new notation was introduced which simplified the analysis of noisy linear circuits. This notation was used to develop cascading and de-embedding equations for noisy linear two-ports in a simplified form, and was also used to develop some of the new measurement techniques.

Table of Contents

Chapter Page

1. Introduction 1

1.1 Related Literature 3

2. The Circuit Theory of Linear Noisy Devices 17

2.1 The Fourier Analysis of Noise 18

2.2 The Noisy Linear One-Port 25

2.3 The Noisy Linear N-Port 27

2.3.1 The Noisy Linear Two-Port 31

2.3.2 The Noise Parameters of a Passive Two-port 39

2.4 Cascaded Noisy Two-ports 41

3. Estimation of Noise Parameters 49

3.1 Overview of the Noise Parameter Measurement Problem 49

3.1.1 The Multiple Impedance Load 54

3.2 The Conventional Method of Noise Parameter Estimation 56

3.2.1 Systematic Errors 59

3.2.2 The Conventional Method Implemented with the Multiple Impedance Load 59

3.3 Noise Parameter Estimation by Linear Regression of Power Measurements 60

3.3.1 Implementation of the LRPG Method 66

3.3.2 Systematic Errors of the LRPG Method 68

3.3.3 Some Variations of the LRPG Method 69

3.4 Receiver Noise Calibration 70

3.4.1 Minimizing the Receiver Excess Noise Temperature 71

3.4.2 Removal of Receiver Noise from each Measurement 72

3.4.2.1 A Method of Keeping the Receiver Noise Temperature Fixed 73

3.4.3 De-embedding the Receiver after Determining Noise Parameters 76

3.4.4 A Simple Method of Receiver Noise Calibration 78

3.5 Analysis of Least Squares Fitting Uncertainties .81

3.5.1 The Classical Estimate 83

3.5.2 Error Analysis Using Norms 85

3.5.2.1 Estimation of the Spectral Norm ...87

3.5.2.2 The Singular Value Decomposition ..88

3.5.2.3 The Generalized Inverse 90

3.5.3 Estimation Using the Singular Value Decomposition 92

3.5.3.1 The Full Rank Case 94

3.5.3.2 The Rank Deficient Case 94

3.5.3.3 The Nearly Rank Deficient Case 96

3.5.4 Application to Noise Parameter Estimation .98

4. Experimental Apparatus 100

4.1 The PIN Diode Multiple Impedance Load 100

4.1.1 Theory of Operation 101

4.1.2 Design and Construction 105

4.1.2.1 Mechanical Design 108

4.1.2.2 Choice of Dielectric 112

4.1.2.3 The Switchable Terminations 114

4.1.2.4 Circuit Element Models 116

4.1.2.5 The In-phase Networks 119

4.1.2.6 Other Circuit Elements 120

4.1.3 Small Signal Behavior 121

4.1.4 Noise Temperature 121

4.2 The Relay Multiple Impedance Load 127

4.3 The Noise Measurement Receiver 130

4.3.1 Frequency Stabilisation 130

4.4 The Test Fixture and Calibration Standards 138

5. Calibration Techniques 143

5.1 Noise Generator Calibration 143

5.1.1 Calibration From One Power Measurement ...143

5.1.2 Calibration From Two Power Measurements ..145

5.2 S-parameter Calibration 146

6. Measurement Errors 155

6.1 Instrument Errors 155

6.1.1 S-Parameter Measurement Errors 156

6.1.2 Analysis of Frequency Related Errors 157

6.1.3 Power Measurement Errors 164

7. Experimental Procedure and Results 169

7.1 Room Temperature Experiments 169

7.1.1 PIN Diode Multiple Impedance Load Noise Calibration 170

7.1.2 Receiver and Noise Generator Calibration .170

7.1.3 FET and Passive DUT Noise Measurements ...171

7.2 The Cryogenic Measurements 174

7.2.1 Cryogenic S-parameter Calibrations 176

7.2.2 Noise Generator Calibration 177

7.2.3 The Passive DUT Noise Measurements 178

7.2.4 The Cryogenic FET Noise Measurements 178

7.2.5 Iterative Improvement of the S-parameter Calibration 179

8. The APL Programs 188
    8.1 The APL Language 189
    8.2 The IMPCAP Workspace 189
        8.2.1 Some Details 195
Conclusions 198
    Recommendations 200
References 204
Appendix 1 - A Brief Description of APL 216
Appendix 2 - A Summary of the Main IMPCAP Functions 219

List of Tables

Table Page

2.1 Notation for Noisy Two-ports........................33

7.1 Room Temperature Passive DUT S-Parameters...........181

7.2 Passive DUT Room Temperature Noise Parameter Estimated from S-Parameters...................181

7.3 Measured Passive DUT Room Temperature Noise Parameters.......................................181

7.4 FET Room Temperature S-Parameters..................182

7.5 FET Room Temperature Noise Parameters...............182

7.6 FET Cryogenic S-Parameters Before Iteration.........183

7.7 FET Cryogenic Noise Parameters Before Iteration.....184

7.8 Passive DUT Cryogenic S-parameters Improved by Iteration......................................184

7.9 Passive DUT Cryogenic Noise Parameters Estimated From S-parameters Improved by Iteration......................................185

7.10 Measured Passive DUT Cryogenic Noise Parameters Improved by Iteration.........................185

7.11 FET Cryogenic Noise Parameters Improved by Iteration186

7.12 FET Cryogenic S-Parameters Improved by Iteration....187

List of Figures

Figure Page

2.1 The Z-parameter Representation of a Noisy N-port.....30

2.2 The Y-parameter Representation of a Noisy N-port.....30

2.3 The S-parameter Representation of a Noisy N-port.....32

2.4 The Terminal Noise Generators of the Voltage-Current Representation of a Noisy Two-port.................................35

2.5 The Terminal Noise Generators of the Wave Representation of a Noisy Two-port...............35

2.6 The Terminal Noise Generators of Noisy Two-ports in Cascade................................43

2.7 The Terminal Noise Generators of the Two-port Equivalent to a Cascade of Noisy Two-ports.......43

3.1 The General Configuration for Noise Measurements.....50

3.2 The Multiple Impedance Load...........................56

3.3 The Configuration for a New Method of Keeping the Receiver Excess Noise Temperature Constant...75

3.4 Flow Diagram for a Receiver and Unilateral Device....80

4.1 Equivalent Circuit of a PIN Diode..................103

4.2 Block Diagram of an In-Phase Network................104

4.3 Nominal Reflection Coefficients of the Multiple Impedance Load.................................106

4.4 Block Diagram of the Multiple Impedance Load........107

4.5 The Stripline Configuration.........................109

4.6 The Stripline Fixture..............................110

4.7 Stripline with Three Layers of Dielectric...........113

4.8 Layout of a Switchable Termination..................115

4.9 Equivalent Circuits for an HP PIN Diode in a
Stripline Package.................................117

4.10 Reflection Coefficients of the PIN Diode
Multiple Impedance Load at 1.2 GHz and 300K.....122

4.11 Reflection Coefficients of the PIN Diode
Multiple Impedance Load at 1.5 GHz and 300K.....123

4.12 Reflection Coefficients of the PIN Diode
Multiple Impedance Load at 1.8 GHz and 300K.....124

4.13 Reflection Coefficients of the PIN Diode
Multiple Impedance Load at 1.2 GHz and 12K......125

4.14 Reflection Coefficients of the PIN Diode
Multiple Impedance Load at 1.5 GHz and 12K......126

4.15 Simplified Diagram of the Relay Multiple
Impedance Load..................................128

4.16 Reflection Coefficients of the Relay Multiple
Impedance Load at 1.2 GHz and 300K.............131

4.17 Reflection Coefficients of the Relay Multiple
Impedance Load at 1.5 GHz and 300K.............132

4.18 Reflection Coefficients of the Relay Multiple
Impedance Load at 1.2 GHz and 14K..............133

4.19 Reflection Coefficients of the Relay Multiple
Impedance Load at 1.5 GHz and 14K..............134

4.20 Block Diagram of the Noise Measurement Receiver.....135

4.21 Equivalent Circuit for the Open Circuit Calibration Standard....................................140

4.22 Equivalent Circuit for the Short Circuit Calibration Standard....................................140

4.23 Equivalent Circuit for the Through Line Calibration Standard....................................141

4.24 Improved Equivalent Circuit for the Open Circuit Calibration Standard.........................141

4.25 Improved Equivalent Circuit for the Short Circuit Calibration Standard.........................142

4.26 Improved Equivalent Circuit for the Through Line Calibration Standard.........................142

5.1 Flow Diagram for the Unknown Two-ports Connected to the Two-port Calibration Standard..148

5.2 Flow Diagram for the Unknown Two-ports Connected to the First One-port Calibration Standard..148

5.3 Flow Diagram for the Unknown Two-ports Connected to the Second One-port Calibration Standard....................................149

6.1 Flow Diagram for a Noise Generator and Receiver Connected by a Transmission Line...............161

6.2 Relative Error Due to a 1 MHz Frequency Offset for Cryogenic Noise Measurement with the PIN Diode MIL...165

6.3 Relative Error Due to the 4 MHz Noise Measurement Bandwidth for Cryogenic Noise Measurement with the Relay MIL..................166

6.4 Relative Error Due to a 1 MHz Frequency Offset for Cryogenic Noise Measurement with the Relay MIL....................................167

7.1 The Room Temperature Noise Measurement Receiver Used for Noise Temperature Calibration of the PIN Diode MIL.............................171

7.2 The Room Temperature Receiver Calibration Configuration.................................172

7.3 The Room Temperature Noise Measurement Configuration173

7.4 The Cryogenic S-parameter Measurement Configuration.175

7.5 The Cryogenic Noise Measurement Configuration.......175

8.1 The Array Structure for Complex Data...............192

Chapter 1

Introduction

Low noise microwave amplifiers are used extensively in radio telescopes, satellite earth stations and radar systems to minimize noise added to the signal by the receiver. The University of Alberta low noise amplifier group is engaged in the design and construction of ultra-low noise amplifiers using gallium arsenide field effect transistors (GaAs FETs) and high electron mobility transistors (HEMTs) cooled to 10K. Such amplifiers are smaller, cheaper, easier to maintain and more stable than other types of low noise amplifiers such as parametric amplifiers and masers.

The objective of this project was to develop the equipment, techniques and software necessary to measure the noise parameters of a cooled low noise GaAs FET in the 1 GHz to 2 GHz frequency range. The transistor selected for this project was the Mitsubishi MGF1412, an n-channel GaAs MESFET. Knowledge of the GaAs FET noise parameters as a function of bias conditions and frequency will allow a designer to select the best transistors from a lot and to design amplifiers optimized for a selected transistor. In addition, the theory required to obtain the noise parameters of a cooled GaAs FET also led to a better understanding of the noise behavior of linear electronic devices.

Noise parameter estimation is a process comprising several steps. The noise parameters of the noise measurement receiver and the noise temperature of the noise generator must each be calibrated. Then, noise power measurements are made with the device under test (DUT) inserted in the noise measurement system. Next, the noise parameters or the excess noise temperature of the DUT and receiver are estimated from the power measurements. Finally, the noise contribution of the noise measurement receiver must be accounted for. There are a number of different ways of accomplishing the entire process and of accomplishing each step, and in the course of this project a number of different procedures were used. This thesis first discusses the individual procedures and then describes how these were used to obtain the final results.

The final experiment alone of this project generated in excess of 2100 noise power measurements and 320 reflection coefficient measurements. The large amount of data and the complexity of many of the equations involved necessitates the use of computer programs to collect and manipulate the data. The data was collected using an HP86 computer and custom software; the details of this system will not be mentioned. The software used to organize and manipulate the data and to estimate noise parameters is described in chapter 8. The approach throughout this project has been that when an algorithm or procedure was required, a program was written to perform it, then verified with dummy data and then used to manipulate the experimental data. This reduces, but does not eliminate, the possibility of errors in calculation.

1.1 Related Literature

During the course of the research for this project, the literature was widely searched and consulted. This section is a review of the thirty or so most useful papers in the list of references, in chronological order.

Rothe, H., Dahlke, W., 1956, "Theory of Noisy Fourpoles"
This paper derives the variation of noise figure with generator admittance (or impedance) from linear circuit theory applied to a two-port with two partially correlated internal noise generators. The internal noise generators are replaced by two uncorrelated voltage and current noise generators and two non-existent admittances connected at the device input.

IRE Subcommittee 7.9 on Noise, 1960, "IRE Standards on Methods of Measuring Noise in Linear Two-Ports"
This paper introduces a method of estimating noise parameters by means of an experimental search for the minimum noise figure. Lossless tuning networks are required at the input and output of the DUT. The measurement of noise figure using a hot-cold noise generator is described.

Fukui, H., 1966, "Available Power Gain, Noise Figure and Noise Measure of Two-Ports and Their Graphical Representations"
This paper derives the loci of constant noise figure, noise measure and available gain on the complex reflection coefficient plane.

Bosma, H., 1967, "On the Theory of Linear Noisy Systems"
This Ph.D. thesis uses elements of Hilbert space to represent the frequency elements of noise exciting a linear network. Correlation matrices and noise amplitude vectors are used to represent noise generated by multiports. The circuit analysis is performed in terms of noise waves, and this is particularly convenient for microwave circuit analysis.

Lange, J., 1967, "Noise Characterization of Linear Two-ports in Terms of Invariant Parameters"
This paper develops a new set of two-port noise parameters which are shown to be invariant to a lossless transformation. It is also shown that one of the noise parameters, N, is related to the VSWR of the optimum (for noise) generator reflection coefficient.

Lane, R.Q., 1969, "The Determination of Device Noise Parameters"
This paper describes the disadvantages of an experimental search for the minimum noise figure. A method of estimating noise parameters by means of a linear least squares fit to a redundant set of noise figure versus generator admittance measurements is described. The author states that the measurement results presented in this paper were corrected for tuner losses and exhibited a high sensitivity to measurement errors.

Gupta, M.S., 1970, "Determination of the Noise Parameters of a Linear Two-Port"
This paper describes fitting noise parameters to a set of noise figure measurements using the method of steepest descent.

Adamian, V., Uhlir, A., 1973, "A Novel Procedure for Receiver Noise Characterization"
This paper estimates noise parameters from a set of power measurements versus generator noise temperature and admittance. Two measurements must be made with fixed admittance and significantly different noise temperatures. The remaining four parameters can be solved by a least squares fit after the equation is linearized. The input admittance of the receiver must be known.

Mamola, G., Sannino, M., 1975, "Source Mismatch Effects on Measurements of Linear Two-Port Noise Temperatures"
This paper describes an iterative procedure to estimate the error in excess noise temperature due to the non-ideal characteristics of the hot-cold noise generator used to make the measurement.

Hillbrand, H., Russer, P.H., 1976, "An Efficient Method of Computer Aided Noise Analysis of Linear Amplifier Networks"
This paper describes a method for computer aided noise analysis of linear networks based on a formal description of noise by means of correlation matrices. This method extends to passive and active one-ports and two-ports. The noise

description is based on voltage and current noise generators.

Caruso, G., Sannino, M., 1977, "Analysis of Frequency Conversion Techniques in Measurements of Microwave Transistor Noise Temperatures"
This paper describes an iterative algorithm to estimate the error in measured excess noise temperature due to an imperfectly rejected image channel. The image channel is assumed to be very close in frequency (implying a very low intermediate frequency).

Meys, R.P., 1978, "A Wave Approach to the Noise Properties of Linear Microwave Devices"
This paper derives the noise properties of linear two-ports in terms of noise waves generated by partially correlated generators at the device input. A measurement procedure is described which requires a matched hot-cold noise generator and an almost lossless hot-cold noise generator having a reflection coefficient of fixed magnitude and variable phase. The noise parameters are estimated by fitting a sinusoidal function to measurements of excess noise temperature versus the phase of the generator reflection coefficient.

Caruso, G., Sannino, M., 1978, "Computer-Aided Determination of Microwave Two-Port Noise Parameters"
This paper introduces the least squares fit of wave type noise parameters to measured values of excess noise temperature versus generator reflection coefficient. It is

suggested that errors in estimated noise parameters reported by Lane (1969) are due to the set of generator reflection coefficients approximating a singular locus. The shape and location of singular loci on the Smith chart is discussed.

Mitama, M., Katoh, H., 1979, "An Improved Computational Method for Noise Parameter Measurement"
This paper describes a method of fitting noise parameters to excess noise temperature versus reflection coefficient by minimizing the total normalized error, that is, the actual distance from the data points to the estimated curve. The normalization of the fitting errors depends on previously estimated noise parameters and numerically obtained derivatives. As a result, the procedure is iterative, and each iteration involves the numerical estimation of derivatives at each data point.

Caruso, G., Sannino, M., 1979, "Determination of Microwave Two-Port Noise Parameters Through Computer-Aided Frequency Conversion Techniques"
This paper describes the application of the least squares fitting technique from Caruso and Sannino (1978) to the situation where the image frequency is imperfectly rejected or not rejected at all. These results are similar to those of Caruso and Sannino (1977).

Sannino, M., 1979, "On the Determination of Device Noise and Gain Parameters"
The author suggests that the measurement errors described by Lane (1979) may be due to ill-conditioning of the data

array. Singular loci of generator admittances, and how to avoid them while using a slide screw tuner, are discussed.

Sannino, M., 1980, "Simultaneous Determination of Device Noise and Gain Parameters Through Noise Measurements Only"
This paper describes a method of estimating the noise parameters and gain parameters of the DUT only, by using an isolator and step attenuator connected between the DUT and the measurement receiver. The noise parameters of the DUT plus receiver are estimated from measurements of noise figure versus generator reflection coefficient by a linear least squares fit procedure. The noise contribution of the receiver and the available gain of the DUT are estimated by making two or more sets of measurements with different step attenuator settings. This procedure is somewhat ambiguous and appears to assume that the noise figure of the isolator is independent of reflection coefficient presented to its input.

Wiatr, W., 1980, "A Method of Estimating Noise Parameters of Linear Microwave Two-ports"
This Ph.D. dissertation from Warsaw Technical University is in Polish and has not yet been translated into English. It appears to describe the estimation of noise parameters of a two-port such as a transistor by fitting noise parameters to measured excess noise temperature versus generator reflection coefficient using a linear least squares fit procedure similar to that of Caruso and Sannino (1978). The

receiver noise contribution is removed using the correlation matrices by Hillbrand and Russer (1976). There appears to be an extensive error analysis.

Strid, E.W., 1981, "Measurement of Losses in Noise Matching Networks"
This paper presents the loss measurements of a "lossless" slide screw tuner obtained using a network analyser. The loss is found to be a strong function of tuner position, and it is shown that back to back tuner measurements will give an incorrect estimate of the tuner loss.

Hecken, R.P., 1981, "Analysis of Linear Noisy Two Ports Using Scattering Waves"
This paper uses signal flow graphs to analyze a noisy two-port driven by a noise generator through a slightly lossy matching network. It is demonstrated that small losses in an input matching network can significantly increase the minimum excess noise temperature of a low noise GaAs FET amplifier. A method of estimating the noise parameters of a DUT plus the receiver is described, which employs a hot-cold noise generator cascaded with a double-slug tuner to experimentally search for the minimum noise figure. The estimated noise parameters of a GaAs FET plus receiver at 2 Ghz are presented (F_{MIN}=0.9 dB).

Sawayama, Y., Mishima, K., 1981, "Evaluation Method of Device Noise Figure and Gain Through Noise Measurements"
This paper describes a method of estimating the noise parameters, output reflection coefficient and available gain

of the DUT only, using a circulator, noise generator and step attenuator connected between DUT and the receiver. It is important to note that the circulator must be tuned for perfect circulation, which is a difficult procedure and very narrowband by nature.

Mishima, K., Sawayama, Y., Sannino, M., 1982, "Comments on 'Simultaneous Determination of Device Noise and Gain Parameters Through Noise Measurements Only'"
Mishima and Sawayama criticize Sannino's paper because he has apparently assumed that the noise figure of an isolator is independent of the reflection coefficient presented to its input. In addition, the estimated noise parameters of a transistor presented by Sannino are shown to be non-physical. Sannino replies that Mishima and Sawayama do not understand his method and their criticisms are invalid. He states that a one-port network analyzer is obviously necessary to measure the DUT output reflection coefficient, with the object of estimating the isolator noise figure. He also states that non-physical noise parameters are routinely obtained as a result of uncorrected second order measurement errors.

Meys, R.P., 1982, "A Microprocessor Controlled Automatic Noise-Temperature Meter"
This paper discusses the errors of measured excess noise temperature due to uncertainties in the generator noise temperature and power ratio (Y-factor) measurement. The limits and corrections for detector nonlinearity are

discussed. The measurement system considered is similar to an HP8970A noise figure meter.

Adamian, V., Uhlir, A., 1982, "Input Reflection and Noise Figure Dependence on Source Reflection: Determination Using Noise Generator"
This paper describes a method of determining the DUT input reflection coefficient from one measurement with a matched calibrated hot-cold noise source and 4 measurements with a mismatched hot-cold noise generator and a lossless line stretcher.

Lane, R.Q., 1982, "A .5-18 GHz Semi-Automatic Noise Parameter Measurement Technique"
This paper describes a method of estimating noise parameter by means of a computer directed search employing a double slug tuner connected before and after the DUT. The generator reflection coefficients are confined to two singular loci near the noise minimum. The author claims the method still has a high sensitivity to measurement errors and that these errors are due to uncorrected tuner losses. He speculates that the errors may be reduced using the fitting algorithms of Mitama and Katoh (1979).

Leake, B.W., 1982, "A Programmable Load for Power and Noise Characterization"
This paper describes a one port load consisting of four or six PIN diodes interconnected by directional couplers. A number of different reflection coefficients are possible, depending on the group of diodes which are forward biased.

Large signal measurements of a power transistor are presented, and a measurement configuration for transistor noise measurements is suggested.

Larock, V.D., Meys, R.P., 1982, "Automatic Noise Temperature Measurement Through Frequency Variation"
This paper describes a method of estimating noise parameters employing a mismatched hot-cold noise generator at the end of a long transmission line. The phase of the noise generator reflection coefficient is varied by slightly changing the measurement frequency. The noise parameters are obtained by fitting a sinusoidal curve to measurements of excess noise temperature versus the phase of the generator reflection coefficient. The loss of the transmission line must be accounted for. The estimated noise parameters of a bipolar transistor plus receiver at 500 Mhz are presented (T_{MIN}=200K).

Martines, G., Sannino, M., 1982, "Determination of Microwave Transistor Noise and Gain Parameters Through Noise Figure Measurements Only"
This paper describes a method of estimating the noise parameters and gain parameters of the DUT only, by using an isolator and step attenuator after the DUT. Tuner losses are estimated from the difference between predicted and measured gain and noise temperature with a matched generator. It is assumed that tuner losses are not a function of the tuner position.

Gupta, M.S., 1983, "Impossibility of Linear Two Port Measurement with a Single Temperature Noise Source" This paper shows that the minimum number of power measurements required to estimate the noise parameters of a two-port is five, and that at least two of the measurements must be with noise generators of substantially different noise temperature. Singular loci of generator admittances are also discussed.

Fanelli, N., 1983, "A New Measurement Method of the Noise Parameters of Two-Port Devices" This paper employs a sliding short and a matched hot-cold noise generator before the DUT, and an isolator between the DUT and receiver, to obtain the noise parameters of the DUT only. The maximum and the minimum power received with the sliding short connected, and the reflection coefficient of the short in the minimum power position, are used to calculate the optimum generator reflection coefficient. Estimated noise parameters of a GaAs FET at 9.5 Ghz are presented (F_{MIN}=2.5 dB).

Calandra, E.F., Martines, G., Sannino, M., 1984, "Characterization of GaAs FET's in Terms of Noise, Gain and Scattering Parameters Through a Noise Parameter Test Set" The noise parameters of the DUT only are determined using an isolator and step attenuator connected between the DUT and the receiver. A one port network analyzer is required to measure the output reflection coefficients of the DUT. The noise figure of the isolator is determined from the output reflection coefficient of the DUT. The scattering parameters are obtained from the DUT available gain with a matched input termination and reflection measurements of the DUT output.

Adamian, V., Uhlir, A., 1984, "Simplified Noise Evaluation of Microwave Receivers"
In this paper noise parameters are estimated by fitting to a set of power measurements and a measurement of excess noise temperature, knowing generator and DUT reflection coefficients and noise temperature. The noise parameters estimated here are non-standard and their conversion to other types of noise parameters is not discussed. This method requires a matched hot-cold noise source and a set of lossless offset shorts. The DUT input reflection coefficient must be known and can be crudely estimated from additional measurements of power with the magnitude of the generator reflection coefficient held constant. The fitting procedure involves fitting the the power measurements to a periodic non-sinusoidal function.

Pospieszalski, M., Wiatr, W., 1986, "Comments on 'Design of Microwave GaAs MESFET's for Broadband, Low Noise Amplifier'"
The authors comment that in Fukui's paper one of four sets of measured noise parameters and three of six sets of noise parameters estimated from a GaAs FET model are nonphysical. The criteria for physically possible noise parameters is discussed.

Martines, G., Sannino, M., 1985, "Simultaneous Determination of Transistor Noise, Gain and Scattering Parameters for Amplifier Design Through Noise Figure Measurements Only"
This paper describes a method of estimating the noise parameters, gain parameters and scattering parameters of the DUT only by employing an isolator and step attenuator connected between the DUT and the receiver. The receiver excess noise temperature is estimated from measurements of the DUT output reflection coefficient. The noise and gain parameters are estimated from measurements of excess noise temperature and estimated receiver excess noise temperature. The DUT S-parameters are estimated from the DUT output reflection coefficient with various (known) generator reflection coefficients and the DUT available gain with a matched generator.

Pospieszalski, M., 1986, "On the Measurement of Noise Parameters of Microwave Two-Ports"
This paper describes a method of estimating the noise parameters of a transistor from a series of excess noise temperature measurements made with a set of quarter wave transformers. The noise contribution of the measurement receiver is removed after the noise parameters have been estimated, using the correlation matrix description of noise discussed by Hillbrand and Russer (1976). The ABCD small signal parameters are used, and the noise of the circuit elements is described in terms of voltage and current

generators.

Pospieszalski, M., 1986, "On the Noise Parameters of Isolator and Receiver with Isolator at the Input"
This paper describes the use of the correlation matrices of Hillbrand and Russer (1976) and the general approach of Twiss (1955) to derive a better expression for the excess noise temperature of an isolator than is currently used in the literature eg. Martines and Sannino (1982), and Sawayama and Mishima (1981).

Chapter 2

The Circuit Theory of Linear Noisy Devices

This chapter describes the circuit theory of noisy linear N-ports, particularly as applied to cascaded two-ports. Circuit theory for incoherent signals (noise) differs from circuit theory for coherent signals in that superposition does not hold, except in special cases (see below). Most texts on circuit theory do not discuss incoherent signals. Probably the most complete presentations are the papers by the IRE Subcommittee 7.9 on Noise ((2),1960) and by Hartman (1976). This chapter combines the results of a number of authors to provide the analytical basis for the rest of the thesis.

The first part of the chapter reviews the Fourier analysis of noise based on texts by Carson (1968) and Papoulis (1965) and papers by the IRE Subcommittee 7.9 on Noise ((2), 1960), Hartmann (1976), Hecken (1981) and Adamian and Uhlir (1984). A new notation is introduced which simplifies the analysis of linear circuits excited by more than one random signal or excited by both coherent and random signals.

The second part of the chapter describes circuit models for noisy linear N-ports. The notation introduced in the first part of the chapter is used to obtain some useful results from the literature, thus demonstrating that the notation is consistent and, at the same time, accomplishing a literature review. In the last part of this chapter the new notation is used to derive hitherto unpublished de-embedding formulae for noisy two-ports. The rest of this thesis assumes that all devices are linear and that the signal may be noise. Henceforth the word linear will be omitted and linearity will be implied.

In the literature no fewer than eleven different sets of parameters are used to describe excess noise temperature as a function of the generator immitance. The relationships between the different parameter sets are often ill-defined, and to further confuse the issue there are notational differences between some authors using the same parameters. This chapter presents a minimum set of parameters, the relationships between these parameters, and their relationships to the elements of three linear circuit models.

2.1 The Fourier Analysis of Noise

The Fourier analysis of noise is reviewed here in order to establish a notation and to clarify the underlying assumptions. This analysis is based on that by Carson (1968, Ch. 3), which is a good exposition of the analysis assumed by Rothe and Dahlke (1956), the IRE Subcommittee 7.9 on Noise (1960,II), Hartmann (1976), Hecken (1981), and others. Additional material from Papoulis (1965) has been included. The use of a separate symbol to indicate a random variable is not common in circuit analysis and it will become evident that this approach is very useful.

Noise is a random signal of voltage, current or electromagnetic wave which is a manifestation of a random electrical process (Carson, 1975). The noise considered in this thesis is a combination of thermal noise and shot noise acted upon by linear circuit elements. Papoulis (1965) shows that thermal noise has a normal distribution, and that shot noise has a normal distribution if its power spectral density is sufficiently high. In actual noise measurements it is usually assumed that all the noise has a normal distribution; this is an assumption that would be very difficult to prove or disprove. Random signals with a normal distribution acted upon by a linear circuit retain a normal distribution. Thus, all the noise considered in this thesis will be assumed to have a normal distribution.

For the purposes of the Fourier analysis below the symbol "~" above a variable will indicate a random variable. Let $\tilde{s}(t)$ be a random signal such as described above; then $<\tilde{s}>$ will be the time average and $E\{\tilde{s}\}$ will be the ensemble average or expected value of $\tilde{s}$.

The auto-correlation, $R_S(\tau)$, of a random signal is defined by:

$$R_S(\tau) = E\{\tilde{s}(t)\tilde{s}(t-\tau)\} = \lim_{K\to\infty} \frac{1}{K}\sum_{i=1}^{K} \tilde{s}_i(t)\tilde{s}_i(t-\tau) \qquad (2.1)$$

Because $\tilde{s}(t)$ is assumed stationary, $E\{\tilde{s}(t)\tilde{s}(t-\tau)\}$ is independent of the time of observation, t, and $R_S(\tau) = R_S(-\tau)$. Thus $R_S(\tau)$ has even symmetry with respect to

$\tau=0$. The maximum value of $R_S(\tau)$ is $R_S(0)$, which is the signal power. Since $\tilde{s}(t)$ is ergodic equation 2.1 can be replaced by:

$$R_S(\tau) = \langle\tilde{s}(t)\tilde{s}(t-\tau)\rangle = \lim_{T\to\infty} \frac{1}{T} \int_{-\frac{T}{2}}^{+\frac{T}{2}} \tilde{s}(t)\tilde{s}(t-\tau)dt \qquad (2.2)$$

Let $G_S(f)$ be the Fourier transform of $R_S(\tau)$. Then:

$$R_S(\tau) = \int_{-\infty}^{+\infty} G_S(f)\, e^{j2\pi f\tau}\, df \qquad (2.3)$$

$G_S(f)$ is real and positive and symmetric about $f=0$. By setting $\tau=0$ we observe that the power spectral density of $\tilde{s}(t)$ is $2G_S(f)$.

The signal $\tilde{s}(t)$ can be approximated by a Fourier series with random coefficients, as follows:

$$\tilde{s}(t) = \sum_{n=-\infty}^{+\infty} \tilde{S}_n e^{jn2\pi f_0 t} \qquad (2.4)$$

where: $\tilde{S}_n$ is the n'th Fourier coefficient of $\tilde{s}(t)$

Substituting the Fourier series into equation 2.2, and assuming that the Fourier coefficients are uncorrelated with each other, $R_S(\tau)$ is related to the Fourier series coefficients by:

$$R_S(\tau) = \langle\tilde{S}_0^2\rangle + 2\sum_{n=1}^{\infty} \langle\tilde{S}_n\tilde{S}_n^*\rangle\, e^{jn2\pi f_0\tau} \qquad (2.5)$$

This approximation implies that $R_S(\tau)$ is periodic in τ. Papoulis (1965, Ch. 10) shows that the autocorrelation of the thermal noise generated by a passive one-port is proportional to $h(|\tau|)$, where $h(t)$ is the impulse response of the one-port, which cannot be periodic. Papoulis (Ch. 13) also shows that if $R_S(\tau)$ is not periodic in τ then the Fourier coefficients are approximately uncorrelated over long periods of time.

In the literature, *e.g.* Carson, it is assumed that each Fourier component can be considered as a sinusoid of random phase and amplitude representing the noise in the frequency interval $(n - \frac{1}{2})f_0$ to $(n + \frac{1}{2})f_0$. The signal power of this component is:

$$P_n = 2\int_{(n-\frac{1}{2})f_0}^{(n+\frac{1}{2})f_0} G_S(f)df = 2\langle\tilde{S}_n\tilde{S}_n^*\rangle \tag{2.6}$$

Assuming that $G_S(f)$ is constant over the frequency interval, the effective amplitude of the component is defined as:

$$S_n = \sqrt{P_n} = \sqrt{2\langle\tilde{S}_n\tilde{S}_n^*\rangle} = \sqrt{2f_0G_S(nf_0)} \tag{2.7}$$

Consider a signal which is the sum of two random signals with arbitrary (possibly zero) correlation. Let the time function of the signal be written as:

$$\tilde{s}(t) = \tilde{u}(t) + \tilde{v}(t) \tag{2.8}$$

Since the Fourier series expansion is linear, the Fourier series coefficients are related by:

$$\tilde{S}_n = \tilde{U}_n + \tilde{V}_n \tag{2.9}$$

By finding the autocorrelation of each side of this equation one obtains:

$$\langle \tilde{S}_n \tilde{S}_n^* \rangle = \langle \tilde{U}_n \tilde{U}_n^* \rangle + \langle \tilde{V}_n \tilde{V}_n^* \rangle + 2\mathrm{Re}\{\langle \tilde{U}_n \tilde{V}_n^* \rangle\} \qquad (2.10)$$

In terms of effective amplitudes (see equation 2.7) this can be rewritten as:

$$S_n^2 = U_n^2 + V_n^2 + 4\mathrm{Re}\{\langle \tilde{U}_n \tilde{V}_n^* \rangle\} \qquad (2.11)$$

Thus, to find the effective amplitude of the sum of two partially correlated random signals, it is necessary to know the effective amplitude of each of the signals as well as the cross-correlation, $\langle \tilde{U}_n \tilde{V}_n^* \rangle$. $\langle \tilde{U}_n \tilde{V}_n^* \rangle$ is a Fourier coefficient of $R_{UV}(\tau)$, the cross-correlation of $\tilde{u}(t)$ and $\tilde{v}(t)$, which is given by:

$$R_{UV}(\tau) = \lim_{T\to\infty} \frac{1}{T} \int_{-\frac{T}{2}}^{+\frac{T}{2}} \tilde{u}(t)\tilde{v}(t-\tau)dt \qquad (2.12)$$

and:

$$R_{UV}(\tau) = \langle \tilde{U}_0 \tilde{V}_0^* \rangle + 2\sum_{n=1}^{\infty} \langle \tilde{U}_n \tilde{V}_n^* \rangle e^{j2n\pi f_0 \tau} \qquad (2.13)$$

Note that $|\langle \tilde{U}_n \tilde{V}_n^* \rangle| \le \frac{1}{2}U_n V_n$. The factor of $\frac{1}{2}$ appears because of the definition of the effective amplitude given in equation 2.7. Two signals are said to be uncorrelated if $\langle \tilde{U}_n \tilde{V}_n^* \rangle = 0$, in which case superposition holds for power. If $\langle \tilde{U}_n \tilde{V}_n^* \rangle = \frac{1}{2}|U_n V_n|$ superposition holds for effective amplitude, as for coherent signals. If neither of these two conditions apply the signals will add with partial correlation and equation 2.10 must be used.

It has been assumed above that noise at different frequencies is uncorrelated. Thus, noise at different frequencies may be treated separately and the results combined by superposition of power. Accordingly, from here on all analysis will be for a single frequency or narrow frequency band and the subscript "n", indicating the frequency multiple, will be dropped from all the Fourier series coefficients. This being the case $2\langle\tilde{U}\tilde{U}^*\rangle$ becomes the autocorrelation of $\tilde{u}(t)$ and $2\langle\tilde{U}\tilde{V}^*\rangle$ becomes the cross-correlation of $\tilde{u}(t)$ and $\tilde{v}(t)$ in the frequency interval from $f_c - \frac{\Delta f}{2}$ to $f_c + \frac{\Delta f}{2}$.

Because partially correlated random signals do not add by superposition of effective amplitude, the response of a circuit excited by random signals will differ from that of a circuit excited by coherent signals. The problem of analysis has been addressed by several authors. Rothe and Dahlke (1956) introduced a representation which adds two noiseless correlation admittances to each two-port in such a way that the terminal noise generators can be considered as uncorrelated and other signals are not affected. Haus and Adler (1958, 1959) extended this representation to a canonical representation of a noisy N-port. These representations have been much used when the terminal quantities are chosen to be voltage and current; however, they have not been extended to wave representations of a noisy circuit. Adamian and Uhlir (1984), in an analysis of a noisy circuit using a wave model, use the symbol "⊕" to indicate addition with partial correlation. This clarifies which operation is being performed, but there is confusion as to whether a symbol represents a random variable or its effective amplitude.

The response of a circuit to a random signal differs from its response to a coherent signal because the signal is different, not because the circuit components behave differently; this difference should be reflected in the model of the signal rather than that of the circuit. It is also useful to distinguish determinate values, such as component values and signal amplitudes, from random processes. Accordingly the symbol Ψ introduced here will be a unitless complex random variable which can be thought of as the phasor representation of a random signal of unity effective amplitude over the bandwidth of observation and having a normal distribution. The frequency components of each random signal will be expressed as $A\Psi_A$ where A is the effective amplitude of that component and Ψ_A embodies all the statistical properties, including those of distribution and correlation. For each pair of random signals, Ψ_I and Ψ_J, a cross correlation $\alpha_{IJ} = \langle\Psi_I\Psi_J^*\rangle$ is defined. The following rules must be followed to find the sum of two random signals:

1. The sum of any two random signals must be another random signal or zero.

2. The effective amplitude of the sum is found as follows:

Let $C\Psi_C = A\Psi_A + B\Psi_B$. (2.14)

Then $C^2 = A^2 + B^2 + 2AB\ \mathrm{Re}\{\alpha_{AB}\}$. (2.15)

3. The magnitude of α_{AB} must be less than or equal to 1.

Bosma(1967) states that the relative delay between the signals to be added must be significantly less than the reciprocal bandwidth of observation, or the magnitude of the correlation will begin to decrease. This may be important where long line lengths or high Q, *i.e.* long decay time, circuits are used.

The notation introduced above is applicable to wave models of circuits and to voltage-current models, and also differentiates between coherent and random signals. It will be seen that this notation is indispensible to the analysis of cascaded noisy two-ports performed in the latter part of this chapter.

2.2 The Noisy Linear One-Port

Consider two passive one-ports connected together via a lossless pair of conductors. The energy delivered to each one-port from the other one-port is thermal radiation. It has been shown by Nyquist (1928) and Kittel (1969) by using the precepts of quantum mechanics that if the system is in thermal equilibrium then the spectral density of the power emitted, *i.e.* the available power, from each one-port on each electromagnetic mode carried by the conductors is:

$$W_A = \frac{hf}{e^{\frac{hf}{kT_{PH}}} - 1} \qquad (2.16)$$

where: f is the frequency of observation
h is Planck's constant
k is Boltzmann's constant
T_{PH} is the absolute physical temperature of the system

For a single mode conductor, and for low frequencies such that $hf \ll kT$, equation 2.16 reduces to

$$W_A = kT_{PH} \qquad (2.17)$$

The fractional error involved in this approximation is $+\frac{hf}{2kT}$, which is 0.02% at 300K and 2GHz, and 0.5% at 10K and 2GHz. The validity of equation 2.17 was verified experimentally by Johnson (1928). Under the assumptions just discussed, the effective amplitude of the terminal noise generator of a passive one-port is a function of the physical temperature and the impedance, and is given here for emergent wave, voltage, and current terminal noise generators respectively:

$$B_G = \sqrt{kT_{PH}\Delta f(1 - |\Gamma_G|^2)} \qquad (2.18)$$

$$V_G = \sqrt{4kT_{PH}\Delta f R_G} \qquad (2.19)$$

$$I_G = \sqrt{4kT_{PH}\Delta f G_G}\ . \qquad (2.20)$$

where: T_{PH} is the physical temperature

Δf is the bandwidth

R_G is the real part of the generator impedance Z_G

G_G is the real part of the generator admittance Y_G

Γ_G is the generator reflection coefficient.

The available noise power spectral density of an active one-port is commonly described by its noise temperature, which is the temperature of a passive one-port having the same impedance and available noise power spectral density. Thus, the effective amplitude of the terminal noise generator of the model of an active one-port is also given by equations 2.18 to 2.20, substituting noise temperature for physical temperature.

2.3 The Noisy Linear N-Port

An N-port has 2N terminal variables which can be modelled either as voltages and currents or as incident and emergent waves. A linear N-port is modelled by choosing N terminal variables to be independent and the other N terminal variables to be dependent. The array of linear coefficients relating the independent to the dependent terminal variables are the small signal parameters. If signals are generated internally, they are modelled by N terminal generators corresponding to the N dependent terminal variables.

The noise generated internally by a noisy N-port can be modelled by N terminal generators connected to a non-generating N-port characterized by small signal parameters (just as for any other internally generated signal). However, when modelling internally generated noise, the terminal noise generators may have some cross-correlation. Noise generated by physically separate devices is assumed to be uncorrelated so that the noise power generated by each device can be found independently and added.

From the discussion above it can be seen that an N-port device can be described by ${}^{2N}C_N$ sets of small signal parameters, if all the parameter sets can be used. The terminal generators corresponding to different sets of small signal parameters are linearly related. If the terminal generators are noise generators then equations 2.14 and 2.15 must be used to relate the effective amplitudes.

When the terminal quantities are chosen to be voltages and currents, two common choices of small signal parameters are impedance or Z parameters (the dependent variables are terminal voltages) and admittance or Y parameters (the dependent variables are terminal currents). The small signal equations for these two parameter sets are given in matrix form below:

$$\underline{v} = \underline{\underline{Z}}\,\underline{i} + \mathrm{Diag}(\underline{\Psi}_Z)\underline{v}_Z \tag{2.21}$$

$$\underline{\alpha}_Z = \langle \underline{\Psi}_Z \times \underline{\Psi}_Z^{*} \rangle \tag{2.22}$$

$$\underline{i} = \underline{Y}\underline{v} + \mathrm{Diag}(\underline{\Psi}_Y)\underline{i}_Y \tag{2.23}$$

$$\underline{\alpha}_Y = \langle \underline{\Psi}_Y \times \underline{\Psi}_Y^* \rangle \tag{2.24}$$

where: $\underline{v}$ is the vector of terminal voltages
$\underline{i}$ is the vector of terminal currents
$\underline{Z}$ is the array of Z-parameters
$\underline{Y}$ is the array of Y-parameters
$\underline{v}_Z$ is the vector of effective amplitudes of the terminal noise voltage generators
$\underline{\Psi}_Z$ is the vector of random signals of the terminal noise voltage generators
$\underline{i}_Y$ is the vector of effective amplitudes of the terminal noise current generators
$\underline{\Psi}_Y$ is the vector of random signals of the terminal noise current generators
$\underline{\alpha}_Z$ is the matrix of auto correlation and cross correlation coefficients associated with the terminal noise voltage generators
$\underline{\alpha}_Y$ is the matrix of auto correlation and cross correlation coefficients associated with the terminal noise current generators

The corresponding circuit models are shown in figure 2.1 and figure 2.2.

When the terminal quantities are chosen to be incident and emergent normalized waves the emergent waves can be chosen as the dependent variables, in which case the parameter set is called the scattering or S-parameters. The S-parameter small signal equations for a noisy N-port are:

$$\underline{b} = \underline{S}\underline{a} + \mathrm{Diag}(\underline{\Psi}_S)\underline{b}_S \tag{2.25}$$

$$\underline{\alpha}_S = \langle \underline{\Psi}_S \times \underline{\Psi}_S^* \rangle \tag{2.26}$$

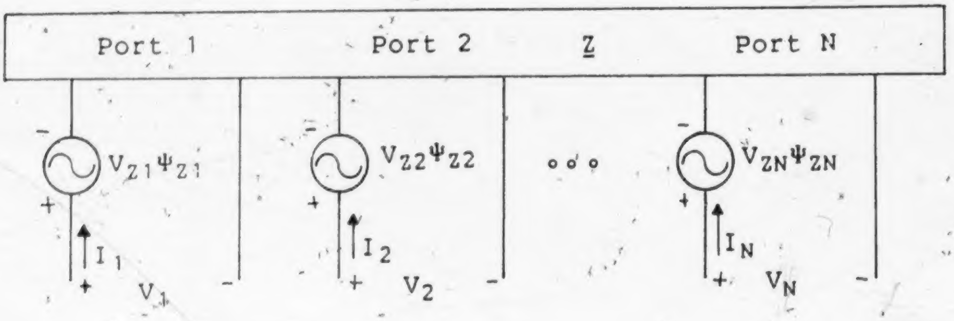
Port 1
Port 2
$\underline{Z}$
Port N
$V_{Z1}\Psi_{Z1}$
$V_{Z2}\Psi_{Z2}$
$V_{ZN}\Psi_{ZN}$
I_1
I_2
I_N
V_1
V_2
V_N

Figure 2.1 The Z-parameter Representation of a Noisy N-port

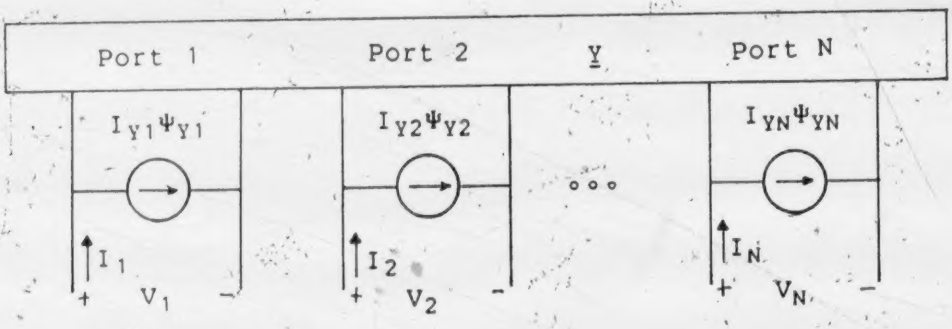
Port 1
Port 2
$\underline{Y}$
Port N
$I_{Y1}\Psi_{Y1}$
$I_{Y2}\Psi_{Y2}$
$I_{YN}\Psi_{YN}$
I_1
I_2
I_N
V_1
V_2
V_N

Figure 2.2 The Y-parameter Representation of a Noisy N-port

where: $\underline{a}$ is the vector of incident waves

$\underline{b}$ is the vector of emergent waves

$\underline{S}$ is the array of S-parameters

$\underline{b}_S$ is the vector of effective amplitudes of the terminal emergent noise wave generators

$\underline{\Psi}_S$ is the vector of random signals of the terminal emergent noise wave generators

$\underline{\alpha}_S$ is the matrix of auto correlation and cross correlation coefficients associated with the terminal emergent noise wave generators

A noisy N-port can be represented by the flow diagram in figure 2.3.

The power spectral density of the terminal noise generators associated with a noisy N-port is commonly described using the passive noisy one-port as a model, choosing either a reference impedance or a reference temperature to be used in equations 2.18 to 2.20. If the terminal noise generators are chosen to be voltage or current generators, a reference temperature of 290K, represented by the symbol T_0, is commonly chosen and the power spectral density is described as a resistance or a conductance. If the terminal generators are chosen to be wave generators, the reference reflection coefficient is commonly chosen to be zero, and the power spectral density is described as a temperature. The effective amplitudes of terminal generators of noisy N-ports (for N > 1) are given by:

$$V = \sqrt{4k\Delta f T_0 R} \tag{2.27}$$

$$I = \sqrt{4k\Delta f T_0 G} \tag{2.28}$$

$$B = \sqrt{k\Delta f T_B} \tag{2.29}$$

$$A = \sqrt{k\Delta f T_A} \tag{2.30}$$

2.3.1 The Noisy Linear Two-Port

Consider a noisy two-port in cascade with a noisy one-port (the "generator") delivering power to a receiver of narrow bandwidth and arbitrary immitance. Suppose the noise

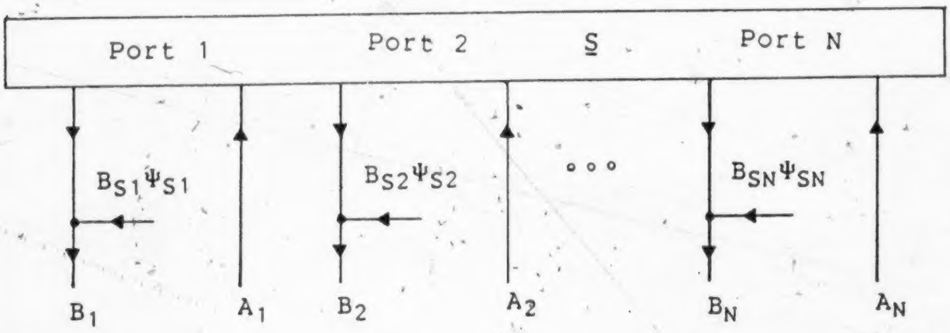

Figure 2.3 The S-parameter Representation of a Noisy N-port

generated by the two-port is attributed to the generator. The resulting apparent increase in the noise temperature of the generator is called the excess noise temperature, T_E, of the two-port. It will be seen below that the excess noise temperature of a two-port is a function of the generator impedance and four noise parameters.

A linear noisy two-port may be represented by twelve sets of small signal parameters and corresponding terminal generators (six sets using terminal voltages and currents and six sets using incident and emergent waves). Only three of the possible twelve representations are used in this thesis. Because the effective amplitude and the correlation properties of a particular terminal generator depend on the choice of the other terminal generator, it is important to establish a clear notation. The notation which will be used in this thesis is given in Table 2.1. The symbols R_n and g_n are in accordance with common usage in the literature. The other symbols listed do not conflict with common usage, so

Table 2.1 Notation for Noisy Two-ports

Common Name of Parameter Set	Dependent Variables		Terminal Generators		Power Spectral Density		Correlation Coeff.
ABCD	i_1	v_1	$I_C\Psi_{IC}$	$V_C\Psi_{VC}$	g_n	R_n	α_C
S	b_1	b_2	$B_{S1}\Psi_{S1}$	$B_{S2}\Psi_{S2}$	T_{S1}	T_{S2}	α_S
T	a_1	b_1	$A_T\Psi_{AT}$	$B_T\Psi_{BT}$	T_{AT}	T_{BT}	α_T

far as the author is able to determine. The cross-correlation coefficients are defined as:

$$\alpha_C = \langle \Psi_{VC}\Psi_{IC}^* \rangle \tag{2.31}$$

$$\alpha_S = \langle \Psi_{S1}\Psi_{S2}^* \rangle \tag{2.32}$$

$$\alpha_T = \langle \Psi_{AT}\Psi_{BT}^* \rangle \tag{2.33}$$

An equation relating the excess noise temperature of a two-port to the generator impedance, admittance or reflection coefficient is nonlinear and has four parameters, called noise parameters. Equations of this sort (and sets of noise parameters) are presented by Rothe and Dahlke (1956), the IRE Subcommittee 7.9 on Noise (1960,II), Lange (1967), Adamian and Uhlir (1973), Caruso and Sannino (1978), Meys (1978), Hecken (1981), Weinreb (1982), Pospieszalski (1984), and others. The twelve equations presented by the above authors can be reduced to a minimum set using a common set of parameters.

If the terminal generators representing the internally generated noise of a two-port are both chosen to be at the port connected to the generator termination then they can be included with the generator without further considering the small signal parameters of the two-port. This choice of terminal generators corresponds to ABCD parameters for a voltage-current model (shown in figure 2.4) and T-parameters for a normalized wave model (shown in figure 2.5). If the two-port terminal noise generators are included with the generator, the three noise generators now considered part of the generator can be replaced by a single noise generator whose noise temperature must be increased so that the voltages and currents at terminals $1'-1'$ or the wave variables at reference plane $A_1'-B_1'$ remain unchanged.

First consider the voltage-current analysis. The open circuit voltage at terminals $1'-1'$ is given by:

$$V_{OC}\Psi_{oc} = V_G\Psi_{VG} - V_C\Psi_{VC} - I_C\Psi_{IC}Z_G \tag{2.37}$$

Finding the autocorrelation of this equation and assuming that the noise generated by the two-port is not correlated with the noise generated by the one-port results in:

$$V_{oc}^2 = V_G^2 + V_C^2 + I_C^2|Z_G|^2 + 2V_CI_C\mathrm{Re}\{\alpha_C Z_G^*\} \tag{2.38}$$

The quantities in equation 2.38 can be written in terms of power spectral densities given by equations 2.19, 2.27 and 2.28 and we can substitute

$$V_{oc}^2 = 4k\Delta f(T_G+T_E)R_G. \tag{2.39}$$

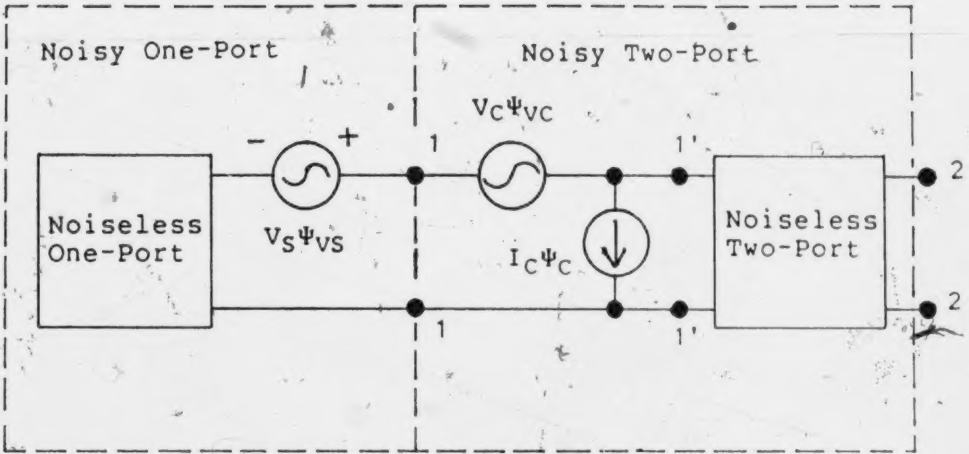
Noisy One-Port
Noisy Two-Port
$V_C\Psi_{VC}$
-
+
1
1'
2
Noiseless One-Port
$V_S\Psi_{VS}$
$I_C\Psi_C$
Noiseless Two-Port
1
1'
2

Figure 2.4 The Terminal Noise Generators of the Voltage-Current Representation of a Noisy Two-port

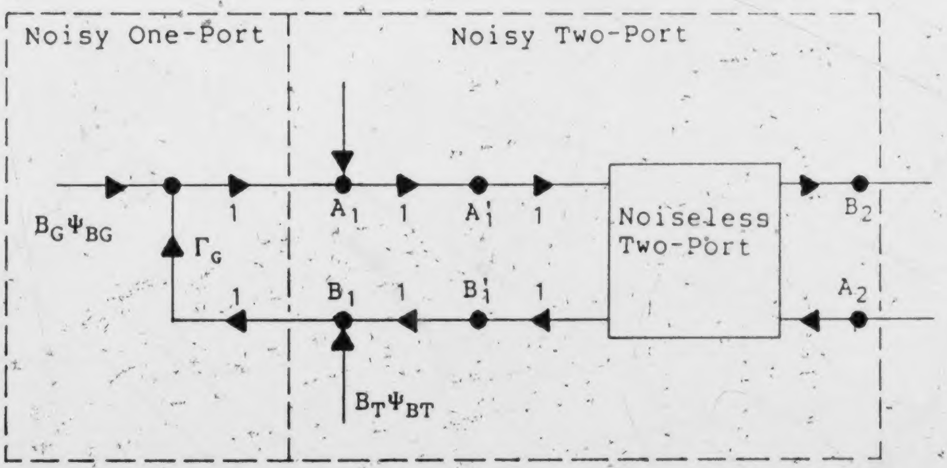
Noisy One-Port
Noisy Two-Port
$B_G\Psi_{BG}$
1
A_1
1
A_1'
1
Noiseless Two-Port
B_2
Γ_G
1
B_1
1
B_1'
1
A_2
$B_T\Psi_{BT}$

Figure 2.5 The Terminal Noise Generators of the Wave Representation of a Noisy Two-port

With these substitutions equation 2.38 becomes:

$$T_E = T_0 \frac{R_n + g_n|Z_G|^2 + 2\sqrt{R_n g_n}\,\mathrm{Re}\{\alpha_C Z_G^*\}}{R_G} \qquad (2.40)$$

In the same manner if a Norton equivalent circuit is used to represent the generator one obtains the result:

$$T_E = T_0 \frac{g_n + R_n|Y_G|^2 + 2\sqrt{R_n g_n}\,\mathrm{Re}\{\alpha_C Y_G\}}{G_G} \qquad (2.41)$$

Equation 2.40 and equation 2.41 can be rearranged into equation 2.42 and equation 2.43, which are equivalent to the equations derived by Lange (1967):

$$T_E = T_{MIN} + T_N \frac{|Z_G - Z_{OPT}|^2}{4R_G R_{OPT}} \qquad (2.42)$$

$$T_E = T_{MIN} + T_N \frac{|Y_G - Y_{OPT}|^2}{4G_G G_{OPT}} \qquad (2.43)$$

where: N (as defined by Lange) is related to T_N by:
$T_N = 4NT_0$.

Lange (1967) has shown that T_{MIN} and T_N are invariant to a lossless transformation and that Y_{OPT} and Z_{OPT} are transformed in the same way as Y_G and Z_G. From the condition $|\alpha_C| \le 1$ it can be shown that (Pospieszalski, 1984):

$$0 \le T_{MIN} \le T_N \qquad (2.44)$$

A similar procedure can be followed for the wave analysis by finding the emergent wave into a reflectionless termination at reference plane $A_1'-B_1'$:

$$B_0\Psi_{B0} = B_G\Psi_{BG} + A_T\Psi_{AT} + \Gamma_G B_T\Psi_{BT} \qquad (2.45)$$

where: $B_0\Psi_{B0}$ is the emergent wave into a reflectionless termination.

Finding the autocorrelation of equation 2.45 results in:

$$B_0^2 = B_G^2 + A_T^2 + B_T^2|\Gamma_G|^2 + 2A_TB_T\mathrm{Re}\{\alpha_T\Gamma_G^*\} \qquad (2.46)$$

Substituting the power spectral densities from equations 2.18, 2.29 and 2.30 and replacing the effective amplitude of the equivalent noise generator by:

$$B_0^2 = k\Delta f(T_G+T_E)(1-|\Gamma_G|^2) \qquad (2.47)$$

equation 2.46 becomes the equation first obtained by Meys (1978):

$$T_E = \frac{T_{AT} + T_{BT}|\Gamma_G|^2 + 2\sqrt{T_{AT}T_{BT}}\,\mathrm{Re}\{\alpha_T\Gamma_G^*\}}{1 - |\Gamma_G|^2} \qquad (2.48)$$

Meys has shown equation 2.48 can be rearranged into the following form:

$$T_E = T_{MIN} + T_D\frac{|\Gamma_G - \Gamma_{OPT}|^2}{1 - |\Gamma_G|^2} \qquad (2.49)$$

This is equivalent to the form:

$$T_E = T_{MIN} + T_N\frac{|\Gamma_G - \Gamma_{OPT}|^2}{[1 - |\Gamma_G|^2][1 - |\Gamma_{OPT}|^2]} \qquad (2.50)$$

This equation was derived by Caruso and Sannino (1978) from equations 2.42 and 2.43. T_N and T_{MIN} are the same constants as in equations 2.42 and 2.43 and Γ_{OPT} is transformed by a lossless transformation in the same way as Γ_G.

In the course of the algebra performed to arrive at equations 2.42 and 2.43 and equation 2.50 the relationships between sets of noise parameters are obtained. Let any cross-correlation coefficient be given by $\alpha = \delta + j\gamma$. The relationships between the noise parameters of equation 2.42, equation 2.43 and the circuit of figure 2.4 are:

$$T_{MIN} = 2T_0\sqrt{R_n g_n}\left[\sqrt{1-\gamma_C^2} + \delta_C\right] \tag{2.51}$$

$$T_N = 4T_0\sqrt{R_n g_n(1-\gamma_C^2)} \tag{2.52}$$

$$Y_{OPT} = \left[\frac{g_n}{R_n}\right]^{\frac{1}{2}}\left[\sqrt{1-\gamma_C^2} + j\gamma_C\right] \tag{2.53}$$

$$Z_{OPT} = \left[\frac{R_n}{g_n}\right]^{\frac{1}{2}}\left[\sqrt{1-\gamma_C^2} - j\gamma_C\right] \tag{2.54}$$

The relationships between the noise parameters of equation 2.50 and those of equation 2.48 are (derived from Meys (1978) and Weinreb (1982)):

$$T_N = \sqrt{(T_{AT} + T_{BT})^2 - 4T_{AT}T_{BT}|\alpha_T|^2} \tag{2.55}$$

$$T_{MIN} = \frac{T_{AT} - T_{BT} + T_N}{2} \tag{2.56}$$

$$T_D = \frac{T_{AT} + T_{BT} + T_N}{2} \tag{2.57}$$

$$\Gamma_{OPT} = \frac{-\alpha_T \sqrt{T_{AT}T_{BT}}}{T_D} \qquad (2.58)$$

The inverse relationships are:

$$T_{BT} = T_D - T_{MIN} \qquad (2.59)$$

$$T_{AT} = T_D|\Gamma_{OPT}|^2 + T_{MIN} \qquad (2.60)$$

$$\alpha_T = \frac{-\Gamma_{OPT}\ T_D}{\sqrt{T_{AT}T_{BT}}} \qquad (2.61)$$

where: $T_D = \frac{T_N}{1-|\Gamma_{OPT}|^2}$

Note that Y_{OPT}, Z_{OPT}, and Γ_{OPT} are all strongly dependent on the cross correlation coefficients and are related by:

$$Y_{OPT} = \frac{1}{Z_{OPT}} \qquad (2.62)$$

$$\Gamma_{OPT} = \frac{Z_{OPT} - Z_0}{Z_{OPT} + Z_0} \qquad (2.63)$$

2.3.2 The Noise Parameters of a Passive Two-port

The excess noise temperature of a passive two-port is determined by its available gain and its physical temperature. If we imagine such a two-port connected in cascade with a passive one-port of the same physical temperature, the noise temperature at the unterminated port of the two-port must be the physical temperature of the composite one-port. From these considerations one can determine that the excess noise temperature is given by:

$$T_E = T_{PH} \left[\frac{1}{G_A} - 1 \right] \tag{2.64}$$

where: G_A is the available gain of the two-port
T_{PH} is the physical temperature of the two-port.

It is possible to determine the noise parameters of a passive two-port from its absolute temperature, T_{PH}, and its small signal parameters. Many authors, for example Haus and Adler (1959), Penfield (1962) and Hecken (1981), ignore the cross correlation coefficient because it can be shown that for an appropriate choice of characteristic impedance the cross correlation between noise wave generators is zero. The appropriate value of the characteristic impedance depends on the small signal parameters of the two-port being modelled. When analyzing a circuit consisting of a number of two-ports it is hardly convenient to work with waves normalized with respect to different, arbitrary impedances. Wait (1968) gives the noise parameters of a passive two-port as:

$$T_{S1} = T_{PH} \left[1 - |s_{11}|^2 - |s_{12}|^2 \right] \tag{2.65}$$

$$T_{S2} = T_{PH} \left[1 - |s_{22}|^2 - |s_{21}|^2 \right] \tag{2.66}$$

$$\alpha_S = \frac{-T_{PH} \left[s_{11} s_{21}^* + s_{12} s_{22}^* \right]}{\sqrt{T_{S1} T_{S2}}} \tag{2.67}$$

where: T_{PH} is the physical temperature of the two-port.

2.4 Cascaded Noisy Two-ports

The noise parameters of a cascade of two noisy two-ports can be determined from the noise parameters of each of the two-ports and the small signal parameters of one of the two-ports. That relationship will be derived in this section, using incident and emergent waves as the terminal quantities. These equations will then be solved for the noise parameters of each of the constituent two-ports, enabling one to de-embed a two-port from a cascade without using any additional equipment to separate the noise contributions of the various elements of the cascade. This approach, although very simple, had not previously been reported in the literature but has now been published (Valk et al.,1988) This approach to de-embedding will be used in this thesis to de-embed the transistor from the receiver and from the lossy lines used to pass signals into the cryostat.

Engberg (1974, 1985) published formulae which can be used to find the noise parameters of a noisy two-port embedded in a lossy feedback network and to find the noise parameters of noisy two-ports in cascade and in parallel. These results were obtained in terms of ABCD parameters and the represenation of noise generators introduced by Rothe and Dahlke (1956). Some of Engberg's results are very difficult to solve for de-embedding and Engberg does not report using his formulae for that purpose. The formulae derived below are solved for de-embedding and are written in terms of the noise parameters of a wave representaton , *i.e.*

T_{AT}, T_{BT} and α_T.

Figure 2.6 shows the two-ports in cascade, the terminal quantities, and the terminal noise generators associated with the T-parameter representation. Figure 2.7 shows the terminal generators and terminal quantities of the two-port equivalent to the cascade. The small signal equations for two-ports "A" and "B" are:

$$\begin{bmatrix} b_{1A} \\ a_{1A} \end{bmatrix} = \begin{bmatrix} t_{11} & t_{12A} \\ t_{21A} & t_{22A} \end{bmatrix} \begin{bmatrix} a_{2A} \\ b_{2A} \end{bmatrix} + \begin{bmatrix} +B_{TA}\Psi_{BTA} \\ -A_{TA}\Psi_{ATA} \end{bmatrix} \qquad (2.68)$$

$$\begin{bmatrix} b_{1B} \\ a_{1B} \end{bmatrix} = \begin{bmatrix} t_{11B} & t_{12B} \\ t_{21B} & t_{22B} \end{bmatrix} \begin{bmatrix} a_{2B} \\ b_{2B} \end{bmatrix} + \begin{bmatrix} +B_{TB}\Psi_{BTB} \\ -A_{TB}\Psi_{ATB} \end{bmatrix} \qquad (2.69)$$

From figure 2.6 it can be seen that $a_{2A}=b_{1B}$ and $b_{2A}=a_{1B}$. Using these relationships equation 2.69 can be substituted into equation 2.68 with the result:

$$\begin{bmatrix} b_{1A} \\ a_{1A} \end{bmatrix} = \begin{bmatrix} t_{11A} & t_{12A} \\ t_{21A} & t_{22A} \end{bmatrix} \begin{bmatrix} t_{11B} & t_{12B} \\ t_{21B} & t_{22B} \end{bmatrix} \begin{bmatrix} a_{2B} \\ b_{2B} \end{bmatrix} + \qquad (2.70)$$

$$\begin{bmatrix} t_{11A} & t_{12A} \\ t_{21A} & t_{22A} \end{bmatrix} \begin{bmatrix} +B_{TB}\Psi_{BTB} \\ -A_{TB}\Psi_{ATB} \end{bmatrix} + \begin{bmatrix} +B_{TA}\Psi_{BTA} \\ -A_{TA}\Psi_{ATA} \end{bmatrix}$$

Comparing figure 2.6 and figure 2.7, it can be seen that $b_{1C}=b_{1A}$, $a_{1C}=a_{1A}$, $b_{2C}=b_{2B}$ and $a_{2C}=a_{2B}$. Using these relationships the quantities in equation 2.70 can be identified with quantities in the small signal equation for the cascade:

$$\begin{bmatrix} b_{1C} \\ a_{1C} \end{bmatrix} = \begin{bmatrix} t_{11C} & t_{12C} \\ t_{21C} & t_{22C} \end{bmatrix} \begin{bmatrix} a_{2C} \\ b_{2C} \end{bmatrix} + \begin{bmatrix} +B_{TC}\Psi_{BTC} \\ -A_{TC}\Psi_{ATC} \end{bmatrix} \qquad (2.71)$$

The following relationships are obtained from the

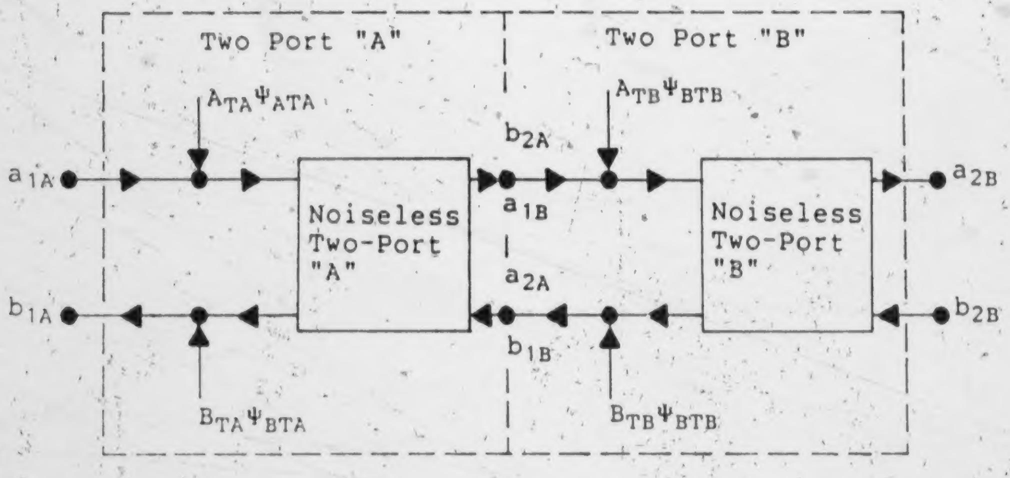
Two Port "A"
Two Port "B"
$A_{TA}\Psi_{ATA}$
$A_{TB}\Psi_{BTB}$
b_{2A}
a_{1A}
a_{1B}
a_{2B}
Noiseless Two-Port "A"
Noiseless Two-Port "B"
a_{2A}
b_{1A}
b_{1B}
b_{2B}
$B_{TA}\Psi_{BTA}$
$B_{TB}\Psi_{BTB}$

Figure 2.6 The Terminal Noise Generators of Noisy Two-ports in Cascade

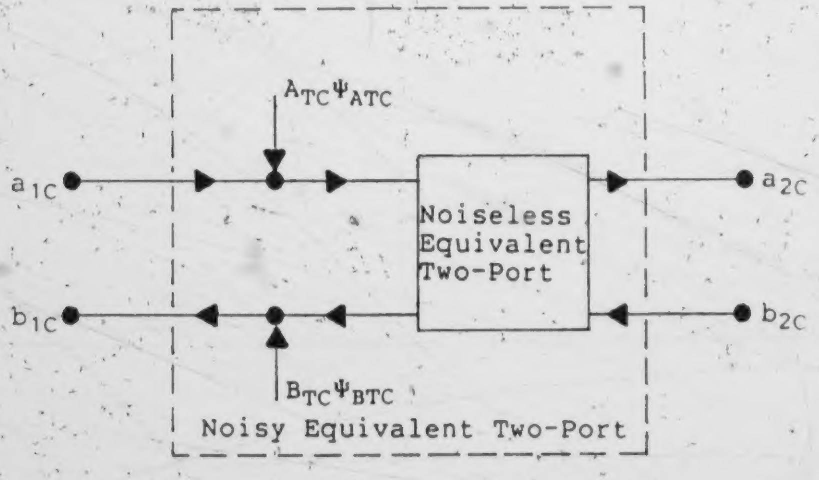
$A_{TC}\Psi_{ATC}$
a_{1C}
a_{2C}
Noiseless Equivalent Two-Port
b_{1C}
b_{2C}
$B_{TC}\Psi_{BTC}$
Noisy Equivalent Two-Port

Figure 2.7 The Terminal Noise Generators of the Two-port Equivalent to a Cascade of Noisy Two-ports

comparison:

$$B_{TC}\Psi_{BTC} = B_{TB}\Psi_{BTB}t_{11A} - A_{TB}\Psi_{ATB}t_{12A} + B_{TA}\Psi_{BTA} \qquad (2.72)$$

$$A_{T_C}\Psi_{AT_C} = -B_{T_B}\Psi_{BT_B}t_{21A} + A_{T_B}\Psi_{AT_B}t_{22A} + A_{T_A}\Psi_{AT_A} \tag{2.73}$$

Note that these relationships are independent of the small signal parameters of two-port "B". Finding the autocorrelation of equation 2.72 and substituting the relationships of equations 2.29, 2.30, and 2.33 (and assuming that the noise generated by two-port "A" is uncorrelated with the noise generated by two-port "B") results in:

$$T_{BT_C} = T_{BT_B}|t_{11A}|^2 + T_{AT_B}|t_{12A}|^2 + T_{BT_A} - 2\sqrt{T_{BT_B}T_{AT_B}}\,\mathrm{Re}\{\alpha_{T_B}t^*_{11A}t_{12A}\} \tag{2.74}$$

Similarly, from equation 2.73:

$$T_{AT_C} = T_{BT_B}|t_{21A}|^2 + T_{AT_B}|t_{22A}|^2 + T_{AT_A} - 2\sqrt{T_{BT_B}T_{AT_B}}\,\mathrm{Re}\{\alpha_{T_B}t^*_{21A}t_{22A}\} \tag{2.75}$$

With the same substitutions and assumptions the cross-correlation coefficient can be found from the crosscorrelation of equation 2.72 and equation 2.73 to be:

$$\alpha_{T_C} = \frac{1}{\sqrt{T_{AT_C}T_{BT_C}}}\Big[\alpha_{T_A}\sqrt{T_{BT_A}T_{AT_A}} - T_{BT_B}t^*_{11A}t_{21A} - T_{AT_B}t^*_{12A}t_{22A} + \sqrt{T_{BT_B}T_{AT_B}}\,(\alpha^*_{T_B}t^*_{12A}t_{21A} + \alpha_{T_B}t^*_{11A}t_{22A})\Big] \tag{2.76}$$

Equations 2.74, 2.75 and 2.76 can easily be solved for T_{AT_A}, T_{BT_A} and α_{T_A}, thus de-embedding two-port "A" from the cascade (see Valk et al., 1988). This important result will be used in later parts of this thesis to de-embed the transistor from the receiver.

Solving for T_{AT_B}, T_{BT_B} and α_{T_B} is more difficult. The (attempted) solution of equations 2.74, 2.75 and 2.76 for these noise parameters is very tedious and complicated. A better strategy is to proceed by solving equation 2.72 and equation 2.73 for $B_{T_B}\Psi_{BT_B}$ and $A_{T_B}\Psi_{AT_B}$:

$$B_{T_B}\Psi_{BT_B} = \left[\frac{t_{22_A}}{t_{11_A}t_{22_A} - t_{12_A}t_{21_A}}\right]\left[B_{T_C}\Psi_{BT_C} + A_{T_C}\Psi_{AT_C}\frac{t_{12_A}}{t_{22_A}} - A_{T_A}\Psi_{AT_A}\frac{t_{12_A}}{t_{22_A}} - B_{T_A}\Psi_{BT_A}\right] \qquad (2.77)$$

$$A_{T_B}\Psi_{AT_B} = \left[\frac{t_{11_A}t_{22_A} - t_{12_A}t_{21_A}}{t_{21_A}}\right]\left[B_{T_C}\Psi_{BT_C} + A_{T_C}\Psi_{AT_C}\frac{t_{11_A}}{t_{21_A}} - A_{T_A}\Psi_{AT_A}\frac{t_{11_A}}{t_{21_A}} - B_{T_A}\Psi_{BT_A}\right] \qquad (2.78)$$

These equations are much simplified by converting the small signal parameters to reverse transfer scattering parameters. These are defined by:

$$\begin{bmatrix} b_2 \\ a_2 \end{bmatrix} = \begin{bmatrix} r_{11} & r_{12} \\ r_{21} & r_{22} \end{bmatrix}\begin{bmatrix} a_1 \\ b_1 \end{bmatrix} \qquad (2.81)$$

The following cross-correlations, which are required below, can be found from the cross-correlation of equation 2.72 and equation 2.73 with Ψ_{AT_A} and Ψ_{BT_A}:

$$\langle \Psi_{AT_C}\Psi^{*}_{AT_A} \rangle = \frac{A_{T_A}}{A_{T_C}} \qquad (2.79)$$

$$<\Psi_{BT_C}\Psi^*_{BT_A}> = \frac{B_{T_A}}{B_{T_C}} \tag{2.80}$$

$$<\Psi_{AT_C}\Psi^*_{BT_A}> = \frac{A_{T_A}}{A_{T_C}}\alpha_{T_A} \tag{2.82}$$

$$<\Psi_{AT_A}\Psi^*_{BT_C}> = \frac{B_{T_A}}{B_{T_C}}\alpha_{T_A} \tag{2.83}$$

Finding the autocorrelation of equation 2.77 and equation 2.78 and using the substitutions mentioned above results in:

$$\begin{aligned} T_{BT_B} = {} & |r_{22_A}|^2(T_{BT_C} - T_{BT_A}) + |r_{21_A}|^2(T_{AT_C} - T_{AT_A}) \\ & - 2\mathrm{Re}\{r_{21_A}r^*_{22_A}[\alpha_{T_C}\sqrt{T_{BT_C}T_{AT_C}} - \alpha_{T_A}\sqrt{T_{BT_A}T_{AT_A}}]\} \end{aligned} \tag{2.84}$$

and:

$$\begin{aligned} T_{AT_B} = {} & |r_{12_A}|^2(T_{BT_C} - T_{BT_A}) + |r_{11_A}|^2(T_{AT_C} - T_{AT_A}) \\ & - 2\mathrm{Re}\{r_{11_A}r^*_{12_A}[\alpha_{T_C}\sqrt{T_{BT_C}T_{AT_C}} - \alpha_{T_A}\sqrt{T_{BT_A}T_{AT_A}}]\} \end{aligned} \tag{2.85}$$

The cross-correlation coefficient can be found from the cross-correlation of equation 2.77 and equation 2.78:

$$\alpha_{T_B} = \frac{1}{\sqrt{T_{AT_B} T_{BT_B}}} \Big[r_{12_A} r_{22_A}^{*} (T_{BT_A} - T_{BT_C}) \tag{2.86}$$

$$+ r_{11_A} r_{21_A}^{*} (T_{AT_A} - T_{AT_C})$$

$$+ \sqrt{T_{BT_C} T_{AT_C}} \, (r_{12_A} r_{21_A}^{*} \alpha_{T_C}^{*} + r_{11_A} r_{22_A}^{*} \alpha_{T_C})$$

$$- \sqrt{T_{BT_A} T_{AT_A}} \, (r_{12_A} r_{21_A}^{*} \alpha_{T_A}^{*} + r_{11_A} r_{22_A}^{*} \alpha_{T_A}) \Big]$$

Using equations 2.84, 2.85 and 2.86 two-port "B" can be de-embedded from a cascade. This important result will be used later to de-embed the transistor from the lossy input lines used in cryogenic measurements.

It should be noted that Engberg's(1985) results are easily solveable for the noise parameters of two-port "A"; however, they would be difficult to solve for the noise parameters of two-port "B". If required, the results derived by Engberg (1985) for noisy two-ports in parallel can be easily solved for (parallel) de-embedding. These results may be required to de-embed the transistor from a lossy fixture model. Engberg's formulae for a noisy two-port embedded in a lossy feedback network do not appear to be easily solveable for de-embedding, and also assume that the feedback network is at 290K. If these relationships must be derived for other network physical temperatures, or if they must be solved for de-embedding, it may be expedient to start from scratch using the notation introduced in this chapter.

Chapter 3

Estimation of Noise Parameters

This chapter begins with an overview of the noise parameter measurement problem, and a review of conventional noise parameter measurement techniques. An improved measurement method which does not suffer from the systematic errors of the conventional method is presented. Two new methods of accounting for receiver noise are introduced. The use of the singular value decomposition to estimate the sensitivity of the estimated noise parameters to measurement errors is also introduced. Finally, improved methods of calibrating the noise temperature of a mismatched noise generator are discussed.

3.1 Overview of the Noise Parameter Measurement Problem

The configuration used to measure the noise parameters of a two-port (called the "device under test" or DUT) is shown in figure 3.1. In general the receiver must have high, adjustable gain, narrow bandwidth, and low excess noise temperature. The bandwidth is assumed sufficiently narrow that the noise and small signal parameters of all other system components are constant over the bandwidth. The effective bandwidth is given by:

$$\Delta f = \int_0^\infty \frac{G_{TREC}(f)}{G_{TREC}(f_0)} df \qquad (3.1)$$

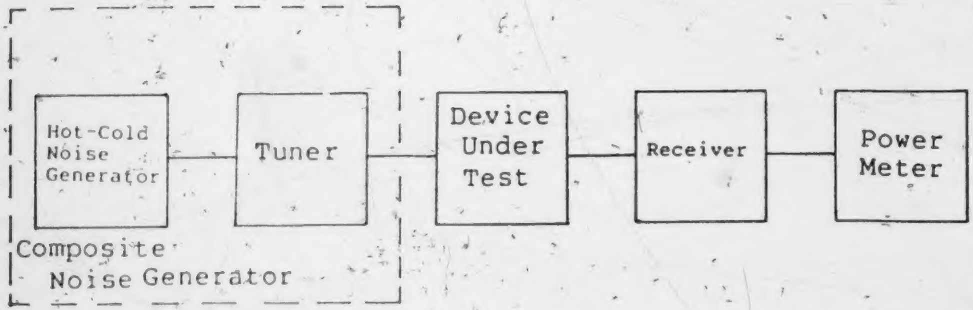
Hot-Cold
Noise
Generator
Tuner
Device
Under
Test
Receiver
Power
Meter
Composite
Noise Generator

Figure 3.1 The General Configuration for Noise Measurements

where: G_{TREC} is the transducer gain of the receiver
f_0 is the nominal operating frequency of the receiver

The receiver gain must be high and adjustable so that the noise within the system bandwidth can be adjusted to indicate near full scale of the power meter.

Each of the four system components generates some noise. The noise generated by the power meter is usually of no consequence due to the high receiver gain; alternatively because the receiver is unilateral any noise generated by the power meter is fixed and can be attributed to the receiver. By either argument the power meter can be considered noiseless. The power measured by the power meter can be given as:

$$P = k\Delta f((T_G+T_{DUT})G_{ADUT}G_{TREC}+T_{REC}G_{TREC}) \tag{3.2}$$

where: k is Boltzmann's constant

T_G is the noise temperature of the noise generator

G_{ADUT} is the available gain of the DUT

T_{REC} is the excess noise temperature of the receiver

T_{DUT} is the excess noise temperature of the DUT.

T_{DUT} and G_{ADUT} are functions of the reflection coefficient of the noise generator, Γ_G, and T_{REC} and G_{TREC} are functions of the reflection coefficient presented to the receiver input, which is a function of Γ_G and the S-parameters of the DUT.

Power measurements in the configuration of figure 3.1, using noise generators of fixed reflection coefficient and variable noise temperature, are sufficient only to determine one of the excess noise temperatures and one gain in equation 3.2. Equation 3.2 can be rewritten in terms of the parameters of the composite two-port consisting of the DUT and the receiver (called the "receiver under test" or RUT) as:

$$P = k\Delta f(T_G + T_{RUT})G_{TRUT} \tag{3.3}$$

where: T_{RUT} is the excess noise temperature of the RUT

G_{TRUT} is the transducer gain of the RUT.

T_{RUT} and G_{TRUT} are functions of Γ_G. By comparing equation 3.2 to equation 3.3 we see that

$$G_{TRUT} = G_{ADUT}G_{TREC} \tag{3.4}$$

and

$$T_{RUT} = T_{DUT} + \frac{T_{REC}}{G_{ADUT}} \qquad (3.5)$$

The important problem of how to account for the receiver noise must be dealt with by any scheme to measure T_{DUT}. In order to determine T_{DUT} using equation 3.5, one must know T_{REC}, T_{RUT} and G_{ADUT} for the same noise generator reflection coefficient. This problem becomes more sensitive to measurement error when the DUT output is mismatched.

In order to find the noise parameters of the RUT, which describe the variation of T_{RUT} as a function of Γ_G, power measurements must be made in the configuration of figure 3.1 using a number of different known values of noise generator noise temperatures and reflection coefficients (Gupta, 1983). Both the method of finding noise parameters and the method of accounting for receiver noise depend in part on the choice of noise generator. It is convenient to choose the noise generator so that the noise temperature and reflection of some of the states are known a-priori. It is usually not difficult to measure the reflection coefficient of a noise generator; however, measuring the noise temperature of a noise generator accurately can be difficult, especially if its reflection coefficient is large.

The conventional type of noise generator used for noise measurements is capable of assuming one of two noise temperatures while maintaining substantially the same reflection coefficient. The reflection coefficient is usually small. The two states are typically known as "hot" (for high noise temperature), and "cold" (for low noise temperature), and these noise generators will be referred to as "hot-cold" noise generators in this thesis. Hot-cold noise generators in which the noise is not thermally generated, *e.g.* hot-cold noise generators which are on, require noise temperature calibration near each frequency of interest.

Some authors, *e.g.* Fanelli (1983), Weinreb (1982), Adamian and Uhlir (1973), Meys (1978) and others have developed measurement schemes using passive devices with fixed noise temperature but variable reflection coefficients as noise generators. The great advantage of these noise generators is that their noise temperature can be determined from their physical temperature. These measurement schemes require unconventional methods to estimate noise parameters.

The noise generators with variable reflection coefficient referred to above have a common disadvantage in that the reflection coefficient is controlled by mechanical means, *i.e.* by adjusting a tuner or a sliding short or replacing a termination. This is a great disadvantage when one is attempting to measure the noise parameters of a device at cryogenic temperatures. If the noise generator is located inside the cooling apparatus (cryostat) with the DUT, then provision must be made to manipulate the tuning apparatus from outside the cryostat, or the cryostat must be cycled every time the reflection coefficient is changed. If the noise generator is located outside the cryostat then the noise contribution of the transmission line from room temperature to cryogenic temperature must be accounted for, which is also a matter of considerable difficulty. In either case, unless the tuning apparatus is constructed so that the settings are repeatable, the reflection coefficient of the noise generator must be measured after every adjustment of the tuning apparatus.

3.1.1 The Multiple Impedance Load

Leake (1982) described a broad band microwave load having a reflection coefficient which can be set to one of sixteen values using D.C. control voltages and currents of small amplitude. Leake suggests that the excess noise temperature of such a load is small (experimental methods and accuracy not stated) which implies that the noise temperature of the load should be equal to its physical temperature. Because of its repeatability and because the noise measurements can be completely controlled by computer, this device is potentially very useful for cryogenic noise measurements. Also, its use should result in a decrease in measurement time and in reduced susceptibility to human error.

A load of the type described by Leake, to operate in the 1.2 GHz to 1.8 GHz band was built by the author, with a

10dB coupler incorporated as shown in figure 3.2. The construction of this load is described in chapter 4. Sixteen distinct values of reflection coefficient are available at port 2. A hot-cold noise generator connected to port 1 will also allow the noise temperature at port 2 of the load to be varied, thus allowing the load to be used in the conventional method described below. With a noise generator connected to port 1 the noise temperature at port 2 of the multiple impedance load is:

$$T_G = (T_{HC} + T_{MIL})G_{AMIL} \tag{3.6}$$

where: G_{AMIL} is the available gain from port 1 to port 2
T_{HC} is the noise temperature of the hot-cold noise generator
T_{MIL} is the excess noise temperature of the multiple impedance load (referred to port 1).
T_G is the noise temperature of the composite noise generator (at port 2 of the multiple impedance load).

The first problem which had to be solved after building the multiple impedance load was measuring the excess noise temperature of the load. This was difficult because the load has -6 dB to -10 dB available gain and a large mismatch at port 2, depending on the frequency and the state of the load. As a result the receiver noise had to be carefully accounted for in the measurement.

If the Leake load behaves as a passive device T_{MIL} is,

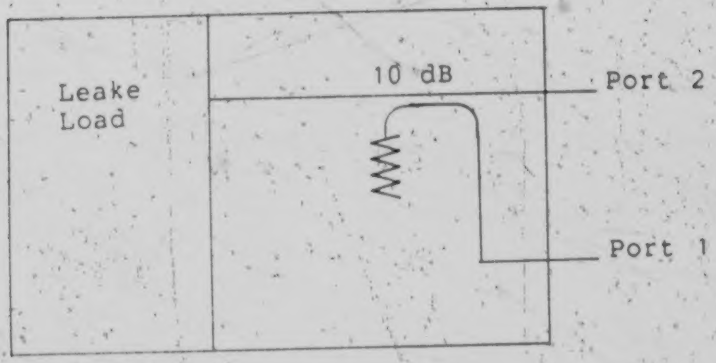

Figure 3.2 The Multiple Impedance Load

given by equation 2.64 so that equation 3.6 is reduced to:

$$T_G = T_{HC} G_{AMIL} + T_{PH}(1 - G_{AMIL}) \qquad (3.7)$$

where: T_{PH} is the physical temperature of the multiple impedance load.

If T_{HC} is substantially different from the physical temperature then T_G must be calibrated. Since G_{AMIL} varies from -6 dB to -10 dB across the 1.2 GHz to 1.8 GHz band of operation and also depends on the state of the multiple impedance load, T_G must be calibrated at each frequency of operation and for each state which will be used with T_{HC} not equal to the physical temperature of the load.

3.2 The Conventional Method of Noise Parameter Estimation

The conventional method is described by many authors, for example the IRE Subcommittee 7.9 on Noise (1959), Lange (1967), Lane (1969), Caruso and Sannino (1978), Lane (1982), and Martines and Sannino (1985). This method uses a hot-cold noise generator and a two-port tuner to measure the excess noise temperature of the RUT for different generator reflection coefficients. To obtain a calibrated hot-cold noise generator with a variable reflection coefficient a lossless tuner can be connected to a calibrated noise generator. If this tuner (sometimes called the input tuner because it is located at the DUT input) is indeed lossless then its available gain will be unity and the noise temperature of the composite noise generator will be that of the calibrated noise generator. At microwave frequencies slide screw and stub tuners are often used.

Consider the configuration of figure 3.1 when the noise generator is a hot-cold noise generator whose reflection coefficient is the same in both states. Then the quantities T_{RUT} and $G_{T_{RUT}}$ in equation 3.3 will be the same for the hot and the cold states of the noise generator. Let Y be the ratio of the power measured with the noise generator in the hot state to the power measured with the noise generator in the cold state. From equation 3.3 Y is given by:

$$Y = \frac{T_h + T_{RUT}}{T_c + T_{RUT}} \qquad (3.8)$$

where: T_h is the noise temperature of the noise generator in the hot state

T_c is the noise temperature of the noise generator in the cold state

This equation can be manipulated to obtain:

$$T_{RUT} = \frac{T_h - YT_c}{Y-1} \quad . \tag{3.9}$$

The noise parameters of the RUT can be determined by measuring T_{RUT} with different values of Γ_G. One can search for the minimum T_{RUT} while varying Γ_G as described by the IRE Subcommittee 7.9 on Noise (1959), Lange (1967) and others. The minimum value of T_{RUT} is T_{MIN} and the corresponding value of Γ_G is Γ_{OPT}. Γ_{OPT} can be difficult to determine accurately since the gradient of T_{RUT} with respect to Γ_G approaches zero near $\Gamma_G = \Gamma_{OPT}$. T_N can be found by measuring the excess noise temperature for one different, known, value of Γ_G.

Improved methods are described by Lane (1969), Gupta (1970), Caruso and Sannino (1978), and others. Measurements of T_{RUT} are made for a redundant set of arbitrary (known) values of Γ_{AC} using the procedure described above. The noise parameters can be obtained by an iterative search for the minimum error in equation 2.50 as described by Gupta (1979) and Mitima and Katoh (1979), or equation 2.50 can be linearized and a least squares fit performed as described by Lane (1969) and Caruso and Sannino (1978). There are some sets of values of Γ_G which cannot be used to uniquely determine a set of noise parameters. These singular loci are described by Caruso and Sannino (1978) and Gupta (1983).

3.2.1 Systematic Errors

There are two systematic errors in the conventional method due to the non-idealities of hot-cold noise generators and loss-less tuners. The reflection coefficient of a practical hot-cold noise generator undergoes a small change between the cold and the hot state[1,2] causing G_{TRUT} and T_{RUT} to change. Also, even the best tuners have a small loss (Strid, 1981), dependent on the tuner setting. As a result the noise temperature of the composite noise generator differs from that of the hot-cold noise generator, especially in the hot state. If these changes are not accounted for, substantial errors in the excess noise temperatures and noise parameters can occur.

3.2.2 The Conventional Method Implemented with the Multiple Impedance Load

The systematic errors inherent in the conventional method of noise parameter estimation are reduced if the conventional method is implemented using a composite noise generator consisting of a hot-cold noise generator connected to port 1 of the multiple impedance load. This configuration can be used as a hot-cold noise generator with sixteen possible reflection coefficients. The available gain from port 1 to port 2 of the multiple impedance load varies from -6 dB to -10 dB; the change in reflection coefficient at

---

[1] Hewlett Packard 346A, 346B, 346C Noise source Operating and Service Manual, 1983, Hewlett Packard Co., California

[2] AILTECH 70 Hot-cold Standard Noise Generator Manual, AILTECH New York

port 2 of the multiple impedance load due to the change in the reflection coefficient of the hot-cold noise generator is attenuated by this amount, thus reducing unwanted variations in the transducer gain and excess noise temperature of the RUT. Because of these same high losses, the "hot" noise temperature of each state of the composite noise generator must be calibrated. Since each of the sixteen states must be calibrated for "hot" noise temperature at each frequency of interest, this method can become impossible if the calibration method is too time consuming. If the "cold" noise temperature can be assumed to be the physical temperature of the multiple impedance load, and if that does not differ appreciably from the "cold" noise temperature of the hot-cold noise generator, then the "cold" noise temperature need not be calibrated.

3.3 Noise Parameter Estimation by Linear Regression of Power Measurements

It is in some cases necessary to estimate noise parameters using a noise generator which cannot assume different noise temperatures for a given reflection coefficient. In this situation excess noise temperatures cannot be determined directly, and the noise parameters must be estimated directly from the power measurements. The method which is introduced here is based on an idea introduced by Adamian and Uhlir(1973) but the implementation is quite different. A short description of this method is "linear regression of power measurements referred to the generator" and so this method will be referred to as the "LRPG" method. The measurement procedure must be performed at each frequency of interest and requires noise generators of various noise temperatures and reflection coefficients; however, hot-cold noise generators are not required. In addition the input reflection coefficient of the RUT must be known. This method can be implemented using the multiple impedance load with a hot-cold noise generator connected to port 1, and can also be implemented using the multiple impedance load and a separate "hot" noise generator. Alternatively, it can be implemented using a calibrated "hot" noise source and a separate (not necessarily lossless) tuner. The method is insensitive to non-idealities of hot-cold noise generators and tuners. The computational complexity is similar to that of the least squares fit of the conventional method and is less than that of the conventional method corrected for non-idealities of the hot-cold noise generator and tuner.

Consider the configuration of figure 3.1, where the noise parameters of the RUT are unknown. The objective is to estimate the noise parameters from a set of noise power measurements and a minimum set of scattering parameter measurements. The transducer gain of the RUT is (from

Gonzalez, 1984):

$$G_{TRUT} = \frac{1-|\Gamma_G|^2}{|1-\Gamma_G\Gamma_{IN}|^2}\,|s_{21}|^2\,\frac{1-|\Gamma_L|^2}{|1-s_{22}\Gamma_L|^2} \tag{3.10}$$

where: s_{21} and s_{22} are scattering parameters of the RUT
Γ_L is the reflection coefficient of the load (power meter)
Γ_G is the reflection coefficient of the generator
Γ_{IN} is the input reflection coefficient of the RUT.

Note that the second and third factors are not a function of Γ_G and are therefore the same for all measurements. It will become obvious that s_{21}, s_{22} and Γ_L remain unknown. The excess noise temperature of the RUT can be written as:

$$T_{RUT} = T_{MIN} + T_D\,\frac{|\Gamma_G-\Gamma_{OPT}|^2}{1-|\Gamma_G|^2} \tag{3.11}$$

where: T_{MIN}, T_D and Γ_{OPT} are the (unknown) noise parameters of the RUT.

Equation 3.10 and equation 3.11 can be substituted into equation 3.3 and rearranged to obtain:

$$P\,\frac{|1-\Gamma_{IN}\Gamma_G|^2}{1-|\Gamma_G|^2} = k\Delta f G_0(T_G + T_{MIN} + T_D\,\frac{|\Gamma_G-\Gamma_{OPT}|^2}{1-|\Gamma_G|^2}) \tag{3.12}$$

where

$$G_0 = |s_{21}|^2\,\frac{1-|\Gamma_L|^2}{|1-s_{22}\Gamma_L|^2} \tag{3.13}$$

Let a number of power measurements be made with a number of noise generators with various values of T_G and Γ_G. Corresponding to the i^{th} measurement there will be a set of known values P_i, T_{Gi} and Γ_{Gi}. After some manipulation (similar to those of Caruso and Sannino, 1978) to reduce the number of terms, equation 3.12 can be rewritten in linear form as:

$$P_i \frac{|1-\Gamma_{IN}\Gamma_{Gi}|^2}{1-|\Gamma_{Gi}|^2} = k\Delta f G_0 \Big(T_{MIN} - T_D + T_{Gi} + T_D \frac{1+u_{OPT}^2+v_{OPT}^2-2u_{Gi}u_{OPT}-2v_{Gi}v_{OPT}}{1-u_{Gi}^2-v_{Gi}^2}\Big) \tag{3.14}$$

where: $\Gamma_{Gi} = u_{Gi} + jv_{Gi}$
$\Gamma_{OPT} = u_{OPT} + jv_{OPT}$
the unknowns are T_{MIN}, T_D, Γ_{OPT} and $k\Delta f G_0$

Assuming only that Γ_{IN} is known, equation 3.14 can be rewritten in a standard linear form (Bard, 1974):

$$Y_i = \Theta_1 X_{1_i} + \Theta_2 X_{2_i} + \Theta_3 X_{3_i} + \Theta_4 X_{4_i} + \Theta_5 X_{5_i} \tag{3.15}$$

where the (known) variables in equation 3.15 are given by:

$$Y_i = P_i \frac{|1-\Gamma_{IN}\Gamma_{Gi}|^2}{1-|\Gamma_{Gi}|^2} \tag{3.16}$$

$$X_{1_i} = 1 \tag{3.17}$$

$$X_{2_i} = T_{Gi} \tag{3.18}$$

$$X_{3_i} = \frac{1}{1-u_{Gi}^2-v_{Gi}^2} \tag{3.19}$$

$$X_{4i} = \frac{u_{Gi}}{1-u_{Gi}^2-v_{Gi}^2} \quad (3.20)$$

$$X_{5i} = \frac{v_{Gi}}{1-u_{Gi}^2-v_{Gi}^2} \quad (3.21)$$

The (unknown) coefficients in equation 3.15 are given by:

$$\Theta_1 = k\Delta f G_0 \, (T_{MIN}-T_D) \quad (3.22)$$

$$\Theta_2 = k\Delta f G_0 \quad (3.23)$$

$$\Theta_3 = k\Delta f G_0 T_D \, (1+u_{OPT}^2+v_{OPT}^2) \quad (3.24)$$

$$\Theta_4 = -2k\Delta f G_0 T_D u_{OPT} \quad (3.25)$$

$$\Theta_5 = -2k\Delta f G_0 T_D v_{OPT} \quad (3.26)$$

The dependent variable in the linear equation is Y_i, and the independent variables are X_{Ki} (K=1,2,3,4,5). If five or more sets of measurements are taken with a set of non-singular values of Γ_{Gi} (Gupta, 1983) then the coefficients of the linear equation can be solved for by least squares fitting. It should be noted that since Y_i is approximately proportional to the generator noise temperature, (see equation 3.14 and equation 3.13), the least squares fitting procedure will approximately minimize the RMS error in excess noise temperature.

Once equation 3.14 has been solved to find the linearized noise parameters, Θ_1 through Θ_5, equations 3.22 to 3.26 must be inverted to find a set of noise parameters. The original set of noise parameters in equation 3.12 can be determined from:

$$T_D = \frac{1}{2\Theta_2}\left(\Theta_3 + \sqrt{\Theta_3^2 - \Theta_4^2 - \Theta_5^2}\right) \qquad (3.27)$$

$$T_{MIN} = \frac{\Theta_1}{\Theta_2} + T_D \qquad (3.28)$$

$$\Gamma_{OPT} = -\frac{\Theta_4 + j\Theta_5}{2\Theta_2 T_D} \qquad (3.29)$$

The other unknown in equation 3.12 can be determined from:

$$k\Delta f G_0 = \Theta_2 \qquad (3.30)$$

An important caveat is that there be no constraints on the least squares fitting procedure to ensure that the linearized parameters can be inverted or, if they can be inverted, that the noise parameters are physically possible. It should be verified that: $0 \le T_{MIN} \le T_N$, where T_N is a noise parameter found in equation 2.50. T_N can be directly determined from the linearized parameters by:

$$T_N = \frac{\sqrt{\Theta_3^2 - \Theta_4^2 - \Theta_5^2}}{\Theta_2} \qquad (3.31)$$

If the measurement errors are too large, the term $\Theta_3^2 - \Theta_4^2 - \Theta_5^2$ may become negative, making evaluation of equation 3.27 and equation 3.31 impossible.

The difficulties described above may be bypassed by converting the linearized noise parameters into the noise parameters of equation 2.48, as follows:

$$T_{AT} = \frac{\Theta_3 + \Theta_1}{\Theta_2} \tag{3.32}$$

$$T_{BT} = -\frac{\Theta_1}{\Theta_2} \tag{3.33}$$

$$\alpha_T = \frac{\Theta_4 + j\Theta_5}{2\sqrt{-\Theta_1(\Theta_3 + \Theta_1)}} \tag{3.34}$$

These noise parameters correspond to the noise temperature and correlation of incident and emergent noise wave generators at the input of the RUT. For this set of noise parameters, physical realizability demands that $|\alpha_T| \le 1$ and that T_{AT} and T_{BT} be positive. If $|\alpha_T|$ is slightly greater than unity this can be attributed to measurement errors, and $|\alpha_T|$ can be estimated as one or some value slightly less than one, keeping the argument of α_T constant. This technique could also be adapted to the conventional method.

3.3.1 Implementation of the LRPG Method

The LRPG method of noise parameter measurement can be used with a variety of noise generators, which can be chosen to minimize other experimental difficulties. If the noise generators are chosen to minimize noise calibration errors, then highly mismatched noise generators should be passive so that their noise temperatures can be determined from their physical temperatures, and noise generators requiring noise temperature calibration, *e.g.* noise diodes, should be well matched.

The LRPG method can be implemented using two separate noise sources; a hot-cold noise generator, and a two-port tuner connected to a passive termination. This is the same hardware used in the conventional method. The hot-cold noise generator need only be used in the "hot" state. The tuner need not be lossless; however, the tuner and termination should be at the same physical temperature. If a noise diode is used as the hot-cold noise source it is advantageous to use the noise diode only in its on condition, as cycling the noise diode causes its physical temperature to cycle, thus leading to uncertainty in the "off" noise temperature of the noise diode.

Another implementation is to use a hot-cold noise generator and the multiple impedance load separately. Any termination at port 1 of the multiple impedance load must be at the same temperature as the multiple impedance load, and the hot-cold noise generator need only be used in a state with a noise temperature substantially different from the physical temperature of the multiple impedance load.

A third implementation is to use the multiple impedance load terminated at port 1 with a hot-cold noise generator, the same configuration as used in the modified conventional method. For convenience the hot-cold noise generator should be chosen so that one of its states (probably the cold state) has the same noise temperature as the physical temperature of the multiple impedance load. Then, in the cold state, the noise temperature of the composite noise generator will be the same as the physical temperature of the load. In the hot state, the noise temperature of the composite load is given by equation 3.7, and must be calibrated for each state of the multiple impedance load which is used (at each frequency of interest). For convenience, only one state of the multiple impedance load need be used with the hot-cold noise generator in the hot state, and the state with the lowest reflection coefficient can be chosen.

3.3.2 Systematic Errors of the LRPG Method

The systematic errors in the conventional method due to tuner loss and the change in the reflection coefficient of the hot-cold noise generator do not occur in the LRPG method. The systematic errors which affect the LRPG method are calibration errors, such as errors in noise generator temperature calibration and errors in the reflection coefficient measurements. A common source of these errors is the use of an HP 346 series noise source which has just been powered off. The author has observed that when these devices are on, the case becomes 5K warmer than the surroundings and the noise diode may be hotter still. This will probably make no significant difference in the hot noise temperature; however, when these noise sources are powered off they take about ten minutes to cool to the temperature of the surroundings, causing a change in the cold noise temperature of at least 1.5%. Using the LRPG method this error is easily avoided because it is not necessary to use the hot-cold noise generator in the cold state.

3.3.3 Some Variations of the LRPG Method

A point of some interest is that the real and imaginary parts of the input reflection coefficient of the RUT, which were assumed to be known in the previous solution of equation 3.12, could be treated as two unknown parameters. The advantage obtained would be that, after calibrating the noise generators, no further S-parameter measurements would be required. However, to solve equation 3.12 using a linearized least squares approach, equation 3.12 would have to be manipulated into a linear form having seven terms. Such a linearization has not yet been found. An iterative solution is possible (perhaps some circuit analysis program could be modified to handle a number of simultaneous configurations), but this has not been attempted.

Another possible variation, which has been explored with fair results, can reduce the number of required noise generators. Consider the situation where the DUT and a multiple impedance load are located inside a cryostat, and the receiver is outside the cryostat. The noise parameters and gain of the receiver can be measured using some implementation of the LRPG method. If we now examine equation 3.12 and equation 3.13 as applied to the RUT, we see that G_0 of the RUT is proportional to G_0 of the receiver. This leads to:

$$G_{0RUT} = G_{0REC} \cdot \frac{|s_{21}|^2}{|1 - s_{22}\Gamma_{IN}|} \tag{3.35}$$

where: s_{21} and s_{22} are scattering parameters of the DUT
Γ_{IN} is the input reflection coefficient of the receiver

Thus by making use of the S-parameters of the DUT, one of the unknown parameters of the RUT can be determined. When equation 3.12 is linearized, one linear parameter, Θ_2, is removed and the minimum number of required noise power measurements is reduced to four. By examining equation 3.15 (the linearization of equation 3.12) one can see that there is no longer any requirement for noise generators of different noise temperatures when measuring the RUT. This could be of considerable advantage if the receiver were at room temperature but the DUT were cooled.

3.4 Receiver Noise Calibration

One of the important aspects of noise parameter measurement is accounting for the noise contribution of the receiver. There are three approaches: the receiver noise can be made so small as to be insignificant, it can be removed from each measurement of noise temperature or power, or it can be removed after the noise parameters of the RUT have been found.

The method of minimizing receiver noise cannot be used at all times. If the DUT noise measure is low, a sufficiently low noise amplifier may not be available. If the DUT gain is very high, attenuation may have to be added at the receiver input to prevent the DUT from oscillating, raising the receiver noise temperature. Even if it is low, the receiver noise must be accounted for in at least one measurement to verify that it is truly insignificant.

3.4.1 Minimizing the Receiver Excess Noise Temperature

A number of authors *e.g.* Lange (1967), Larock and Meys (1982), Adamian and Uhlir (1973) and Weinreb (1982) ignore the receiver noise. The receiver noise can be ignored if it is less than some fraction, say 2%, of the noise generated by the DUT. This condition is difficult to evaluate for all Γ_G; however, as an approximation one is tempted to evaluate this condition using the minimum excess noise temperature, the associated gain of the DUT, and the minimum excess noise temperature of the receiver. This can lead to some error as the excess noise temperature of the receiver may be much higher than its minimum value when the DUT input is terminated so that the DUT generates the minimum excess noise. In any case the receiver noise may be negligible for some values of Γ_G and not others.

A better approach, and one not much more difficult to implement, is to perform a trial de-embedding of noise parameters as described later in this section. If the differences between the noise parameters of the RUT and those of the DUT are negligible, the noise contribution of the receiver can be ignored.

3.4.2 Removal of Receiver Noise from each Measurement

When measuring the excess noise temperature of a DUT using the conventional method described in section 3.4.4 above, the noise contribution of the receiver can be removed using equation 3.5 if the available gain of the DUT and the excess noise temperature of the receiver are known. This excess noise temperature of the receiver can be measured with a noise generator having the same reflection coefficient as the output of the DUT, a simple task only if the output of the DUT is well matched. This task is especially difficult if the noise measurements are being made with various reflection coefficients presented to the input of the DUT, *i.e.* when attempting to measure noise parameters. To simplify matters it is desirable to measure the available gain of the DUT using as little extra equipment as possible.

A number of authors, for example Sannino (1980), Martines and Sannino (1982), and Sawayama (1981), have published noise parameter measurement schemes which modify the conventional approach by placing a circulator and a second noise generator, or an isolator, at the receiver input. By manipulating the second noise generator or an attenuator placed between the isolator and receiver, the excess noise temperature of the receiver and the available gain of the DUT can be determined at the same time as the excess noise temperature of the RUT. The excess noise temperature of the DUT is then determined using equation 3.5.

The method proposed by Sawayama requires a well matched and lossless circulator, which is a narrow band device and difficult to make. Numerous variations have been proposed by Sannino and his co-workers Martines, Calandra and Caruso. Those methods, which are exact, assume a perfectly matched isolator. In all cases knowledge of the DUT S-parameters and the S-parameters of the additional components added to the receiver are required (Sannino, 1982).

3.4.2.1 A Method of Keeping the Receiver Noise Temperature Fixed

The method described below has been published (Valk et al., 1987). The noise contribution of the receiver can easily be accounted for if it can be kept constant, even if the generator coefficient is being changed by large amounts. This can be accomplished by placing a lossless tuner between the DUT and the receiver and adjusting it to present the receiver input with a fixed reflection coefficient. The question is, how can the tuner be adjusted in some simple manner to give a repeatable reflection coefficient? One approach is to present a desired generator reflection coefficient to the DUT input and to connect a reflectometer or S-parameter test set to the output of the tuner attached to the DUT output. The tuner can then be set to some constant reflection coefficient value, limited only by the resolution and drift of the reflectometer or S-parameter test set.

The output tuner can be easily adjusted using no additional instrumentation, however, if the configuration in figure 3.3 is used. Consider the transducer gain from noise generator B to the power meter. If the circulator has no reverse circulation, then this gain can be reduced to zero, by adjusting the output tuner so that the reflection coefficient presented to port 1 of the circulator is zero. It is shown in Valk et al.(1987) that if the circulator does not have perfect circulation then the gain can still be nulled by adjusting the output tuner to present a particular reflection coefficient at port 1 of the circulator. The transducer gain from noise generator B to the power meter can be observed by cycling noise generator B and measuring the power ratio with the power meter. Thus, by adjusting the tuner until the power ratio is unity, one ensures that a unique reflection coefficient is presented to port 1 of the circulator, and that the excess noise temperature of the receiver is kept constant. Noise generator B need not be calibrated, nor is it necessary to know either the reflection coefficient required to null the gain or the reflection coefficient of the DUT output.

After performing the tuning step just described, the excess noise temperature of the RUT can be determined, using equation 3.9, from the power ratio measured with only noise generator A cycling. The excess noise temperature of the

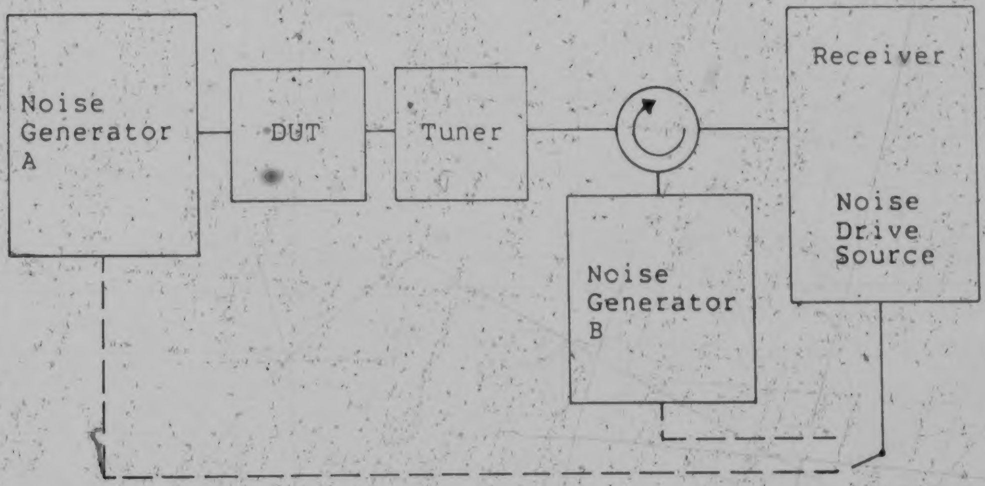
Noise Generator A
DUT
Tuner
Receiver
Noise Drive Source
Noise Generator B

Figure 3.3 The Configuration for a New Method of Keeping the Receiver Excess Noise Temperature Constant

composite receiver (comprising the receiver and circulator) can be measured by following the above procedure with no DUT connected between the noise generator A and the receiver. Because the input reflection coefficient presented to the receiver input has been kept constant G_{TREC} is kept constant. Since $G_{TRUT} = G_{ADUT}\, G_{TREC}$, G_{ADUT} can be determined from:

$$G_{ADUT} = \frac{P_1 - P_2}{P_3 - P_4} \tag{3.36}$$

where: P_1 is the power measured with the DUT inserted and the noise generator in the hot state

P_2 is the power measured with the DUT inserted and the noise generator in the cold state

P_3 is the power measured with the DUT not inserted and the noise generator in the hot state

P_4 is the power measured with the DUT not inserted and the noise generator in the cold state

3.4.3 De-embedding the Receiver after Determining Noise Parameters

Consider the DUT in cascade with the receiver as shown in figure 3.1. It has been shown in chapter 2 (equation 2.74 through equation 2.76) that the noise parameters of two two-ports in cascade can be determined from the noise parameters and small signal parameters of each of the two-ports. These equations are applicable to the configuration of figure 3.1 and can easily be solved to find the noise parameters of the DUT, as follows (Valk et al., 1988, equations 13-15):

$$T_{BT_A} = T_{BT_C} - T_{BT_B}|t_{11_A}|^2 - T_{AT_B}|t_{12_A}|^2 + 2\sqrt{T_{AT_B}T_{BT_B}}\,\mathrm{Re}\{\alpha_{T_B}t_{12_A}t^*_{11_A}\} \qquad (3.37)$$

$$T_{AT_A} = T_{AT_C} - T_{BT_B}|t_{21_A}|^2 - T_{AT_B}|t_{22_A}|^2 + 2\sqrt{T_{AT_B}T_{BT_B}}\,\mathrm{Re}\{\alpha_{T_B}t_{22_A}t^*_{21_A}\} \qquad (3.38)$$

$$\alpha_{T_A} = \frac{1}{\sqrt{T_{AT_A} T_{BT_A}}} \Big[\alpha_{T_C} \sqrt{T_{AT_C} T_{BT_C}} + T_{BT_B} t_{21_A} t^*_{11_A} + T_{AT_B} t_{22_A} t^*_{12_A} - \sqrt{T_{AT_B} T_{BT_B}} \, (t_{21_A} t^*_{12_A} \alpha^*_{T_B} + t_{22_A} t^*_{11_A} \alpha_{T_B}) \Big] \qquad (3.39)$$

where: T_{AT_A}, T_{BT_A} and α_{T_A} are noise parameters of the DUT

t_{11_A}, t_{21_A}, t_{12_A} and t_{22_A} are the transfer scattering parameters of the DUT

T_{AT_B}, T_{BT_B} and α_{T_B} are noise parameters of the receiver

T_{AT_C}, T_{BT_C} and α_{T_C} are noise parameters of the RUT

In order to evaluate these equations, the small signal parameters of the receiver need not be known. Although these equations are too complex to provide insight, they allow one first to measure the noise parameters of the RUT in any convenient manner, then to measure the noise parameters of the receiver separately, and finally, knowing the small signal parameters of the DUT, to find the noise parameters of the DUT.

The noise parameters used for this de-embedding method can be obtained directly from the linearized parameters of the LRPG method using equations 3.32 to 3.34. After equations 3.37 to 3.39 have been applied it will probably be convenient to convert the noise parameters of the DUT to the set T_{MIN}, T_N and Γ_{OPT}.

3.4.4 A Simple Method of Receiver Noise Calibration

While performing cryogenic measurements, the multiple impedance load is inaccessible, and a method is required to estimate the receiver noise parameters quickly and without using the multiple impedance load. Accordingly, a method was devised to estimate the noise parameters of a receiver from a single noise temperature measurement, given that the front end of the receiver is a unilateral, passive element with known S-parameters. When this method is used in the cryogenic noise measurements the unilateral, passive element comprises a bias-tee cascaded with an attenuator and an isolator.

Pospieszalski (1986) discusses such a method; however, he assumes a well matched isolator which may not be preceded by an attenuator. Martines and Sannino (1987) describe another such method; however, their technique is valid only if the ambient temperature is near 290K, and it does not give noise parameters directly. In addition, it is unnecessarily complicated (Pospieszalski, 1988).

The noise behavior of a two-port such as a receiver can be modelled by two partially correlated noise wave generators at the receiver input (see section 2.3.1) If a unilateral device, such as an isolator, is cascaded with the receiver, the reflection coefficient presented to the receiver input is fixed, but not necessarily zero. In this case the excess noise temperature of the receiver is fixed, and the noise behavior of the receiver can be modelled by a single noise wave generator at the receiver input. If the noise parameters and small signal parameters of the unilateral device are known, and the excess noise temperature of the receiver is known, it is possible to find the noise parameters of the composite receiver. However, the noise temperature of the receiver when cascaded with the unilateral device is often imperfectly known, since in general it is unlikely that a calibrated noise generator is available which presents the same reflection coefficient as the unilateral device.

A better estimate of the noise parameters of the composite receiver can be obtained from a noise temperature measurement of the composite receiver. Let the noise behavior of the composite receiver and its components be modelled as shown in figure 3.4. The notation used has been introduced in chapter 2. This situation is equivalent to having T_B of the receiver equal to zero. By using equations 2.74, 2.75 and 2.76, the noise parameters of the composite receiver are easily obtained as the following:

$$T'_{AT} = T_{AT} + |t_{22}|^2 T_U \tag{3.40}$$

$$T'_{BT} = T_{BT} + |t_{12}|^2 T_U \tag{3.41}$$

$$\alpha'_T = \frac{}{\sqrt{T'_{AT} T'_{BT}}} \left(\sqrt{T_{AT} T_{BT}}\, \alpha_T - t_{22} t^*_{12} T_U\right) \tag{3.42}$$

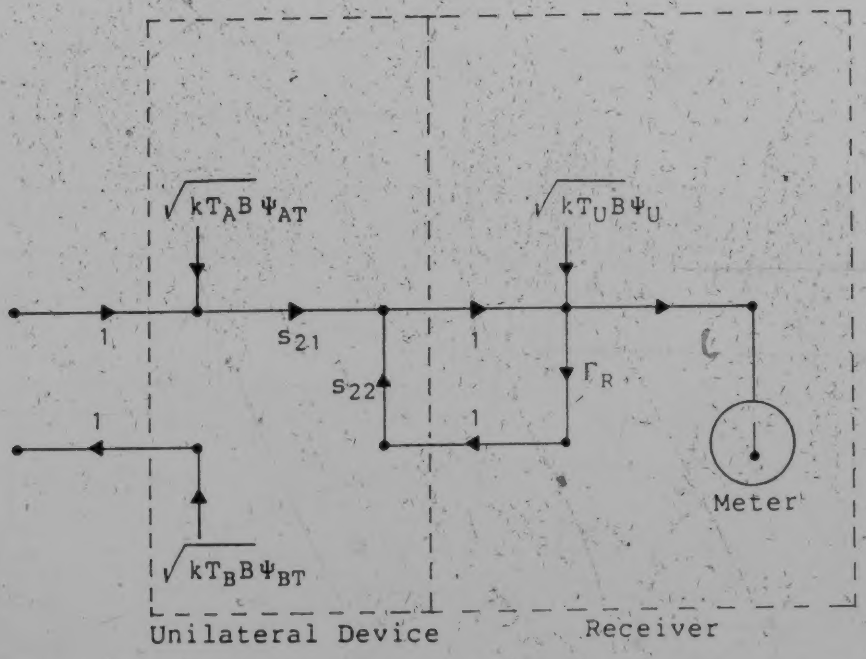
$\sqrt{kT_A B \Psi_{AT}}$
$\sqrt{kT_U B \Psi_U}$
1
s_{21}
1
s_{22}
Γ_R
1
1
Meter
$\sqrt{kT_B B \Psi_{BT}}$
Unilateral Device
Receiver

Figure 3.4 Flow Diagram for a Receiver and Unilateral Device

where: T_{AT}, T_{BT} AND α_T are the noise parameters of the unilateral device

T'_{AT}, T'_{BT} AND α'_T are the noise parameters of the composite receiver

T_U is the noise temperature of a noise wave source shown in figure 3.4

t_{12} and t_{22} are the transfer scattering parameters of the unilateral device.

Since the unilateral device is passive, its noise parameters may be deduced from its S-parameters and its physical temperature. The excess noise temperature of the unilateral device can be obtained from its noise parameters or its available gain. The noise temperature, T_U, of the remaining noise wave generator can be obtained by substituting the results of equation 3.40, equation 3.41 and equation 3.42 into equation 2.49, and then solving for T_U. After some algebra, the following result is obtained:

$$T_U = \frac{(T_{em} - T_{eu})(1 - |\Gamma_G|^2}{|t_{22} - \Gamma_G t_{12}|^2} \qquad (3.43)$$

where: T_{em} is the measured noise temperature of the composite receiver
T_{eu} is the noise temperature of the unilateral device
Γ_G is the reflection coefficient of the noise generator

The value obtained for T_U, and the noise parameters of the unilateral device can now be substituted back into equation 3.40, equation 3.41 and equation 3.42 to obtain the noise parameters of the composite receiver. This method was used to calibrate the noise measurement receiver for all the cryogenic noise measurements.

3.5 Analysis of Least Squares Fitting Uncertainties

A number of the methods described in this chapter use least squares fitting to estimate noise parameters. It is not easy to determine the uncertainty of the estimated noise parameters given the measurement uncertainties. This section does not give a definitive solution to that problem, but will perhaps give some insight.

Consider the system described by the linear equation below:

$$y = x_1\theta_1 + x_2\theta_2 + \ldots + x_n\theta_n \tag{3.44}$$

where: θ_i are parameters of the system
x_i are independent variables
y is the dependent variable
n is the number of parameters.

If a constant term is required, one of the independent variables may be set to one. Suppose that one is trying to estimate the parameters from m observations of the independent variables and the dependent variable. In the absence of measurement errors, the observations are related to the unknown parameters by:

$$\underline{y} = \underline{\underline{X}}\,\underline{\theta} \tag{3.45}$$

where: $\underline{y}$ is the m-vector of observations of the dependent variable
$\underline{\theta}$ is the n-vector of parameters
$\underline{\underline{X}}$ is the m×n matrix of observations of the independent variables
m is the number of observations.

In our experiments, as in many others, there are both random and systematic errors in the measurements of the dependent and independent variables, resulting in uncertainty of the estimated parameters. The purpose of this analysis is to develop techniques to estimate this uncertainty, and to develop estimation techniques which reduce it. Roman letters denote known variables, and Greek letters denote unknown variables. The true (but unknown) value of a variable 'a' is $\hat{a}$ and the measured or estimated value is $\tilde{a}$. Underlined upper case letters are matrices; underlined lower case letters are column vectors.

Let the measurement errors in the dependent variable be $d\underline{y} = \tilde{\underline{y}} - \hat{\underline{y}}$ and the measurement errors in the independent variables be $d\underline{X} = \tilde{\underline{X}} - \hat{\underline{X}}$. By substituting these relationships into equation 3.45, one obtains equation 3.46 below:

$$\tilde{\underline{y}} = \tilde{\underline{X}}\hat{\underline{\theta}} - d\underline{X}\hat{\underline{\theta}} + d\underline{y} = \tilde{\underline{X}}\hat{\underline{\theta}} + \hat{\underline{\epsilon}} \qquad (3.46)$$

where: $\hat{\underline{\epsilon}}$ is the true total error.

Given only $\tilde{\underline{X}}$ and $\tilde{\underline{y}}$, it is generally not possible to estimate both $d\underline{X}$ and $d\underline{y}$, but only the total error. An estimated set of parameters, $\tilde{\underline{\theta}}$, implies a corresponding estimated error:

$$\tilde{\underline{\epsilon}} = \tilde{\underline{y}} - \tilde{\underline{X}}\tilde{\underline{\theta}} \qquad (3.47)$$

The often unsupported premise of least squares fitting is that the best solution to equation 3.46 is the linear function of $\tilde{\underline{y}}$ which minimizes the sum of the squared errors of fit, often expressed as:

$$\chi^2 = \tilde{\epsilon}^T\tilde{\underline{\epsilon}} = \|\tilde{\underline{\epsilon}}\|^2 \qquad (3.48)$$

where: $\|\tilde{\underline{\epsilon}}\|$ is the Euclidian vector norm of $\tilde{\underline{\epsilon}}$.

3.5.1 The Classical Estimate

The classical error analysis assumes that there are no errors in the independent variables, that the errors in the dependent variable are random, that $m \geq n$ and that the rank of $\underline{X}$ is n. Under these conditions, the estimate which minimizes

χ^2 is:

$$\underline{\tilde{\theta}} = (\underline{\tilde{X}}^T\underline{\tilde{X}})^{-1}\underline{\tilde{X}}^T\underline{\tilde{y}} \qquad (3.49)$$

This estimate has zero bias, $E\{\tilde{\theta}-\hat{\theta}\}$, if there are no errors in the independent variable. If, in addition, the errors in the dependent variable are uncorrelated and have a fixed variance, the estimate of equation 3,49 has minimum variance, $E\{(\tilde{\theta}-E\{\tilde{\theta}\})^2\}$. If all these assumptions hold, the elements of the variance-covariance matrix, $\underline{\Sigma} = (\underline{\tilde{X}}^T\underline{\tilde{X}})^{-1}$, can be interpreted as:

$$\Sigma_{ij} = \frac{1}{\sigma_y^2} E\{(\tilde{\theta}_i \; E\{\tilde{\theta}_i\})(\tilde{\theta}_j \; E\{\tilde{\theta}_j\})\} \qquad (3.50)$$

where: σ_y^2 is the variance of the errors in the dependent variable.

Corrections can be made if the errors in the dependent variable are random, but correlated or not of fixed variance.

This error analysis has a number of short-comings. The estimate of equation 3.49 fails, and the variance-covariance matrix becomes nonexistent, if $\underline{\tilde{X}}^T\underline{\tilde{X}}$ is singular. As a result, it is difficult to investigate the behavior of the estimated parameters as $\underline{\tilde{X}}^T\underline{\tilde{X}}$ approaches singularity. The next section will show that the near singularity of $\underline{\tilde{X}}^T\underline{\tilde{X}}$ is an important factor in the uncertainty of the estimated parameters. It should be noted that the variance-covariance matrix gives the statistics of the estimated parameters only if there are no errors at all in the independent variable and no systematic errors in the dependent variable. Given such errors as have just been excluded, one is left with no information regarding the uncertainty of the estimated parameters.

3.5.2 Error Analysis Using Norms

Penrose(1955) has shown, independent of the rank and shape of $\underline{X}$, that the linear solution to equation 3.46 which has the smallest norm and which minimizes $\|\tilde{\underline{\varepsilon}}\|$ is:

$$\tilde{\underline{\theta}} = \tilde{\underline{X}}^I \tilde{\underline{y}} \qquad (3.51)$$

where: $\underline{X}^I$ denotes the generalized inverse of $\underline{X}$.

The generalized inverse of $\underline{X}$, which exhibits a set of properties independent of the shape and rank of $\underline{X}$, is discussed in detail in a subsequent section. In the case where m≥n and $\tilde{\underline{X}}^T\tilde{\underline{X}}$ is not singular, the generalized inverse is given by:

$$\tilde{\underline{X}}^I = (\tilde{\underline{X}}^T\tilde{\underline{X}})^{-1}\tilde{\underline{X}}^T. \qquad (3.52)$$

Ben-Israel(1966) has derived an upper limit for the error of estimate, $d\underline{\theta} = \tilde{\underline{\theta}} - \hat{\underline{\theta}}$, in terms of the generalized inverse. From Ben-Israel's results the author has derived a limit to $\|D\underline{\theta}\|$ which is tighter than Ben-Israel's limit and is in a more convenient form. First, some definitions are required. The Euclidian norm of a vector $\underline{a}$ is $\|\underline{a}\|$. The spectral norm of a matrix $\underline{A}$ is $\|\underline{A}\|_s$, defined by:

$$\|\underline{A}\|_s = \max_{\underline{a}} \frac{\|\underline{A}\underline{a}\|}{\|\underline{a}\|} \qquad (3.53)$$

Subsequent sections discuss the estimation and the exact evaluation of the spectral norm. The error of estimate is related to the errors of measurement by equation 3.54, below:

$$\hat{\underline{\theta}} + d\underline{\theta} = (\hat{\underline{X}} + d\underline{X})^I(\hat{\underline{y}} + d\underline{y}) \qquad (3.54)$$

The limit for $\|d\underline{\theta}\|$ which was derived by the author is:

$$\frac{\|d\underline{\theta}\|}{\|\tilde{\underline{\theta}}\|} \le \frac{\kappa(\tilde{\underline{X}})}{1-\kappa(\tilde{\underline{X}})\dfrac{\|d\underline{X}\|_s}{\|\tilde{\underline{X}}\|_s}} \left[\frac{\|d\underline{X}\|_s}{\|\tilde{\underline{X}}\|_s} + \frac{\|d\underline{y}\|}{\|\tilde{\underline{y}}-\tilde{\underline{\epsilon}}\|}\right] \qquad (3.55)$$

$$\text{Given: } \frac{\|d\underline{X}\|_s}{\|\tilde{\underline{X}}\|_s} \le \frac{1}{\kappa(\tilde{\underline{X}})};$$

where: $\kappa(\tilde{\underline{X}}) = \|\tilde{\underline{X}}\|_s\|\tilde{\underline{X}}^I\|_s$.

With direct substitution of $\kappa(\hat{\underline{X}})$ the inequality derived by Ben-Israel leads to a limit proportional to $\kappa^2(\hat{\underline{X}})$. $\kappa(\underline{X})$ is known as the condition number of $\underline{X}$. $\kappa(\underline{X})$ has a minimum value of 1 for a matrix with orthogonal rows, $\underline{X}\underline{X}^T = \underline{I}$, or orthogonal columns, $\underline{X}^T\underline{X} = \underline{I}$, and approaches positive infinity as $\underline{X}^T\underline{X}$ approaches singularity.

Equation 3.55 holds for matrices, $\underline{X}$, of any rank or shape, since it is derived from equation 3.51 which has no restrictions on the rank or shape of $\underline{X}$. The condition given in equation 3.55 is equivalent to: $\|\tilde{\underline{X}}^I\|_s\|d\underline{X}\|_s \le 1$. This can be interpreted as a requirement that the magnitude of the uncertainty in $\underline{X}$ must be less than the "distance" to the "nearest" matrix of lesser rank. In other words, the uncertainty in the measurements of the independent variables must not be so great that the rank of the matrix $\underline{X}$ is indeterminate.

The limit given in equation 3.55 can be used to determine the maximum error in the estimated parameters given the (estimated) maximum error in the dependent and independent variables. This limit is the maximum error of estimate for all errors in the dependent variable of magnitude $\|d\underline{y}\|$ and all errors in the independent variables of magnitude $\|d\underline{X}\|_S$. Thus, row and column scaling should be used so that the estimated maximum error in each measurement of the dependent variable is the same, and so that the estimated maximum error in each measurement of each of the independent variables is the same. In the absence of such scaling, the uncertainty of the estimated parameters may be overestimated.

3.5.2.1 Estimation of the Spectral Norm

The spectral norm can be estimated using the Euclidian matrix norm:

$$\|\underline{X}\|_E = \sqrt{\sum_{ij} x^2} \tag{3.56}$$

Anticipating a result below (equation 3.64), the spectral norm is bracketed by the Euclidian norm as follows:

$$\frac{\|\underline{X}\|_E}{\sqrt{k}} \leq \|\underline{X}\|_S \leq \|\underline{X}\|_E \tag{3.57}$$

where: m is the number of rows of $\underline{X}$
n is the number of columns of $\underline{X}$
k = min(m,n)

Thus, the condition number is bracketed by the following estimates:

$$\frac{\|\underline{X}\|_E \|\underline{X}^I\|_E}{k} \leq \kappa(\underline{X}) \leq \|\underline{X}\|_E \|\underline{X}^I\|_E \tag{3.58}$$

If $\underline{X}$ is of full rank (see below), $\underline{X}^I$ can be obtained from equation 3.52.

3.5.2.2 The Singular Value Decomposition

The exact value of the spectral norm can be determined from the singular value decomposition of the matrix. The singular value decomposition can also be used to calculate the generalized inverse of a matrix. The singular value decomposition applies to any real or complex matrix of any shape; however, only real matrices will be considered here. It can be shown (Ben Isreal, 1966) that any m×n matrix, $\underline{X}_{mn}$, can be expressed as the product:

$$\underline{X}_{mn} = \underline{U}_{mm} \underline{S}_{mn} \underline{V}_{nn}^T \tag{3.59}$$

where: $\underline{U}$ and $\underline{V}$ are real and orthogonal ($\underline{U}\underline{U}^T = \underline{I}$ and $\underline{V}\underline{V}^T = \underline{I}$)
the s_i are real and nonnegative

and the matrix $\underline{S}$ can be written as:

$$\underline{S}=\begin{bmatrix} s_1 & & & \\ & s_2 & & \\ & & \ddots & \\ & & & s_n \\ & & 0 & \end{bmatrix} \qquad m\geq n \qquad (3.60)$$

$$\underline{S}=\begin{bmatrix} s_1 & & & & \\ & s_2 & & & \\ & & \ddots & & 0 \\ & & & s_m & \end{bmatrix} \qquad m\leq n. \qquad (3.61)$$

This is known as the singular value decomposition of $\underline{X}$. The elements, s_i, are the singular values of $\underline{X}$ and, for convenience, they are usually arranged in decreasing order. A change in the order of the singular values implies a corresponding change in the order of the columns of $\underline{U}$ and $\underline{V}$. The singular values are the positive square roots of the eigenvalues of $\underline{X}^T\underline{X}$. The columns of $\underline{U}$ are eigenvectors of $\underline{X}\underline{X}^T$, and the columns of $\underline{V}$ are eigenvectors of $\underline{X}^T\underline{X}$. It has been shown that the eigenvector-eigenvalue decomposition of $\underline{X}^T\underline{X}$ becomes numerically unstable as $\underline{X}$ approaches singularity. Better algorithms are offered by IMSL and LINPACK subroutines, which can be called from APL with some difficulty.

The number of nonzero singular values is the rank of the matrix. (The rank, r, of a matrix is the number of linearly independent rows or columns.) A matrix is said to be of full rank if $r=\min(m,n)$ and is said to be rank deficient if $r<\min(m,n)$. A square matrix which is rank deficient is singular.

The singular values of a matrix have a number of useful interpretations. The largest singular value, s_1, is the spectral norm of the matrix. The reciprocal of the smallest nonzero singular value is the spectral norm of the generalized inverse of the matrix (this is shown in section 3.5.2.3 below). Thus the condition number of a matrix is:

$$\kappa(\underline{X}) = \frac{s_1}{s_r} \qquad (3.62)$$

where: s_r is the smallest nonzero singular value
r is the rank of the matrix

The smallest singular value is the "distance" to the nearest matrix of smaller rank, if the distance between two matrices $\underline{A}$ and $\underline{B}$ is defined as $\|\underline{A} - \underline{B}\|_S$ or $\|\underline{A} - \underline{B}\|_E$. Two other useful properties are:

$$\mathrm{Det}(\underline{X}) = \prod_i s_i \qquad (3.63)$$

$$\|\underline{X}\|_E = \sqrt{\sum_i s_i^2} \qquad (3.64)$$

This last equation relates the Euclidian matrix norm and the spectral norm. If one considers the limiting cases where all the singular values but one are zero and where all the singular values are equal, equation 3.64 leads to equation 3.57.

3.5.2.3 The Generalized Inverse

The generalized inverse was first described by E.H. Moore(1920) and later by R. Penrose(1954,1955). The properties of this inverse are given below. This inverse, also known as the pseudoinverse or Moore-Penrose inverse, is a generalization of the ordinary inverse with special relevance to least squares fitting problems. Penrose (1955) has shown that the general solution to equation 3.46 is:

$$\underline{\tilde{\theta}} = \underline{\tilde{X}}^{I}\underline{\tilde{y}} + [\underline{I} - \underline{\tilde{X}}^{I}\underline{\hat{X}}]\underline{\alpha} \qquad (3.65)$$

where: $\underline{\tilde{X}}^{I}$ denotes the generalized inverse of $\underline{\hat{X}}$
$\underline{\alpha}$ is an arbitrary vector which may be determined
by some other experiment.

If $\underline{X}$ is of full rank, and m≥n, the term $\underline{I} - \underline{X}^{I}\underline{X}$ is zero, and equation 3.65 reduces to equation 3.51. The generalized inverse exhibits the following properties:

$$\underline{X}\underline{X}^{I}\underline{X} = \underline{X} \qquad (3.66)$$

$$\underline{X}^{I}\underline{X}\underline{X}^{I} = \underline{X}^{I} \qquad (3.67)$$

$$\underline{X}^{I}\underline{X} = [\underline{X}^{I}\underline{X}]^{T} \qquad (3.68)$$

$$\underline{X}\underline{X}^{I} = [\underline{X}\underline{X}^{I}]^{T} \qquad (3.69)$$

If $\underline{X}$ is of full rank, the generalized inverse is given by:

$$\begin{aligned} \underline{X}^{I} &= \underline{X}^{T}[\underline{X}\underline{X}^{T}]^{-1} && m\le n \qquad (3.70) \\ &= \underline{X}^{-1} && m=n \\ &= [\underline{X}^{T}\underline{X}]^{-1}\underline{X}^{T} && m\ge n \end{aligned}$$

By replacing $\underline{X}$ by its singular value decomposition in equation 3.70, one obtains:

$$\underline{X}^{I} = \underline{V}\underline{S}^{I}\underline{U}^{T} \qquad (3.71)$$

where:

$$\underline{S}^I = \begin{bmatrix} s_1^{-1} & & & \\ & s_2^{-1} & & \\ & & \ddots & \\ & & & s_n^{-1} \\ & & \underline{0} & \end{bmatrix} \qquad m \geq n \qquad (3.72)$$

$$\underline{S}^I = \begin{bmatrix} s_1^{-1} & & & & \\ & s_2^{-1} & & & \\ & & \ddots & & \underline{0} \\ & & & s_m^{-1} & \end{bmatrix} \qquad m \leq n. \qquad (3.73)$$

This relationship holds even if $\underline{X}$ is rank deficient, with the modification:

$$\underline{S}^I_{nm} = \begin{bmatrix} s_1^{-1} & & & & \\ & s_2^{-1} & & & \\ & & \ddots & & \underline{0} \\ & & & s_r^{-1} & \\ & & \underline{0} & & \underline{0} \end{bmatrix} \qquad (3.74)$$

where: r is the rank of $\tilde{\underline{X}}$.

From this last equation it is immediately obvious that the spectral norm of the generalized inverse of $\underline{X}$ is the reciprocal of the smallest nonzero singular value of $\underline{X}$.

3.5.3 Estimation Using the Singular Value Decomposition

The following analysis develops better insight into the case when $\underline{X}$ is rank deficient and leads to a method whereby the estimated parameters can be made less sensitive to measurement errors. The objective is to estimate $\underline{\theta}$ given $\tilde{\underline{X}}$

and $\tilde{\underline{y}}$. We assume that $m \geq n$, that there are errors in the dependent and independent variables, and that r, the rank of $\tilde{\underline{X}}$, is less than or equal to n. The parameters are estimated by minimising $\chi = \|\tilde{\underline{\epsilon}}\|$ which can be expressed as:

$$\chi = \|\tilde{\underline{\epsilon}}\| = \|\tilde{\underline{y}} - \tilde{\underline{X}}\tilde{\underline{\theta}}\| \qquad (3.75)$$

It can be shown that $\|\underline{r}\| = \|\underline{U}\underline{r}\|$ if $\underline{U}$ is orthogonal ($\underline{U}\underline{U}^T = \underline{I}$ and $\underline{U}^T\underline{U} = \underline{I}$). Applying these properties to equation 3.75, and replacing $\tilde{\underline{X}}$ by its singular value decomposition, one obtains:

$$\chi = \|\underline{U}^T\tilde{\underline{\epsilon}}\| = \|\underline{U}^T[\tilde{\underline{y}} - \underline{U}\underline{S}\underline{V}^T\tilde{\underline{\theta}}]\| = \|\underline{U}^T\tilde{\underline{y}} - \underline{S}\underline{V}^T\tilde{\underline{\theta}}\| \qquad (3.76)$$

where: $\tilde{\underline{X}} = \underline{U}\underline{S}\underline{V}^T$.

We can now collect terms to obtain the following:

$$\chi = \|\underline{b} - \underline{S}\underline{\alpha}\| = \left\| \begin{bmatrix} b_1 \\ b_2 \\ \vdots \\ b_n \\ b_{n+1} \\ \vdots \\ b_m \end{bmatrix} - \begin{bmatrix} s_1\alpha_1 \\ s_2\alpha_2 \\ \vdots \\ s_n\alpha_n \\ 0 \\ \vdots \\ 0 \end{bmatrix} \right\| \qquad (3.77)$$

where: $\underline{b} = \underline{U}^T\tilde{\underline{y}}$
$\underline{\alpha} = \underline{V}^T\tilde{\underline{\theta}}$

Note that $\underline{\alpha}$ is unknown. Given an estimate for $\underline{\alpha}$, $\tilde{\underline{\theta}}$ can be obtained from:

$$\tilde{\underline{\theta}} = \underline{V}\tilde{\underline{\alpha}} \qquad (3.78)$$

The analysis now splits into three parts. The full rank case will be discussed first, followed by the rank deficient case, followed by the nearly rank deficient case.

3.5.3.1 The Full Rank Case

If $\underline{X}$ is of full rank, all the singular values are nonzero and the solution for minimum χ is:

$$\tilde{\alpha}_i = \frac{b_i}{s_i} \qquad 1 \leq i \leq n \tag{3.79}$$

The estimated parameters are:

$$\underline{\tilde{\theta}} = \underline{V}\underline{\tilde{\alpha}} = \underline{V} \begin{bmatrix} \frac{b_1}{s_1} \\ \frac{b_2}{s_2} \\ \vdots \\ \frac{b_n}{s_n} \end{bmatrix} \tag{3.80}$$

Note that $\underline{\tilde{\alpha}} = \underline{S}^I \underline{b}$, so that equation 3.80 can be written as:

$$\underline{\tilde{\theta}} = \underline{V}\underline{S}^I \underline{U}^T \underline{\tilde{y}} = \underline{\tilde{X}}^I \underline{\tilde{y}} \tag{3.81}$$

which is the usual least squares solution, in which χ^2 is given by:

$$\chi^2 = \sum_{i=n+1}^{m} b_i^2 \tag{3.82}$$

3.5.3.2 The Rank Deficient Case

If $\underline{X}$ is of rank $r<n$ the last $n-r$ singular values will be zero. Referring to equation 3.77, the solution for

minimum x is:

$$\tilde{\alpha}_i = \frac{b_i}{s_i} \qquad 1 \le i \le r \tag{3.83}$$

The last n-r components of $\tilde{\underline{\alpha}}$ are arbitrary and can perhaps be obtained by some other method. The estimated parameters are obtained by applying equation 3.78 with the result:

$$\tilde{\underline{\theta}} = \underline{V}\tilde{\underline{\alpha}} = \underline{V} \begin{bmatrix} \frac{b_1}{s_1} \\ \frac{b_2}{s_2} \\ \vdots \\ \frac{b_r}{s_r} \\ \tilde{\alpha}_{r+1} \\ \vdots \\ \tilde{\alpha}_n \end{bmatrix} = \underline{V} \begin{bmatrix} \frac{b_1}{s_1} \\ \frac{b_2}{s_2} \\ \vdots \\ \frac{b_n}{s_n} \\ 0 \\ \vdots \\ 0 \end{bmatrix} + \underline{V} \begin{bmatrix} 0 \\ \\ \vdots \\ 0 \\ \tilde{\alpha}_{r+1} \\ \vdots \\ \tilde{\alpha}_n \end{bmatrix} \tag{3.84}$$

This result has a fixed part and an arbitrary part, not unlike the natural and forced solutions to a differential equation. The fixed part of $\tilde{\underline{\alpha}}$ can be written as $\underline{S}^I b$, so that equation 3.84 can be manipulated into the following form:

$$\tilde{\underline{\theta}} = \tilde{\underline{X}}^I \tilde{\underline{y}} + \tilde{\alpha}_{r+1}\underline{v}_{r+1} + \tilde{\alpha}_{r+2}\underline{v}_{r+2} + \ldots + \tilde{\alpha}_n\underline{v}_n \tag{3.85}$$

where: $\underline{v}_i$ is the i^{th} column of $\underline{V}$.

The sensitivity of the fixed part of the estimated parameters is given by equation 3.55, as for the full rank case. Note that the columns of $\underline{V}$ will indicate the linear dependencies in $\tilde{X}$. χ^2 for the rank deficient case is:

$$\chi^2 = \sum_{i=r+1}^{m} b_i^2 \tag{3.86}$$

3.5.3.3 The Nearly Rank Deficient Case

It is rare that a matrix of observations, such as $\underline{X}$ is exactly rank deficient. For example, consider the case where the true value of an m×n matrix, m>n, of m observations of n variables has a rank of n-1. This implies that one column is an exact combination of the other n-1 columns. The columns are all m-element vectors and they span a subspace with n-1 dimensions. If a change orthogonal to the subspace, however small, occurs in any of the columns, then the matrix is no longer exactly rank deficient, but will have a large condition number. Put another way, if the matrix of observations is to be rank deficient, there can be no fluctuation orthogonal to the subspace. Thus, if all the variables are measured independently, this matrix of independent variables is likely not to be of full rank and is likely to have a very large condition number.

Suppose that the last q singular values of $\underline{X}$ are unacceptably small compared to the largest singular value. One hopes that q is one or at worst two. Because the last q singular values are the smallest, the corresponding elements of $\tilde{\underline{\alpha}}$ are most sensitive to measurements errors. Referring to equation 3.77, one can see that if these elements of $\tilde{\alpha}$ are constrained to be some arbitrary value, the solution for minimum x under these constraints is given by equation 3.79 for the remainder of the elements. Thus we leave the last q values of $\tilde{\underline{\alpha}}$ to be determined by other experiments and choose the first n-q values as before. The estimated parameters are now given by:

$$\tilde{\underline{\theta}} = \underline{V}\tilde{\underline{\alpha}} = \underline{V}\begin{bmatrix} \frac{b_1}{s_1} \\ \frac{b_2}{s_2} \\ \vdots \\ \frac{b_{n-q}}{s_{n-q}} \\ \tilde{\alpha}_{n-q+1} \\ \vdots \\ \tilde{\alpha}_n \end{bmatrix} = \underline{V}\begin{bmatrix} \frac{b_1}{s_1} \\ \frac{b_2}{s_2} \\ \vdots \\ \frac{b_{n-q}}{s_{n-q}} \\ 0 \\ \vdots \\ 0 \end{bmatrix} + \underline{V}\begin{bmatrix} 0 \\ \\ \vdots \\ 0 \\ \alpha_{n-q+1} \\ \vdots \\ \tilde{\alpha}_n \end{bmatrix} \qquad (3.87)$$

The estimated parameters consist of a fixed part and an arbitrary part. In effect, the fixed part of the solution is obtained by setting the q smallest singular values of $\underline{X}$ to zero. The fixed part of $\tilde{\underline{\alpha}}$ can be written as $\tilde{\underline{S}}^I\underline{b}$, where $\tilde{\underline{S}}$ is $\underline{S}$ with the q smallest singular values set to zero. Using this notation, equation 3.87 can also be expressed as:

$$\tilde{\underline{\theta}} = \tilde{\underline{X}}^I\underline{y} + \tilde{\alpha}_{1+n-q}\underline{v}_{1+n-q} + \tilde{\alpha}_{2+n-q}\underline{v}_{2+n-q} \cdots + \ldots + \tilde{\alpha}_n\underline{v}_n \qquad (3.88)$$

where: $\tilde{\underline{X}} = \underline{U}\tilde{\underline{S}}\underline{V}^T$.

The sensitivity of the fixed part of the estimated parameters to measurement errors is given by equation 3.55, as before. The condition number is now smaller:

$$\kappa(\underline{X}) = \frac{s_1}{s_{n-q}} \tag{3.89}$$

Thus, the sensitivity to measurement errors has been reduced. The modified matrix, $\underline{\tilde{X}}$, is the nearest matrix of rank n-q to $\underline{X}$. Therefore, the change in $\underline{X}$ is the minimum possible to achieve the desired sensitivity. χ^2 is given by:

$$\chi^2 = \sum_{i=n-q+1}^{n} (b_i - s_i \tilde{\alpha}_i)^2 + \sum_{i=n+1}^{m} b_i^2 \tag{3.90}$$

Because the last q singular values are small, χ is least sensitive to variations in the corresponding elements of $\underline{\alpha}$. If these elements of $\underline{\alpha}$ are later chosen near to the value given by equation 3.79 then χ will be approximately minimum.

3.5.4 Application to Noise Parameter Estimation

Although the preceding analysis was the best which could be obtained, it is not easily applied to noise parameter estimation because the noise parameters are related to the coefficients of the linear equations in a very nonlinear manner. The uncertainties in the noise parameters will be related to the uncertainties in the linear coefficients by the Jacobian of the transformation, which has not been found. Noise parameter estimation by rank reduced least squares estimation was tried by the author. However, the estimated noise parameters were no more accurate than the the results obtained using the ordinary least squares fitting algorithm, possibly because the effect of the transformation was ignored, or possibly due to the lack of accurate experimental data. In any case, the condition number does express the uncertainty of the least squares fit very conveniently, and is a useful tool for the experimental design of noise measurements. As far as is known by the author, this approach to noise parameter estimation has never been tried before.

Chapter 4

Experimental Apparatus

This project necessitated the construction and modification of a number of pieces of experimental apparatus. Particularly, the noise figure meter was modified to improve its frequency stability and frequency offset. A test fixture was constructed, and calibration standards were made for this fixture to enable S-parameter calibration to be made to the transistor socket. In order to more accurately and conveniently measure the noise of transistors at cryogenic temperatures two microwave loads were built, each load having a number of separate and distinct states, with each state having a different and fixed reflection coefficient. These loads will be referred to as multiple impedance loads or MIL's. One of these loads was built using PIN diodes; it will be referred to as the 'PIN diode multiple impedance load'. The other load was built using coaxial relays; it will be referred to as the 'relay multiple impedance load'. This chapter discusses the design, construction and performance of these items.

4.1 The PIN Diode Multiple Impedance Load

A multiple impedance load of this type for room-temperature use was first described by Leake (1982). The reflection coefficient of the load described here can be controlled by small D.C. voltages and currents, thus allowing it to be placed inside the cryogenic enclosure directly connected to the transistor fixture, and controlled from outside the enclosure. In our implementation, an additional coupler is included, allowing extra noise to be coupled into the load.

4.1.1 Theory of Operation

The operation of the PIN diode multiple impedance load depends on "switchable" terminations, which are terminations that can be switched between two states, these states having reflection coefficients which are (nearly) of magnitude one and opposite phase. These terminations are interconnected by directional couplers so as to form a one-port which can assume a reflection coefficient which is one of a number of values evenly distributed over a central portion of the reflection coefficient plane.

The switchable terminations are realized using a PIN diode connected in shunt to a transmission line. A PIN diode has an almost intrinsic region between heavily doped P and N type regions (White, 1981). A PIN diode is ideal for our purpose because the circuit characteristics are not strongly dependent on bias conditions, and rectification does not occur at microwave frequencies. When the PIN diode is reverse biased, the equivalent circuit at microwave frequencies is that shown in figure 4.1-a with C_J typically less than 3 pF and R_R as much as 5000 Ohms. When the PIN diode is forward biased the equivalent circuit at microwave frequencies is given by figure 4.1-b with R_F typically less than 1 Ohm (White, 1981, p80).

If we now consider the PIN diode connected in shunt, we see that the reflection coefficient in the reverse biased state falls in the lower half of the reflection coefficient plane approximating an open circuit, and the reflection coefficient in the forward biased state falls in the upper half plane approximating a short circuit. If R_R is sufficiently large the diode can be connected in series with a small inductance, resonant with C_J, so as to cause the reflection coefficient in the forward and reverse biased states to approach -1 and +1 respectively. The series inductance can be thought of as a mismatching element because it maximizes the magnitude of the two reflection coefficients and the angular difference between them.

The switchable terminations are interconnected using quarter wave directional couplers. Such a coupler is a lossless reciprocal 4-port and has the following scattering matrix (Beatty, 1973, p77):

$$\underset{\sim}{S} = \begin{bmatrix} 0 & j\sqrt{1-c^2} & 0 & c \\ j\sqrt{1-c^2} & 0 & c & 0 \\ 0 & c & 0 & j\sqrt{1-c^2} \\ c & 0 & j\sqrt{1-c^2} & 0 \end{bmatrix} \qquad (4.1)$$

where c is the voltage coupling coefficient of the coupler. If port three of the coupler is connected to a nonreflective termination, and ports two and four are connected to terminations having reflection coefficients of Γ_2 and Γ_4

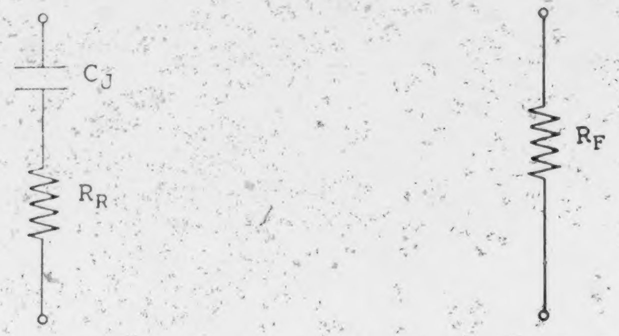

a) Reverse Biased b) Forward Biased

Figure 4.1 Equivalent Circuit of a PIN Diode

respectively, then the reflection coefficient of the network (observed at port one) will be given by:

$$\Gamma_1 = c^2 \Gamma_4 - (1-c^2) \Gamma_2 \tag{4.2}$$

A basic building block (called an in-phase network; see figure 4.2) of the multiple impedance load is a quarter wave directional coupler with port three terminated in a nonreflecting load and ports two and four terminated with a matched pair of the switchable terminations discussed earlier. Let the switchable terminations have reflection coefficients of $+\beta e^{j\alpha}$ or $-\beta e^{j\alpha}$, where β is just less than 1 and α is some arbitrary angle. Then Γ_1 can take on the values:

$$\Gamma_1 = \pm\beta e^{j\alpha} \ , \ \pm(2c^2-1)\beta e^{j\alpha} \tag{4.3}$$

These values of Γ_1 lie on a straight line passing through the origin of the Γ plane, rotated an angle α from the real

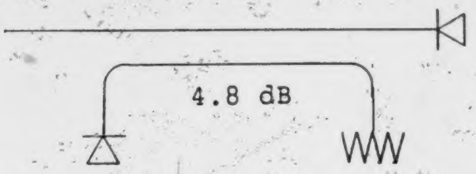

Figure 4.2 Block Diagram of an In-Phase Network

axis. The coupling constant, c, is chosen to be $\frac{1}{\sqrt{3}}$, so that the possible values of Γ_1 are equally spaced on this line. These reflection coefficients are:

$$\Gamma = \pm\beta e^{j\alpha}, \ \pm\frac{1}{3}\beta e^{j\alpha} \tag{4.4}$$

The PIN diode multiple impedance load consists of two in-phase networks connected to a 3 dB coupler as shown in figure 4.4. This coupler has a coupling coefficient of $\frac{1}{\sqrt{2}}$. Substituting into equation 4.2, the reflection coefficient at port one will be given by:

$$\Gamma_1 = \frac{1}{2}\Gamma_4 - \frac{1}{2}\Gamma_2 \tag{4.5}$$

The reflection coefficients presented to ports two and four of the 3 dB coupler can each assume the values given in equation 4.4. The reflection coefficient at port one of the 3 dB coupler (Γ_1), obtained by substituting equation 4.4 into equation 4.5, can take on any one of the following values:

$$\Gamma = \frac{\beta}{2}e^{j\alpha}\begin{bmatrix} 1+j & \frac{1}{3}+j & -\frac{1}{3}+j & -1+j \\ 1+j\frac{1}{3} & \frac{1}{3}+j\frac{1}{3} & -\frac{1}{3}+j\frac{1}{3} & -1+j\frac{1}{3} \\ 1-j\frac{1}{3} & \frac{1}{3}-j\frac{1}{3} & -\frac{1}{3}-j\frac{1}{3} & -1-j\frac{1}{3} \\ 1-j & \frac{1}{3}-j & -\frac{1}{3}-j & -1-j \end{bmatrix} \tag{4.6}$$

These points are plotted in figure 4.3, assuming that $\alpha=0°$ and $\beta=1$. Note that the points are evenly distributed over a square on the Γ plane, centered at the origin and inscribed within the $\Gamma = \frac{1}{\sqrt{2}}$ circle.

It is desirable to be able to inject additional noise into the PIN diode multiple impedance load so that its noise temperature changes. This is made possible by adding a 10 dB coupler ($c = \frac{1}{\sqrt{10}}$) to the load. The addition of this coupler allows the load to be considered as a lossy two-port. The simplified block diagram of the PIN diode multiple impedance load, not including biasing elements is shown in figure 4.4.

4.1.2 Design and Construction

The PIN diode multiple impedance load was designed to operate from 1.2 GHz to 2 GHz. The design center frequency was chosen to be 1.55 GHz because this is near the geometric center of the band and, with our choices of materials and structure, this gives a quarter wavelength of 1.25 in., which is convenient. Dimensions in this chapter are in inches since the commercially available components and materials are specified and manufactured in inches. Because

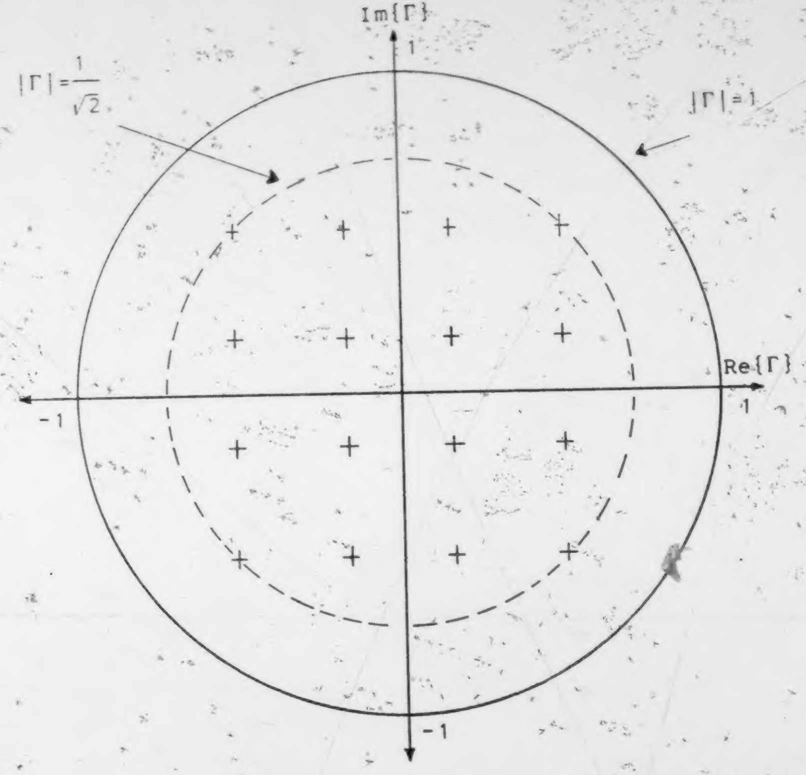

Figure 4.3 Nominal Reflection Coefficients of the Multiple Impedance Load

the wavelength is of the same order as the circuit and component dimensions, the phase shift across a circuit element is significant; the signal must be treated as a wave travelling between a conductor and the ground plane. As a result, the mechanical dimensions of circuit components and the mechanical integrity of the conductors and the ground plane are critical.

The PIN diode multiple impedance load was designed to operate both at 20K and at 300K, and to be able to withstand frequent cycling between these extremes. It would be unreasonable to expect the circuit elements to maintain

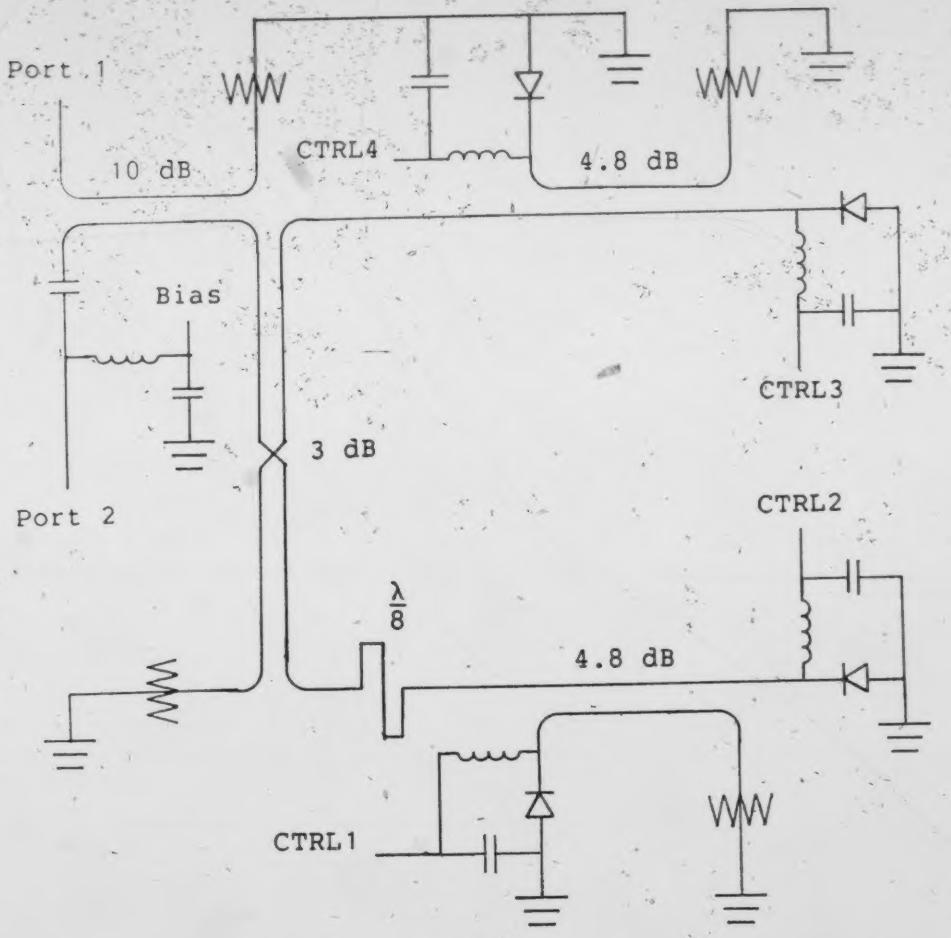
Port 1
10 dB
CTRL4
4.8 dB
Bias
CTRL3
3 dB
Port 2
CTRL2
$\frac{\lambda}{8}$
4.8 dB
CTRL1

Figure 4.4 Block Diagram of the Multiple Impedance Load

their mechanical dimensions over this temperature range. However, the mechanical integrity of the conductors and ground planes must be maintained and large mechanical stresses to components due to temperature cycling must be prevented. This was accomplished by using pressure contacts for all the electrical connections to rigid components within the load; this allowed some the mechanical stresses to be relieved by slippage and creep.

4.1.2.1 Mechanical Design

It was decided to build the PIN diode multiple impedance load using stripline techniques because this technique allows better isolation between adjacent circuitry and easier fabrication of couplers with high coupling coefficients than is possible with microstrip techniques. Stripline construction is illustrated in figure 4.5.

Some of the difficulties encountered in using stripline were:

1. A stripline to coaxial transition was required that had small s_{11} and s_{22} at room temperature and cryogenic temperatures, and was capable of withstanding repeated cycling between these extremes.
2. Most of the components are connected to the ground planes and to the stripline transmission lines by trapping the component leads between the dielectric and the conductor. Pressure on the dielectric sheets had to be maintained over the operating temperature range to ensure reliable electrical connections.
3. The circuit characteristics depend on ground plane spacing. To ensure repeatable circuit performance the ground plane spacing had to be held constant.
4. The dielectric sheets available had a thickness tolerance of ±0.0015 in. This was much larger than the compression of the dielectric due to pressure by the

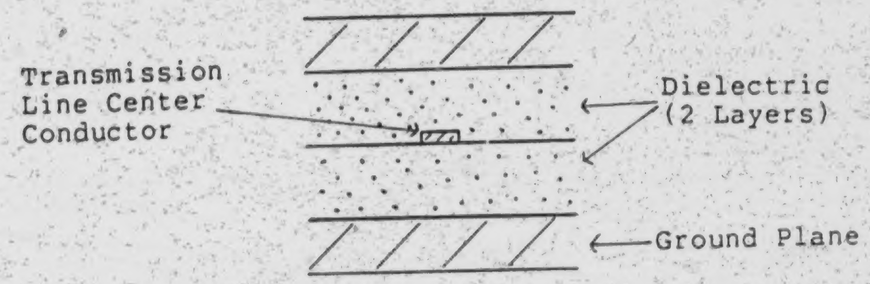

Figure 4.5 The Stripline Configuration

ground planes.

These difficulties were overcome by using the stripline package shown in figure 4.6. This package was developed by building several prototype fixtures, each with a 50 Ohm transmission line between two coaxial ports, and altering the design until the internal reflections were minimized and circuit performance was repeatable.

The ground planes were made of OFHC copper lapped smooth and plated with gold. The OFHC[3] copper ensured high heat conductivity at cryogenic temperatures and the gold plating ensured low resistance electrical and thermal contacts. The pins (marked A) were made of soft steel, which is hard enough to ensure that they would slide within the holes in the ground planes while under lateral pressure. The pins served to align the ground planes and the sheets of dielectric and to provide an anchor for the bolts holding the end plate on. The bolts (marked B) were used to force the ground plane down onto the spacer blocks (marked C)

---

[3] Oxygen Free High Conductivity (OFHC) copper has high thermal conductivity at cryogenic temperatures

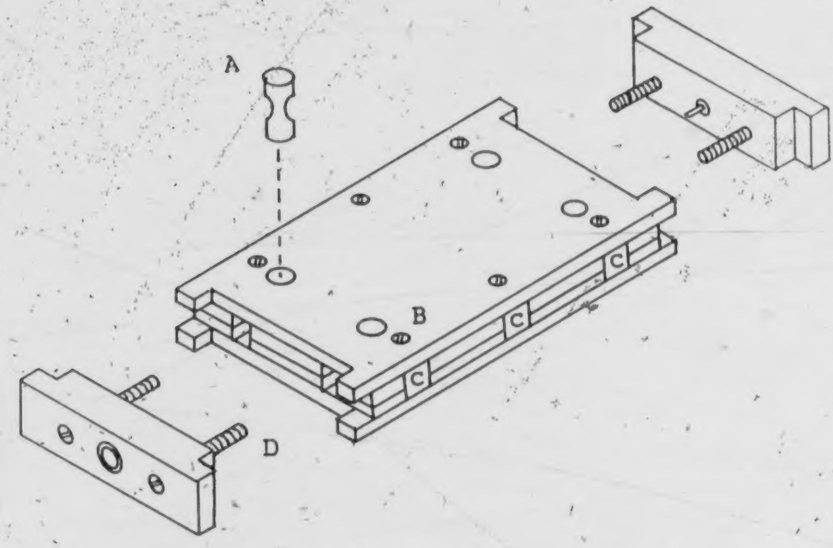

Figure 4.6 The Stripline Fixture

which were fractionally smaller than the thickness of the dielectric sheets plus the thickness of the conductors between the dielectrics. Thus the ground plane spacing was held constant and the dielectric sheets were kept under pressure. The spacer blocks were made of gold plated OFHC copper and were spaced 1.25 in. apart along the edges of the circuit. This ensured that the two ground planes were at the same potential and that the circuit inside the ground planes was isolated from any signals generated outside the ground planes. When the circuit was mounted in a cryostat only one of the ground planes made thermal contact with the cold stage, and the spacer blocks improved the heatsinking of the other ground plane.

The end plates were made of OFHC copper, lapped smooth and plated with gold. They contained a short 50 Ohm coaxial transmission line with a teflon dielectric. The teflon dielectrics and the center conductor were obtained from EMC Inc.[4] When the end plate was fitted onto the ground planes and dielectric, the flat tab on the center conductor fitted between the dielectric sheets, thus connecting to the stripline center conductor and providing vertical alignment. Horizontal alignment was provided by the tabs on the ground planes. The end plates were held onto the ground plates by the bolts (marked D) which were anchored in the alignment pins. Since the alignment pins were able to slide, small variations in dielectric thickness and in the position of the end plate were easily accommodated. To ensure good contact of the end plates to the ground planes, the end faces of the ground planes and the dielectric sheets had to be made coincident. This was ensured by clamping the ground planes and dielectric sheets and then machining all the end faces and alignment holes.

The coaxial connector was held onto the end plate with small machine screws. The annulus around the transmission line in the end plate was necessary for a low inductance ground contact to the coaxial connector.

Although the prototype fixtures were built with two layers of dielectric, (see figure 4.6), the PIN diode multiple impedance load was built with a third layer of dielectric 0.010 in. thick as shown in figure 4.7. The alignment of the three layers of dielectric and the two ground planes depended on the alignment pins. Since this load had only one end plate, extra alignment pins were included. When the prototype fixture was cycled between room temperature and 10K, it was discovered that the dielectric around the alignment pins had been stretched. As a result, the extra alignment pins in the PIN diode multiple impedance load were always removed when the load was cooled so that the dielectric layers could be properly aligned after the load had been disassembled.

---

[4] EMC Technology Inc., 1971 Old Cuthbert Road, Cherry Hill, N.J.

4.1.2.2 Choice of Dielectric

A nominal ground plane spacing of one eighth of an inch was chosen because of the easy availability of PIN diodes and terminations for that ground plane spacing. A number of dielectric materials were available that had a low loss tangent and an unvarying dielectric constant well into the microwave region. Not all of these materials were isotropic. Duroid 5870 was chosen as the dielectric for the following reasons:

1. Its dielectric constant was more isotropic than that of the woven dielectrics.
2. Its dielectric constant (2.33) was one of the lowest of the available materials. As a result circuit dimensions were as large as possible, and this increased the conductor tolerances and made fabrication easier.
3. A report from NASA (Rogers Corp., 1982) indicated that

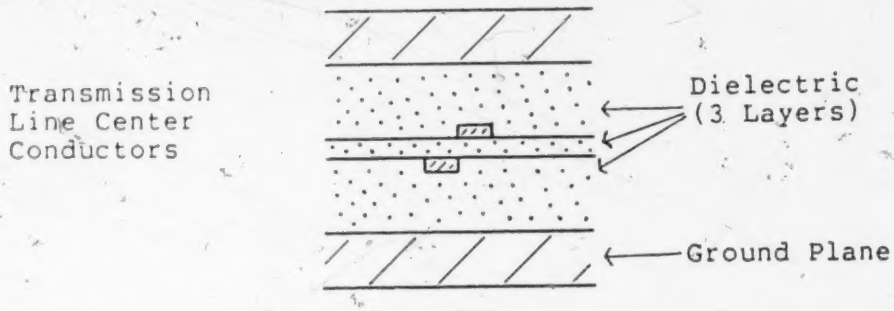

Figure 4.7 Stripline with Three Layers of Dielectric

as Duroid 5870 is cooled the thermal contraction and changes in dielectric constant are such that they compensate and the electrical length of transmission lines remains constant from 300K to 20K.

4. Thermal contraction normal to the plane of the dielectric is low.

To get a nominal ground plane spacing of 0.125 in. two sheets of Duroid 0.062 in. thick were used. A third sheet of Duroid 0.010 in. thick was used between the other two sheets. All the printed circuit elements were etched on either side of the center (0.010 in.) dielectric sheet. The transmission line widths were checked with a travelling microscope, and were found to be within 0.005 in. of the desired width. The directional couplers were realized as overlapping quarter wave-length transmission lines, etched on opposite sides of the center dielectric. This allowed one to build 50 Ohm overlapping couplers with coupling coefficients up to 0.737 (Howe, 1974). Note that the PIN diode multiple impedance load required a 3 dB coupler (c=0.707), so this was just barely adequate.

4.1.2.3 The Switchable Terminations

A switchable termination, described in section 6.1 above, consists of a PIN diode, a mismatching circuit and a bias circuit. The layout is shown in figure 4.8, below. To avoid unwanted reflections the impedance of the bias circuit at the point of connection to the 50 Ohm transmission line was made very high. Rather than making this impedance as high as possible and then ignoring its effects, it was used to mismatch the PIN diode. The mismatching circuitry consisted of the PIN diode lead, the contact pad for the PIN diode, the short section of inductive (narrow) transmission line and the bias circuitry.

The bias circuit consisted of an approximately quarter-wave length of high impedance transmission line terminated in a capacitive short to ground. The length of this transmission line and point of connection to the 50 Ohm transmission line were adjusted to optimize the PIN diode mismatch. In order to increase the isolation between the microwave circuit and external signals, a second quarter-wave section terminated in a capacitive short, followed by a lossy, inductive feedthrough were cascaded with the first section. The feed-through provided broadband isolation of about 20 dB and the two quarter wave sections (center frequency = 1.55 GHz) provided increased isolation between 1 GHz and 2 GHz. The effect of the second quarter

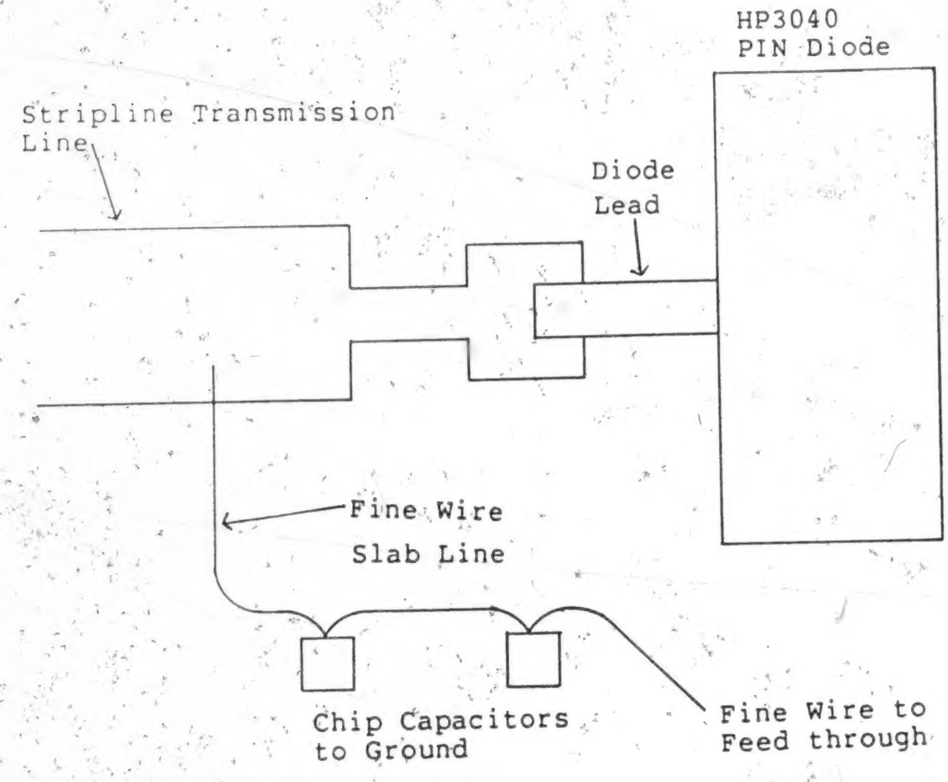
HP3040
PIN Diode
Stripline Transmission Line
Diode Lead
Fine Wire Slab Line
Chip Capacitors to Ground
Fine Wire to Feed through

Figure 4.8 Layout of a Switchable Termination

wave section on the reflection coefficient of the switchable termination was quite small, thus the second quarter wave section, capacitor and feed-through were ignored in the modelling.

Three of the four switchable terminations had a DC connection (through a directional coupler) to a 50 Ohm termination. To minimize the number of microwave components, DC blocking capacitors were not used; instead the current drawn by the 50 Ohm terminations was compensated for by the bias supply.

Once the circuit topology in figure 4.8 was decided upon, a switchable termination was modelled using IMPCAP (see chapter 8). The circuit parameters which could be altered were varied so that the "on" and "off" reflection coefficients of the termination were equal in magnitude, near one, and opposite in phase throughout the 1.2 GHz to 2 GHz band. After optimization, the root mean square deviation from a 180° difference between the phase angles of the "on" reflection coefficient and the "off" reflection coefficient for both diodes at all the design frequencies was 4.2° and the largest deviation was 7°.

4.1.2.4 Circuit Element Models

Hewlett-Packard type 3040 PIN diodes were used because they were easily available and they are mounted in a package especially suitable for stripline with a 0.125 in. ground plane spacing. The published equivalent circuit for a packaged diode is shown in figure 4.9.

The switchable terminations were designed using two-port S-parameter measurements of two of the diodes. These measurements were obtained by modifying one of the prototype fixtures previously discussed to accept a PIN diode, modelling the fixture, and then de-embedding the fixture model from S-parameter measurements of the PIN diodes in the fixture. The PIN diodes were used as one-ports, with the trimmed lead cut off as close as possible to the package. The one-port PIN diodes were modeled as the average of the two two-port S-parameter

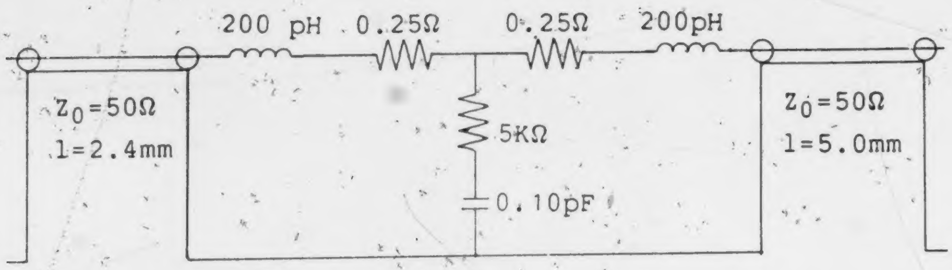
200 pH
0.25Ω
0.25Ω
200pH
Z_0=50Ω
l=2.4mm
5KΩ
0.10pF
Z_0=50Ω
l=5.0mm

a) Reverse Biased

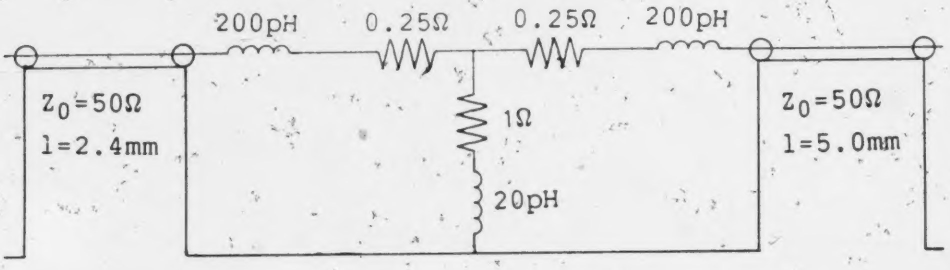
200pH
0.25Ω
0.25Ω
200pH
Z_0=50Ω
l=2.4mm
1Ω
20pH
Z_0=50Ω
l=5.0mm

b) Forward Biased

Figure 4.9 Equivalent Circuits for an HP PIN Diode in a Stripline Package

measurements, with a short section of transmission line at port two to model the discontinuity of the open ended transmission line. After measuring the PIN diodes at several values of forward bias current and reverse bias voltage it was decided to use a forward bias current of 50 mA because at this value of bias current the S-parameters was not strongly dependent on bias current and the power dissipation was low. The S-parameters of the reverse biased PIN diode were only weakly dependent on reverse bias voltage. The reverse bias voltage was chosen to be equal in magnitude to the forward bias voltage so that the power dissipation and hence the temperature of the 50 Ohm terminations should remain unchanged.

At microwave frequencies most capacitors exhibit some series inductance, which had to be included in the circuit model. The capacitors available for use in this circuit were ATC[5] size A (a 0.055 in. cube) and size B (a 0.100 in. cube) with capacitances in 10 percent steps. ATC provides impedance data in graphical form up to the frequency of parallel resonance. Equation 4.7 gives the complex impedance of a capacitor, assuming the only nonideal element is a series inductance.

$$X_C = \omega L - \frac{1}{\omega C} \tag{4.7}$$

By performing a least squares fit of equation 4.7 to selected data points, it was estimated that the series inductance of the A series capacitors was 250 pH ±50 pH and that the series inductance of the B series capacitors was 5500 pH ±50 pH. Both values of series inductance and all the available values of capacitance were allowed in the optimization of the switchable termination.

The high impedance transmission lines in the bias circuit were fabricated as a thin wire trapped between the sheets of dielectric. This is a type of transmission line known as slab line. The equation for the characteristic impedance of slab line is given by Gunston (1971, p70). The thin wire, 0.003 in. in diameter, was obtained from a roll of solder-wick, and has a characteristic impedance of 160 Ohms. In comparison, the narrowest possible printed conductor might be 0.008 in., which would have a characteristic impedance of 137 Ohms. A useful feature of this realization was that, after the printed circuit board was etched, the switchable termination could be tuned by changing the length of the thin wire and its place of attachment (by soldering) to the 50 Ohm transmission line.

---

[5] American Technical Ceramics, 1 Norden Lane, Huntington Station, New York

Formulae from Gupta (1981, p57 and p186) were used to estimate the characteristic impedance of stripline, and to model the step changes in width. From the fixture measurements the loss of the stripline transmission lines was estimated as 0.005 dB/cm.

4.1.2.5 The In-phase Networks

The in-phase networks (described above) consist of two switchable terminations connected by a 4.8 dB directional coupler. Extra sections of transmission line 0.25 in. long were inserted between the switchable terminations and the coupler so that the two circuits did not couple. The couplers were designed for a center frequency of 1.55 GHz and a band of 1.2 GHz to 2 GHz. Following the advice of Howe (1974, p156), , the couplers were overcoupled by 0.2 dB at the center frequency in order to extend the bandwidth of operation. The couplers were fabricated as overlapping conductors printed on opposite sides of the 0.010 in. dielectric sheet. From the design charts in Howe, the conductor width was chosen to be 0.063 in., and the overlap was chosen to be 0.021 in. All the corners were mitred to reduce reflections. The isolated port was terminated by a 50 Ohm resistive element mounted between the ground planes.

4.1.2.6 Other Circuit Elements

The 3 dB coupler was made in crossover configuration. It was designed to be overcoupled by 0.15 dB, and compensation was made for extra coupling in the crossover section. The coupler conductor width was chosen to be 0.054 in. and the overlap was chosen to be 0.042 in. The isolated port of the coupler was connected to one of the coaxial connectors, where it was terminated in 50 Ohms for three of the four couplers.

The 10 dB coupler was connected at the output of the multiple impedance load for the purpose of injecting additional noise. It was designed to be overcoupled by 0.3 dB. The conductors were chosen to be 0.087 in. wide and spaced 0.002 in. apart. The isolated arm was terminated with a 50 Ohm termination mounted between the ground planes.

A D.C. voltage for biasing active devices under test was required at port two of the load (see figure 4.4). However, the stripline conductor leading to this port would already have a D.C. voltage, imparted by the bias circuit for one of the PIN diodes. This situation necessitated the inclusion of the output bias circuit following the 10 dB coupler. The output bias circuit consisted of a series capacitor followed by a bias circuit similar to those used for the switchable terminations.

4.1.3 Small Signal Behavior

The PIN diode multiple impedance load works adequately in band at both room temperature and at cryogenic temperatures. Plots of the reflection coefficients are shown in figure 4.10 through figure 4.14. Note that at 1.55 GHz the center four points are more closely spaced than the exterior points, whereas at 1.2 GHz and 2 GHz the points are evenly spaced. This indicates that the couplers in the in-phase networks are coupled too strongly. The arrangement of the points is also slightly distorted by the output bias circuit. The average phase rotation of the reflection coefficients as a function of frequency is 0.77°/MHz, equivalent to the rotation induced by a 32cm airline.

4.1.4 Noise Temperature

The noise behaviour of the PIN diode multiple impedance load leaves some unanswered questions. With the load at room temperature and configured as a two port tuner, the output noise temperature for each state was measured using the circulator and tuner method described in section 3.4.2.1, and was found to be within 5K of the ambient temperature. These results were confirmed by numerous measurements of passive devices. This result agrees with Leake (1982) who

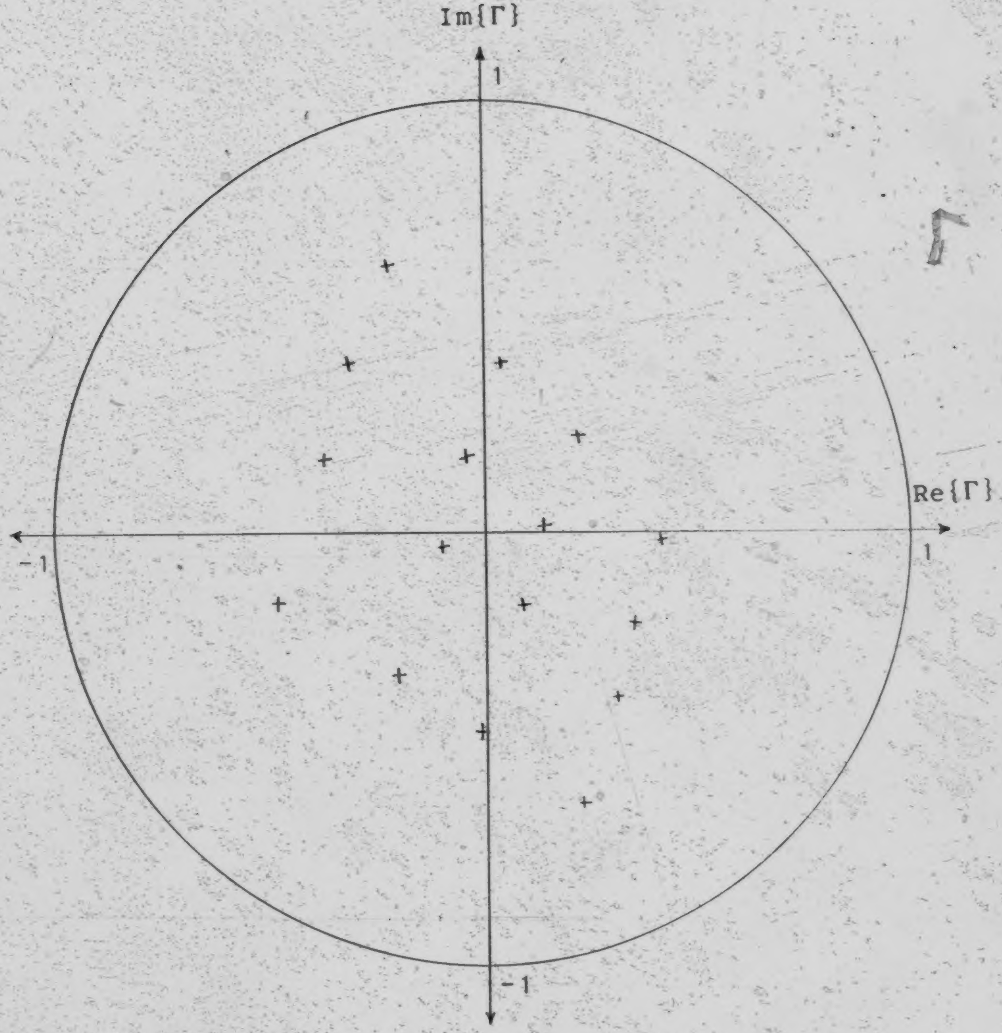

Figure 4.10 Reflection Coefficients of the PIN Diode Multiple Impedance Load at 1.2 GHz and 300K

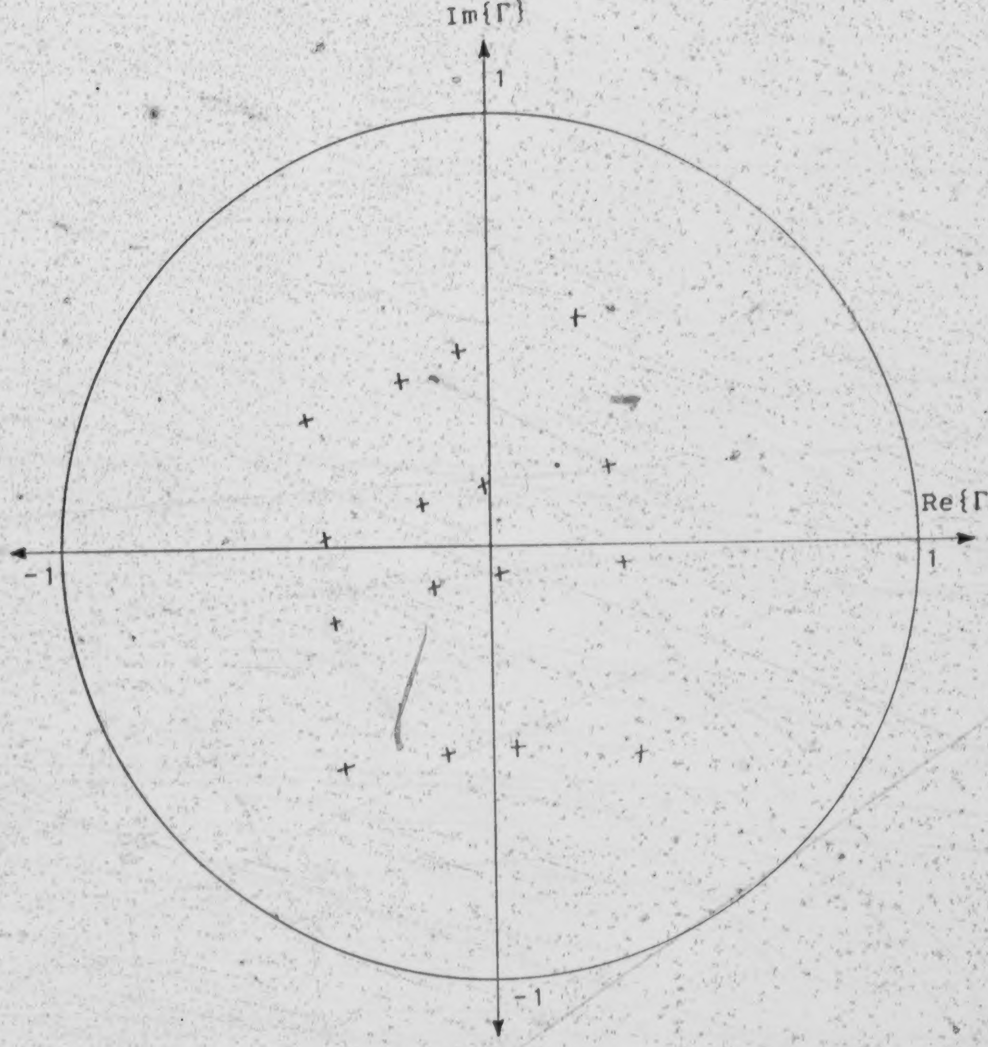

Figure 4.11 Reflection Coefficients of the PIN Diode Multiple Impedance Load at 1.5 GHz and 300K

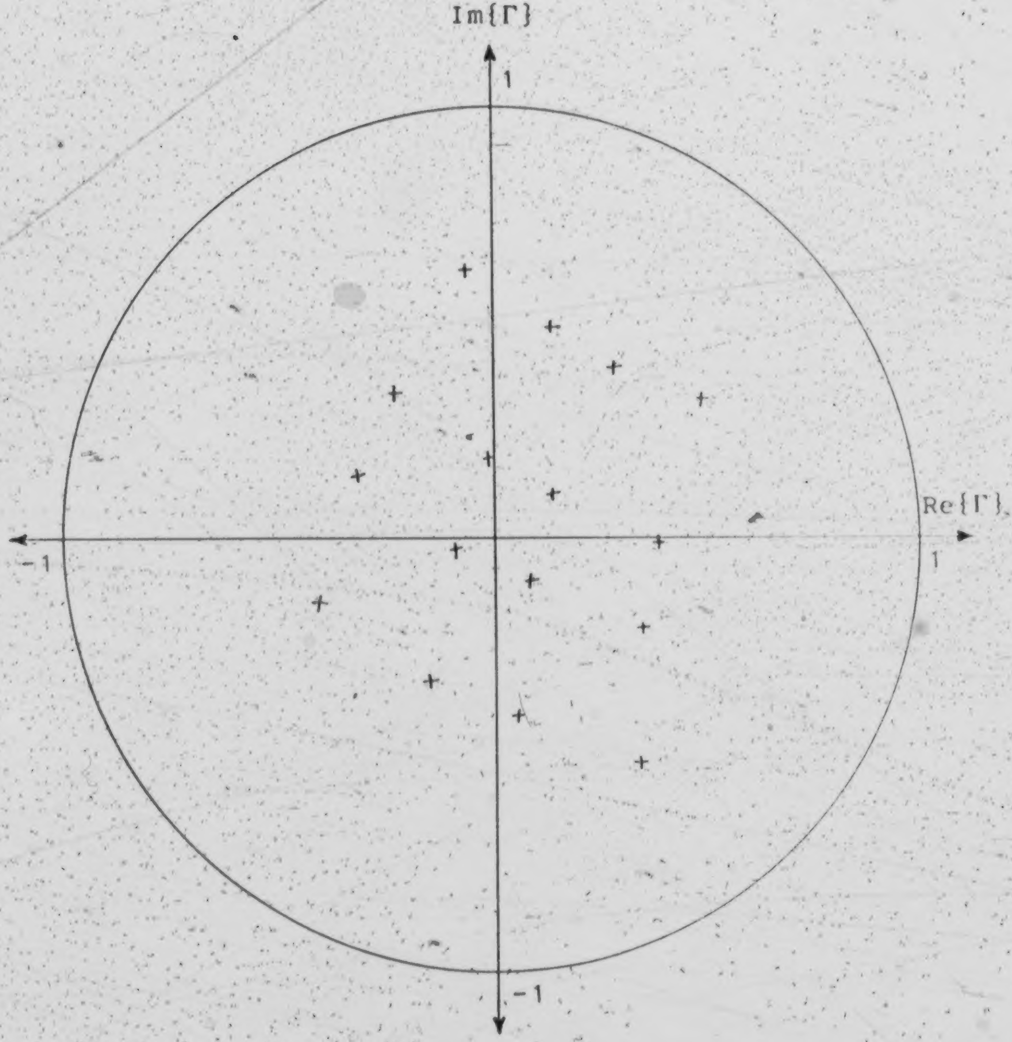

Figure 4.12 Reflection Coefficients of the PIN Diode Multiple Impedance Load at 1.8 GHz and 300K

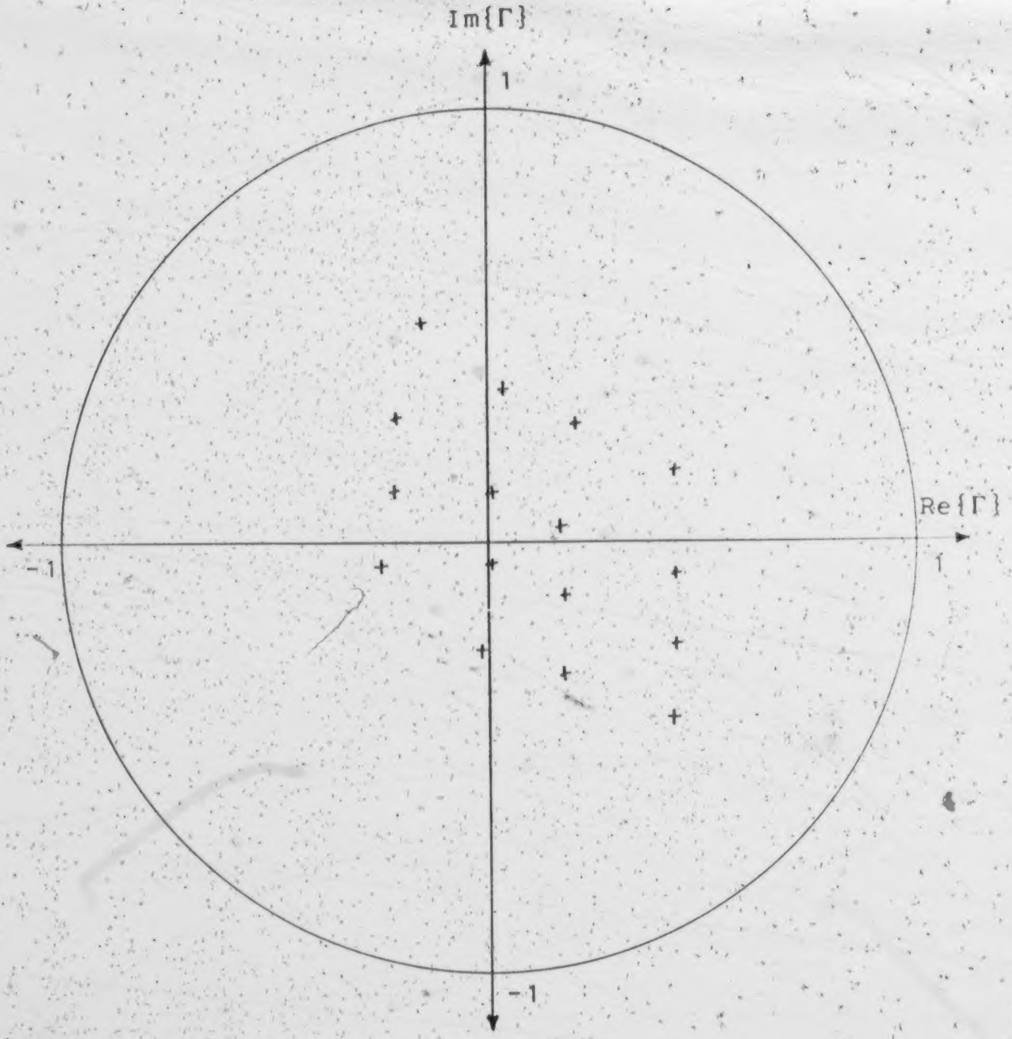

Figure 4.13 Reflection Coefficients of the PIN Diode Multiple Impedance Load at 1.2 GHz and 12K

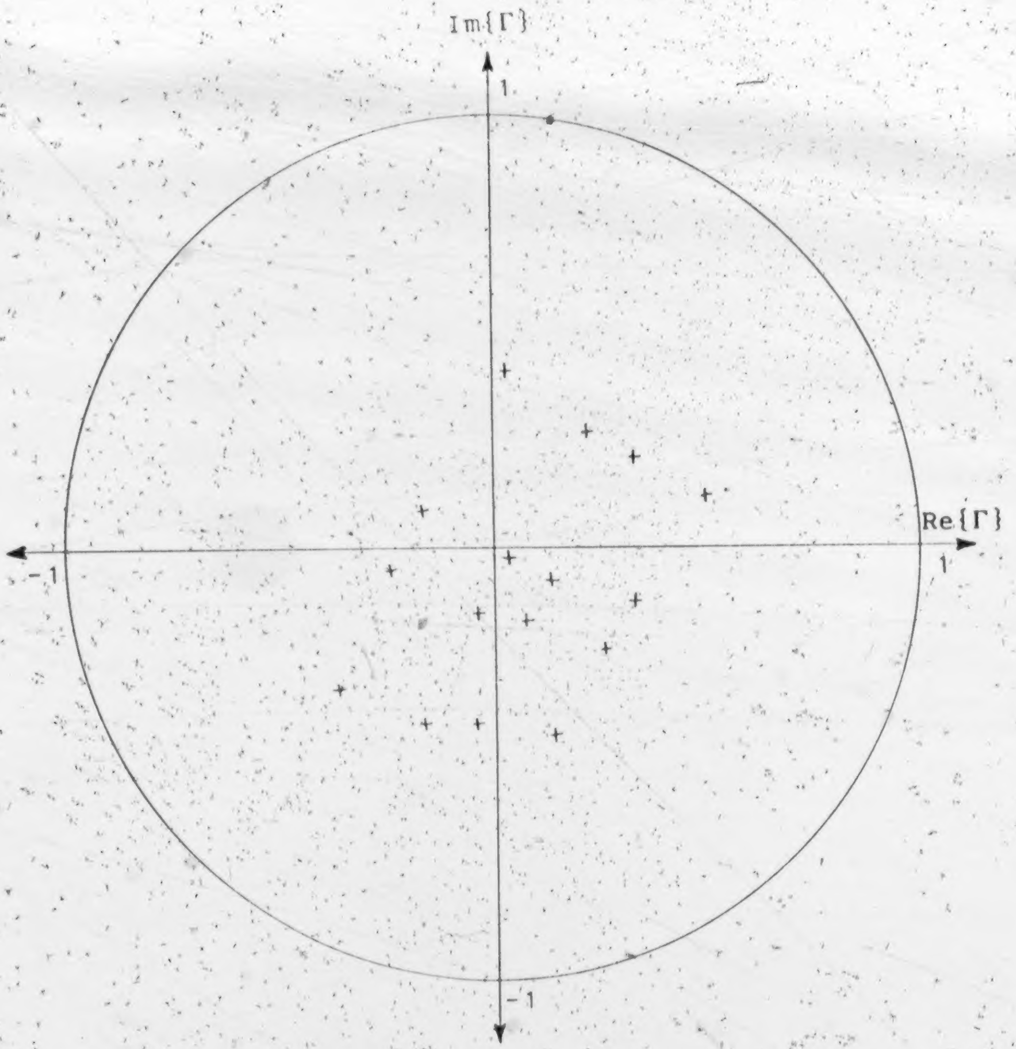

Figure 4.14 Reflection Coefficients of the PIN Diode Multiple Impedance Load at 1.5 GHz and 12K

claims that excess noise generation is low. With the load at 12K and configured as a one port, the noise temperature for each state was measured using the method discussed in section 3.4.4. The output noise temperature was found to vary between 16K and 470K, and to increase in proportion to the number of PIN diodes which were forward biased. It is also evident that some of the PIN diodes contribute more excess noise than others. These results were also confirmed by measuring a passive device. It seems very strange, however, that the output noise temperature of this load should increase when the load is cooled.

4.2 The Relay Multiple Impedance Load

This load was constructed in an attempt to reduce the sensitivity of the noise parameter estimates to measurement errors. The initial room temperature noise parameter estimates displayed an extremely high sensitivity to S-parameter measurement errors, and a sensitivity analysis indicated that this would be reduced by using a noise generator with a number of reflection coefficients spaced evenly around the $|\Gamma_G| = 1$ circle.

The relay multiple impedance load was constructed from six DB* type 2S1G11 coaxial relays and sections of semi-rigid 50 Ohm transmission line, as shown in figure 4.15. The design frequency was chosen to be 1.2 GHz, with the hope of obtaining evenly spaced reflection

---

*DB Products Inc., Pasadena, Ca.

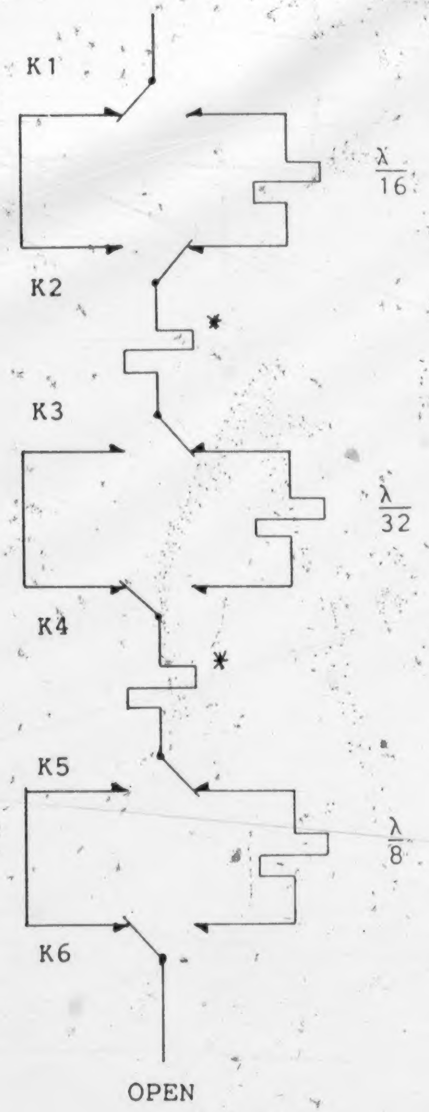
K1
λ/16
K2
*
K3
λ/32
K4
*
K5
λ/8
K6
OPEN

Figure 4.15 Simplified Diagram of the Relay Multiple Impedance Load - the lengths of the transmission lines marked by asterisks were chosen as described in the text

coefficients from 1.2 GHz to 1.5 GHz. This load has 22 states, *i.e.* there are 22 possible distinct reflection coefficients. In 8 of the states, the transmission path is continuous from the terminals of the load to the open end of the stub; in the other 14 states the transmission path terminates in an open circuit inside one of the relays. The load was designed as a 3 bit phase shifter with an incremental phase shift of 11.25°, connected to an open circuit; this determined the length of all but three of the transmission lines. The length of the open stub was chosen so that the 8 states for which the transmission path terminates inside relay K6 have reflection coefficients which are 180° out of phase with the reflection coefficients of the first eight states. These sixteen reflection coefficients should be spaced 22.5° apart at the design frequency. However, because the six relays have VSWR's as large as 1.2, these sixteen reflection coefficients are very unevenly spaced, with gaps as large as 65°. The lengths of the two transmission lines marked by asterisks were chosen so that the reflection coefficients of the remaining 6 states fill in the gaps at 1.2 GHz, 1.3 GHz, 1.4 GHz and 1.5 GHz caused by the relay VSWR. The maximum phase difference between the reflection coefficients of adjacent states is 33° at room temperature. The reflection coefficients of this load are shown in figure 4.16 through figure 4.19 below. The average phase rotation of the reflection coefficients (excluding the reflection coefficients of the last six states which have a much shorter transmission path) as a function of frequency is 1.75°/MHz, equivalent to the phase rotation induced by a 73 cm airline.

4.3 The Noise Measurement Receiver

The noise measurement receiver comprises the HP8970A noise figure meter and additional instruments and components which improve the frequency accuracy and which make it easier to calibrate the noise parameters of the receiver. A block diagram of the receiver is shown in figure 4.20.

4.3.1 Frequency Stabilisation

The characteristics of the noise measurement receiver are determined in part by the characteristics of the HP8970A noise figure meter. The noise figure meter is specified to have a frequency accuracy of ±10 MHz but its frequency stability is not specified. The measurement bandwidth is specified to be 4 MHz. The noise figure meter used for this project was observed to have a typical frequency offset of -3 MHz, and the frequency of its first local oscillator has been observed to change by as much as 300 KHz in 10 minutes. The other two internal local oscillators were observed to have negligible frequency drift compared to the first local oscillator. Without special compensation techniques, the frequency error of the noise measurement receiver as a whole will be equal to or worse than the frequency error of the

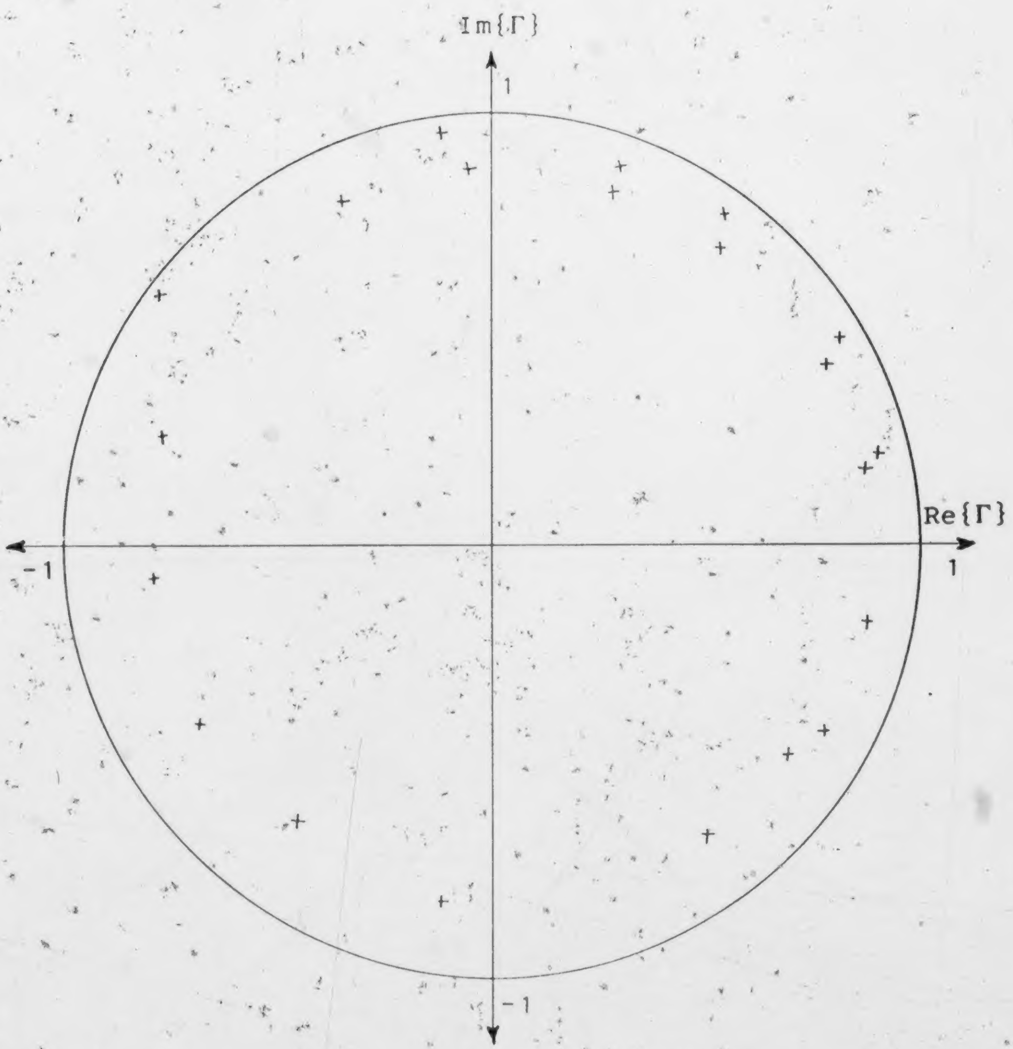

Figure 4.16 Reflection Coefficients of the Relay Multiple Impedance Load at 1.2 GHz and 300K

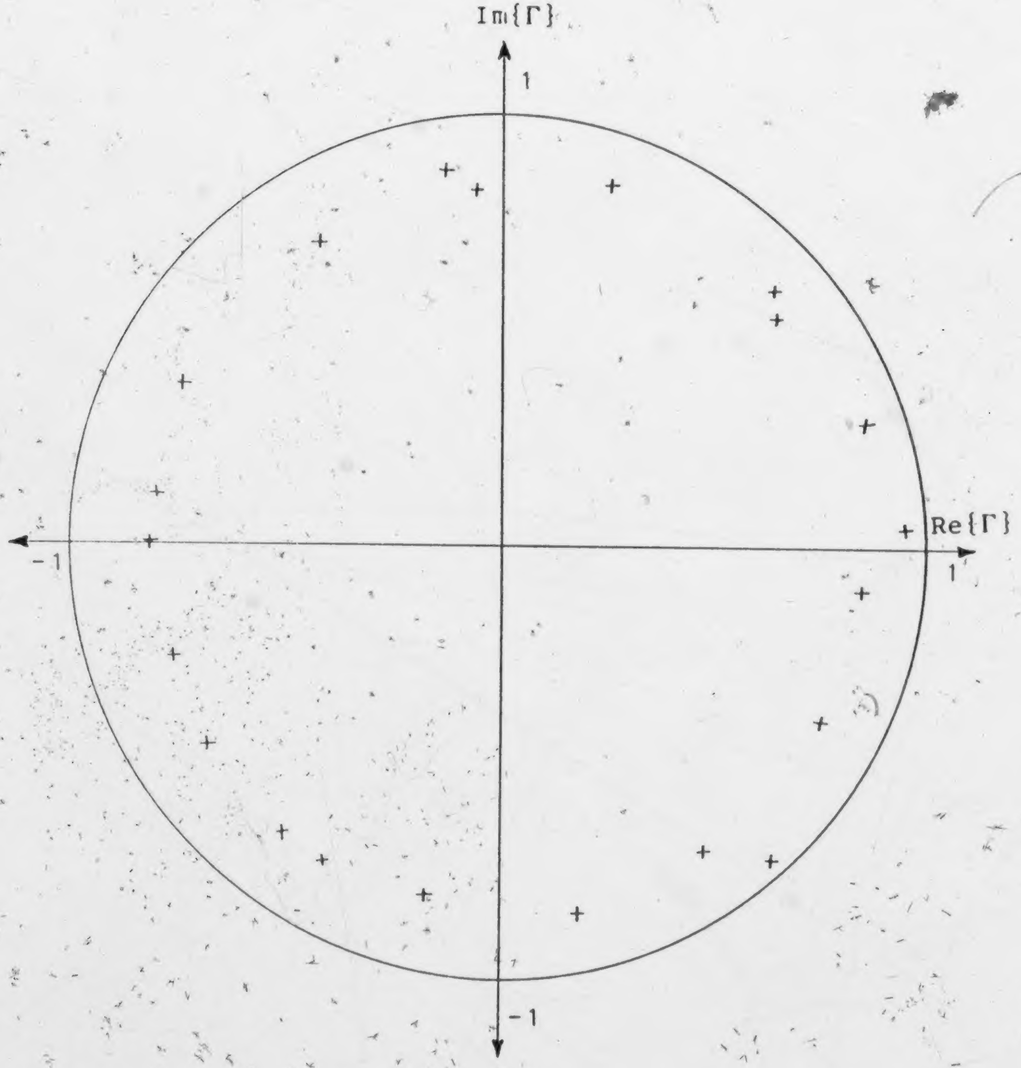

Figure 4.17 Reflection Coefficients of the Relay Multiple Impedance Load at 1.5 GHz and 300K

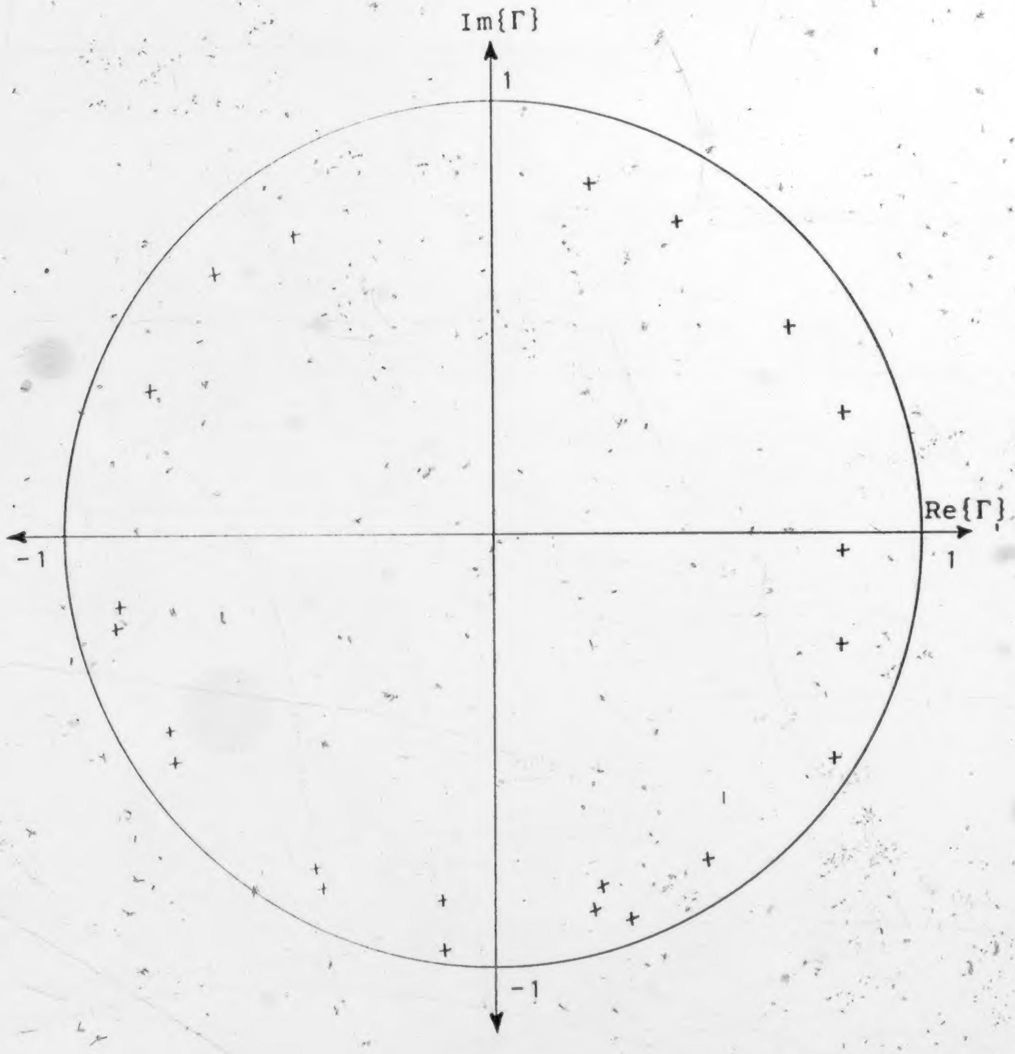

Figure 4.18 Reflection Coefficients of the Relay Multiple Impedance Load at 1.2 GHz and 14K

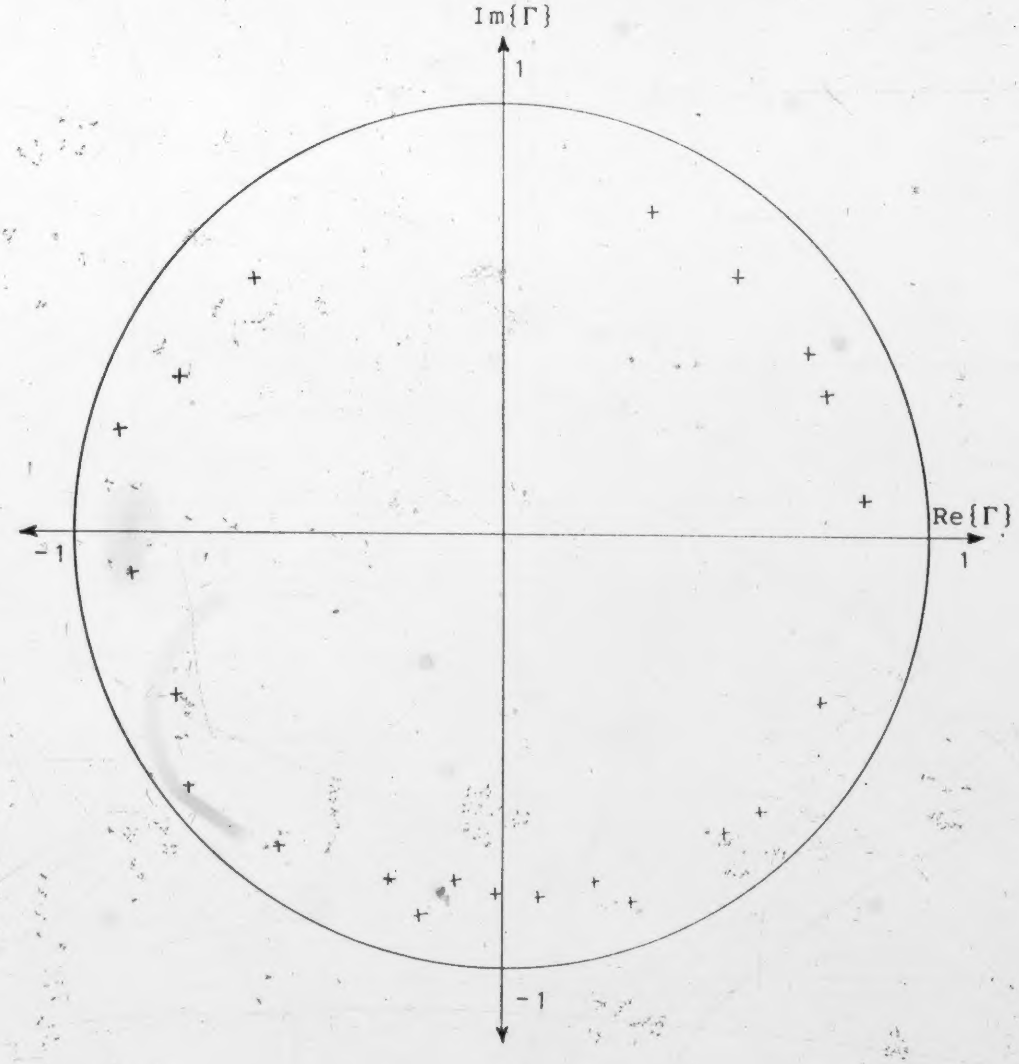

Figure 4.19 Reflection Coefficients of the Relay Multiple Impedance Load at 1.5 GHz and 14K

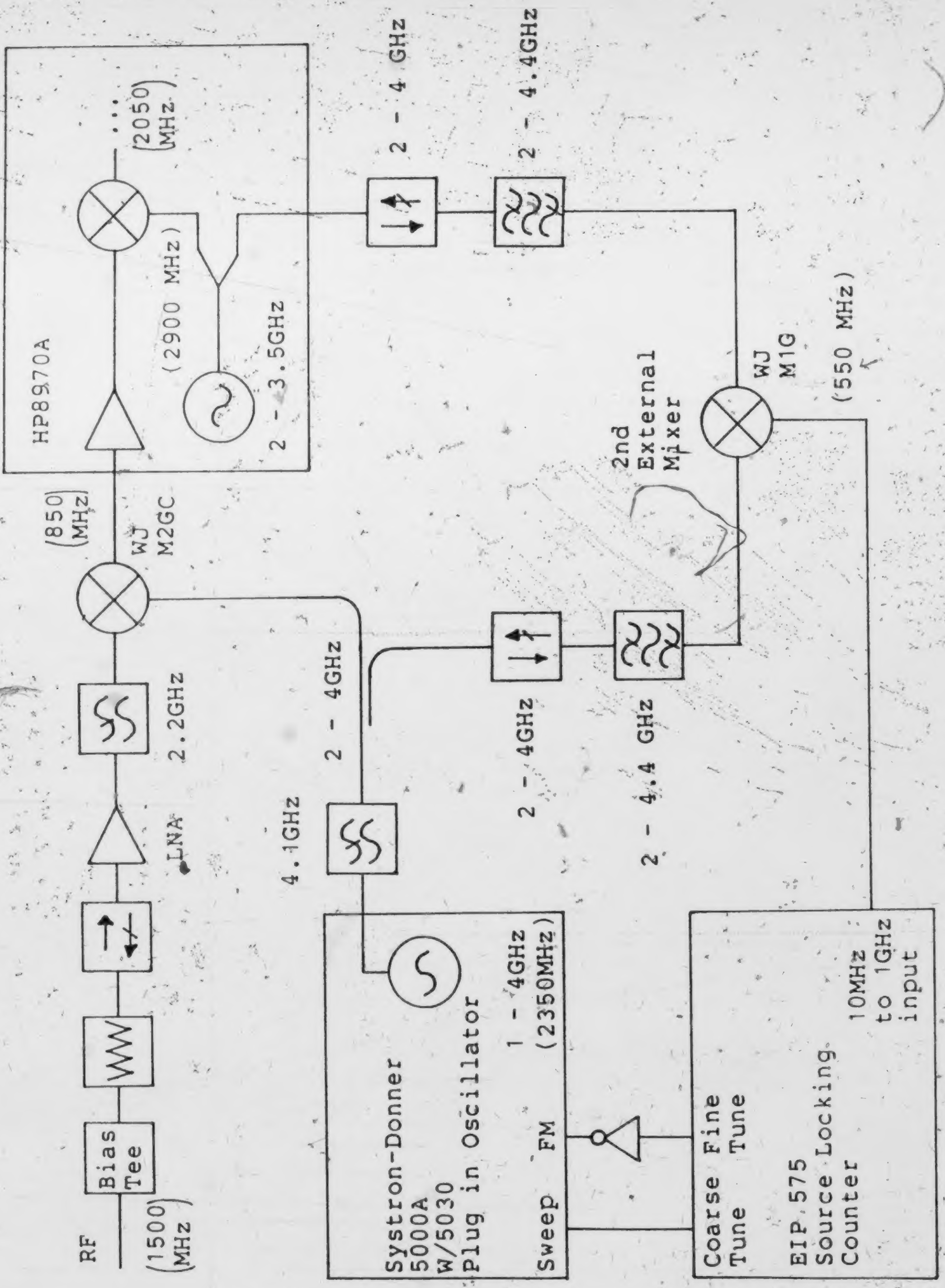
RF
(1500 MHz)
Bias Tee
LNA
2.2GHz
(850 MHz)
WJ M2GC
HP8970A
(2900 MHz)
2 - 3.5GHz
(2050 MHz)
2 - 4 GHz
2 - 4.4GHz
WJ M1G
(550 MHz)
2nd External Mixer
2 - 4GHz
2 - 4.4 GHz
4.1GHz
2 - 4GHz
Systron-Donner 5000A W/5030 Plug in Oscillator
1 - 4GHz (2350MHz)
Sweep
FM
Coarse Tune
Fine Tune
EIP 575 Source Locking Counter
10MHz to 1GHz input

Figure 4.20 Block Diagram of the Noise Measurement Receiver

noise figure meter.

Analysis in chapter 6 shows that the frequency error of the HP8970A noise figure meter is so large as to seriously degrade the accuracy of the noise parameter estimates. In an attempt to alleviate this problem, the frequency compensation system shown in figure 4.20 was developed.

Some of the instruments in figure 4.20 required minor modifications. The first local oscillator signal is available at a jack inside the noise figure meter. A cable was added so that this signal is available at a jack on the rear panel of the noise figure meter. The coarse tune output signal of the counter had to be inverted and level shifted before being fed to the sweep input of the external local oscillator. Most Hewlett-Packard sweep oscillators do not require this modification; instead it is sufficient to reverse the start and the stop markers. The bandpass filters each consist of a tubular 4.4 GHz high pass filter cascaded with a 30 cm section of S-band wave guide.

The arrangement of the mixers is such that the measurement frequency is the sum of the first IF frequency in the noise figure meter (2050±10 MHz) and the frequency difference between the external local oscillator and the first internal local oscillator of the noise figure meter. The source locking counter is connected so that it phase locks the lower side band from the second external mixer, which is the difference frequency of the two local oscillators just discussed, to its internal frequency reference, thus stabilising the measurement frequency. The remaining frequency drift is due to the drift of the source locking counter and the drift of the other two local oscillators in the noise figure meter.

Using this frequency compensation system, the frequency drift was observed to be less than 20 KHz, referenced to the phase locking counter. It was also observed that the noise power readings of the noise figure meter had become more stable.

Due to the frequency drift of the measurement frequency of the HP8970A noise figure meter it is difficult to characterise the passband shape and to estimate the center frequency of the passband. Because the passband gain changes by as much as 0.13 dB in 250 KHz, the frequency drift also makes it difficult to observe the noise figure meter detector linearity. However, using the frequency stabilisation scheme just described and an HP8656 synthesized oscillator as a 950 MHz signal source at the receiver input, it was possible to characterise the passband gain to within ±0.03 dB every 250 KHz. From these measurements it was then possible to estimate the center frequency of the first IF of the noise figure meter as 2049.4 MHz. From this result it can be seen that most of the frequency offset error in the noise figure measurement frequency (3 MHz) is due to the first local oscillator. Different results will undoubtedly be obtained for other noise figure meters of this type, as the frequency accuracy is only specified to be ±10 MHz. Using the frequency compensation system of figure 4.20, the frequency offset should be less than 30 KHz.

The frequency compensation system described above was first used without any filters or isolators. A large number of unwanted low-level signals were observed in this configuration. These unwanted signals were presumably due to the small leakages of coherent signals from the various mixers, propagating throughout the system and forming products in other mixers. One of these unwanted sidebands could potentially cause a serious measurement error if it should occur within the measurement bandwidth of the system. This problem was reduced by introducing the filters and isolators shown, which reduced the level of most of the spurious signals to the point where they could not be observed with a spectrum analyser.

4.4 The Test Fixture and Calibration Standards

The transistor test fixture is a stripline fixture with floating end plates constructed in the same way as the PIN diode multiple impedance load. Two 50 Ohm stripline transmission lines connect the device under test to coaxial connectors mounted in the endplates. The transistor is mounted in the center of the fixture with the gate and drain leads each trapped between the dielectric and a stripline center conductor. The transistor socket comprises two small recesses set into two bars, each one attached to a removable section of the top and bottom ground planes. The source leads of the transistor are trapped between the two bars. The removable ground plane sections allow the transistor to be removed and replaced. Other ground plane sections which fit in place of the above-mentioned sections allow a shorted termination, an open termination, or a short transmission line to be substituted for the transistor. These latter devices allow one to calibrate the S-parameters of the noise measurement system to the transistor socket. These devices were chosen because they were the simplest devices which could be made to fit in the fixture and which would have predictable S-parameters at cryogenic temperatures. Simple equivalent circuits for the three calibration standards, based on their physical dimensions and well known models of the open and the step change in width discontinuities (Gupta, Garg and Chadha, 1981) are shown in figure 4.21 through figure 4.23. More accurate models, arrived at using the iterative procedure described in chapter 7 are shown in figure 4.24 through figure 4.26.

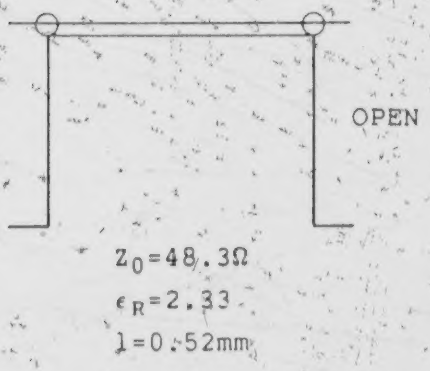
OPEN
$Z_0=48.3\Omega$
$\epsilon_R=2.33$
$l=0.52mm$

Figure 4.21 Equivalent Circuit for the Open Circuit Calibration Standard

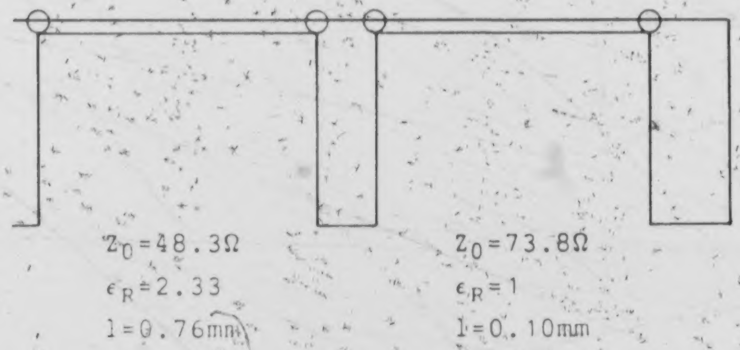
$Z_0=48.3\Omega$
$\epsilon_R=2.33$
$l=0.76mm$
$Z_0=73.8\Omega$
$\epsilon_R=1$
$l=0.10mm$

Figure 4.22 Equivalent Circuit for the Short Circuit Calibration Standard

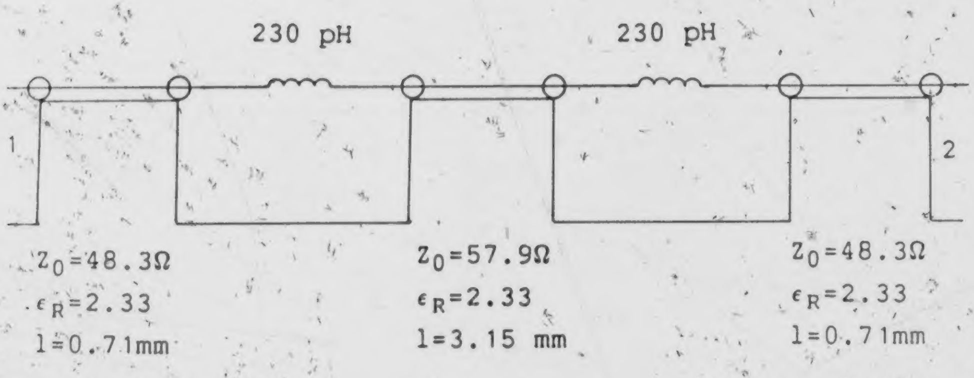
230 pH
230 pH
1
2
Z_0=48.3Ω
ϵ_R=2.33
l=0.71mm
Z_0=57.9Ω
ϵ_R=2.33
l=3.15 mm
Z_0=48.3Ω
ϵ_R=2.33
l=0.71mm

Figure 4.23 Equivalent Circuit for the Through Line Calibration Standard

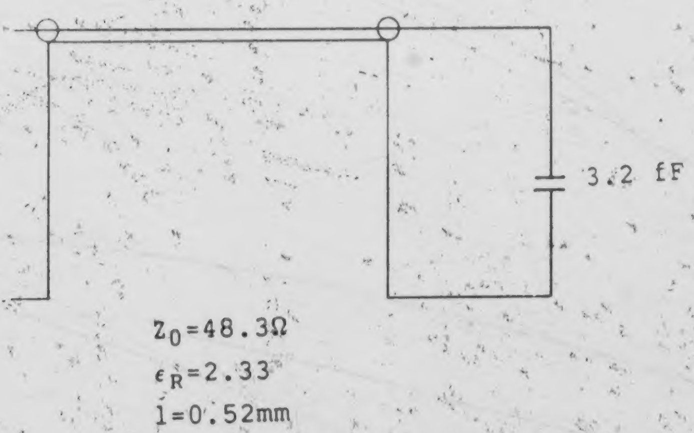
3.2 fF
Z_0=48.3Ω
ϵ_R=2.33
l=0.52mm

Figure 4.24 Improved Equivalent Circuit for the Open Circuit Calibration Standard

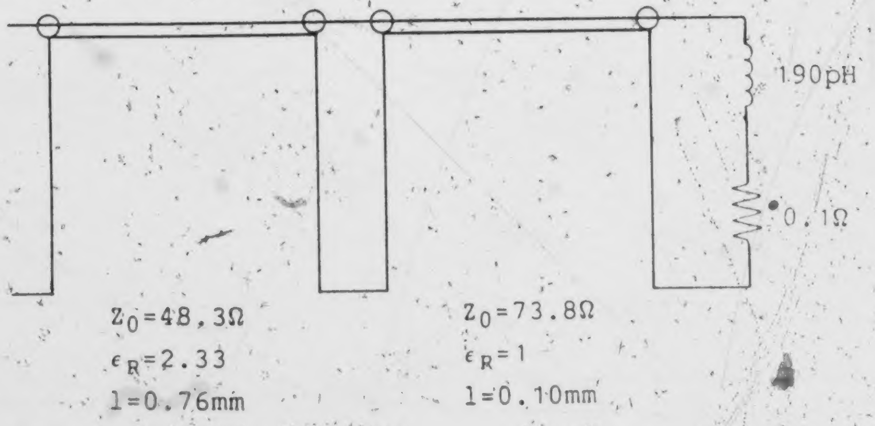
190pH
0.1Ω
$Z_0=48.3\Omega$
$\epsilon_R=2.33$
l=0.76mm
$Z_0=73.8\Omega$
$\epsilon_R=1$
l=0.10mm

Figure 4.25 Improved Equivalent Circuit for the Short Circuit Calibration Standard

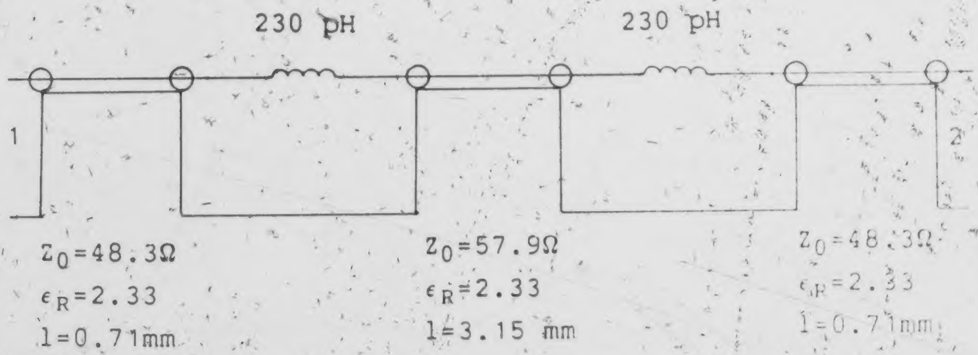
230 pH
230 pH
1
2
$Z_0=48.3\Omega$
$\epsilon_R=2.33$
l=0.71mm
$Z_0=57.9\Omega$
$\epsilon_R=2.33$
l=3.15 mm
$Z_0=48.3\Omega$
$\epsilon_R=2.33$
l=0.71mm

No change

Figure 4.26 Improved Equivalent Circuit for the Through Line Calibration Standard

Chapter 5

Calibration Techniques

In order to complete this project it was necessary develop a number of calibration techniques. The purpose of this chapter is to discuss those techniques.

5.1 Noise Generator Calibration

When a calibrated hot noise generator, such as an HP346, is connected to a two-port tuner, the noise temperature of the composite noise generator must be calibrated. If the tuner is passive and its S-parameters are known, that information is sufficient to determine the noise temperature of the composite noise generator. If the noise temperature of the tuner is unknown then the only possible method of calibration is by noise measurements. In this project, two techniques of generator noise temperature calibration were used. These are discussed below.

5.1.1 Calibration From One Power Measurement

If the noise parameters and the gain-bandwidth product of the noise measurement receiver are known then the noise temperature of a noise generator can be estimated from a single power measurement, made with the unknown noise generator connected to the receiver. By substituting equation 3.13 into equation 3.10, and substituting that result into equation 3.3 the measured power is obtained as:

$$P_{REC} = k\Delta f G_0 (T_G + T_{REC})\mu \tag{5.1}$$

where: k is Boltzmann's constant
T_G is the noise temperature of the noise generator
T_E is the excess noise temperature of the receiver when the noise generator is connected

where:

$$\mu = \frac{1 - |\Gamma_G|^2}{|1 - \Gamma_{IN}\Gamma_G|^2} \tag{5.2}$$

where: Γ_G is the reflection coefficient of the generator
Γ_{IN} is the input reflection coefficient of the receiver.

The noise parameters of the receiver are evaluated for the reflection coefficient of the noise generator to obtain the excess noise temperature of the receiver. The product $k\Delta f G_0$ is available if the receiver has been measured using the LRPG method or the method of section 3.4.4. From this information, the noise generator temperature is obtained as:

$$T_G = \frac{P_{REC}}{\mu k \Delta f G_0} - T_E \tag{5.3}$$

This method may be less accurate than the following method, especially if the receiver noise parameters were determined without using a noise generator having a reflection coefficient near the reflection coefficient of the generator under test.

5.1.2 Calibration From Two Power Measurements

If the noise parameters and gain bandwidth product of the noise measurement receiver are known, and a second calibrated noise generator is available, with a reflection coefficient near the reflection coefficient of the noise generator under test, then the noise temperature of the noise generator under test can be estimated more accurately than by the previous method. Two power measurements are made, one with the calibrated noise generator connected to the receiver and one with the noise generator under test connected to the receiver. If the two noise generators have exactly or nearly the same reflection coefficient, then the results are more accurate because they depend mainly on the noise temperature of the reference noise generator and the gain bandwidth product. The receiver noise parameters are used only to compensate for the shift in generator reflection coefficient, and this is a second order correction. By applying equation 5.3 twice and subtracting, the noise temperature of the noise generator under test is obtained as:

$$T_{G1} = \left[\frac{P_{REC1}}{\mu_1} - \frac{P_{REC2}}{\mu_2}\right] \frac{1}{k\Delta f G_0} + T_{E1} - T_{E2} + T_{G2} \qquad (5.4)$$

The quantities with the subscript "1" refer to the generator under test, and the quantities with the subscript "2" refer to the calibrated noise generator. This approach is from a technique described by Martines and Sannino (1987).

5.2 S-parameter Calibration

In order to estimate the transistor noise and small signal parameters it is necessary to calibrate the S-parameters of the two composite two-ports which connect the the transistor socket in the test fixture to the cryostat ports. Each of these composite two-ports consists of a coaxial feed-through through the cryostat wall, approximately 10 in. of coaxial cable (connecting the feedthrough, which is at 300K, to the fixture which is at 10K), approximately 1 in of stripline transmission line (inside the fixture), various coaxial connectors, and a coaxial to stripline transition. These composite two-ports will be referred to as the "cryostat (transmission) lines". Since the S-parameter test set is outside the cryostat, the terminals inside the cryostat are inaccessible, and the S-parameters of the cryostat lines cannot be measured directly. Furthermore, the 50 Ohm termination normally used for room temperature S-parameter calibration cannot be connected in place of the transistor because of the differing geometry, and in any case its reflection coefficient at cryogenic temperatures is not predicatable. Therefore, the S-parameters of the cryostat lines cannot be estimated using the algorithm used to calibrate the S-parameter test set. An algorithm or method was required to estimate the S-parameters of the cryostat lines from S-parameter measurements made outside the cryostat with various known terminations inserted in place of the transistor.

Krazewski, Stuchly and Stuchly (1983) discuss an analytic procedure to estimate the S-parameters of a two-port from reflection coefficient measurements made at one terminal with three known one-ports connected to the other (inaccessible) terminal. Unfortunately, there were only two one-port calibration standards available (an open and a short) which would fit in the transistor socket, so this method could not be used. A third calibration standard was available (a short transmission line), but this is a two-port. To overcome this problem a calibration procedure was devised to estimate the S-parameters of two (unknown) two-ports from S-parameter measurements made with two known one-port terminations and one known two-port connected to the inaccessible terminals. That procedure was used to calibrate the S-parameters of the cryostat lines.

Figures 5.1, 5.2, and 5.3 show the flow diagrams for the calibration standards and the two-ports to be calibrated. Let M_{11} and M_{12} be the measured reflection coefficients of port 1 measured with port 3 terminated with (known) reflection coefficients of "A" and "C" respectively, as shown in figure 5.2. Let M_{21} and M_{22} be the measured reflection coefficients of port 2 measured with port 4 terminated with (known) reflection coefficients of "B" and

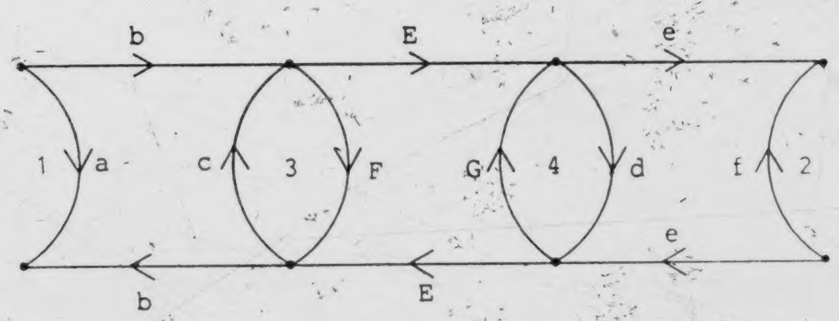
b
E
e
1
a
c
3
F
G
4
d
f
2
e
b
E

Figure 5.1 Flow Diagram for the Unknown Two-ports Connected to the Two-port Calibration Standard

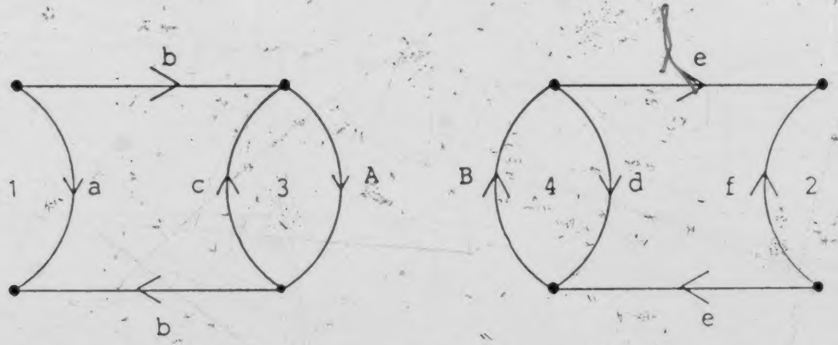
b
e
1
a
c
3
A
B
4
d
f
2
b
e

Figure 5.2 Flow Diagram for the Unknown Two-ports Connected to the First One-port Calibration Standard

"D" respectively, as shown in figure 5.3. Furthermore, let M_{13}, M_{23} and M_{33} be the measured values of s_{11}, s_{22} and s_{21}

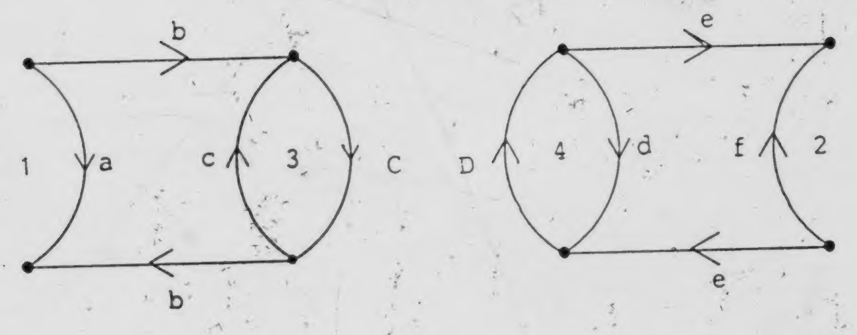

Figure 5.3 Flow Diagram for the Unknown Two-ports Connected to the Second One-port Calibration Standard

when a two port is connected between ports 3 and 4 as shown in figure 5.1, with $s_{11} = F, s_{22} = G$ and $s_{21} = s_{12} = E$. The two (unknown) two-ports are assumed reciprocal, so that the measured values of s_{21} and s_{12} are the same. The relationships between the measured values and the various S-parameters can be found using Mason's Gain rule and are given in equation 5.5 through equation 5.11.

$$M_{11} = \frac{a + (b^2 - ca)A}{1 - Ac} \tag{5.5}$$

$$M_{21} = \frac{f + (e^2 - fd)B}{1 - Bd} \tag{5.6}$$

$$M_{12} = \frac{a + (b^2 - ca)C}{1 - cC} \tag{5.7}$$

$$M_{22} = \frac{f + (e^2 - fd)D}{1 - dD} \tag{5.8}$$

$$M_{13} = \frac{a(1 - Gd) + (b^2 - ca)(F + d(E^2 - FG))}{1 - cF - dG + cd(FG - E^2)} \tag{5.9}$$

$$M_{23} = \frac{f(1 - Fc) + (e^2 - fd)(G + c(E^2 - FG))}{1 - cF - dG + cd(FG - E^2)} \tag{5.10}$$

$$M_{33} = \frac{beE}{1 - cF - dG + cd(FG - E^2)} \tag{5.11}$$

The object is of course, to find the S-parameters of the two outermost (unknown) two-ports; these are the lower case variables. The upper case variables are all known quantities. Equation 5.5 through equation 5.8 can be solved to find the parameters "a", "b", "e" and "f" in terms of the two parameters "c" and "d" and some known intermediate quantities. These relationships are:

$$a = X_1 - X_2c \tag{5.12}$$

$$f = Y_1 - Y_2d \tag{5.13}$$

$$b^2 - ca = X_3 + X_4c \tag{5.14}$$

$$e^2 - fd = Y_3 + Y_4d \tag{5.15}$$

The (known) intermediate quantities X_1 through X_4 and Y_1

through Y_4 are given by the following:

$$X_1 = \frac{\frac{M_{11}}{A} - \frac{M_{12}}{C}}{\frac{1}{A} - \frac{1}{C}} \qquad (5.16)$$

$$X_2 = \frac{M_{11} - M_{12}}{\frac{1}{A} - \frac{1}{C}} \qquad (5.17)$$

$$X_3 = \frac{M_{11} - M_{12}}{A - C} \qquad (5.18)$$

$$X_4 = \frac{\frac{M_{11}}{C} - \frac{M_{12}}{A}}{\frac{1}{A} - \frac{1}{C}} \qquad (5.19)$$

$$Y_1 = \frac{\frac{M_{21}}{B} - \frac{M_{22}}{D}}{\frac{1}{B} - \frac{1}{D}} \qquad (5.20)$$

$$Y_2 = \frac{M_{21} - M_{22}}{\frac{1}{B} - \frac{1}{D}} \qquad (5.21)$$

$$Y_3 = \frac{M_{21} - M_{22}}{A - D} \qquad (5.22)$$

$$Y_4 = \frac{\frac{M_{21}}{D} - \frac{M_{22}}{B}}{\frac{1}{B} - \frac{1}{D}} \qquad (5.23)$$

Equation 5.12 through equation 5.15 can be substituted into equation 5.9 and equation 5.10 and factored to obtain the following two relationships:

$$X_6 = (X_7 + c)(X_8 + d) \qquad (5.24)$$

$$Y_6 = (Y_7 + c)(Y_8 + d) \tag{5.25}$$

The (known) intermediate quantities X_5 through X_8 and Y_5 through Y_8 are given by the following:

$$X_5 = (M_{13} + X_4)(E^2 - FG) + GX_2 \tag{5.26}$$

$$X_6 = \frac{M_{13} - X_1 - X_3F}{X_5} + X_7X_8 \tag{5.27}$$

$$X_7 = \frac{(M_{13} - X_1)G + (E^2 - FG)X_3}{X_5} \tag{5.28}$$

$$X_8 = \frac{(M_{13} + X_4)F - X_2}{X_5} \tag{5.29}$$

$$Y_5 = (M_{23} + Y_4)(E^2 - FG) + FY_2 \tag{5.30}$$

$$Y_6 = \frac{M_{23} - Y_1 - Y_3G}{Y_5} + Y_7Y_8 \tag{5.31}$$

$$Y_7 = \frac{(M_{23} + Y_4)G - Y_2}{Y_5} \tag{5.32}$$

$$Y_8 = \frac{(M_{23} - Y_1)F + (E^2 - FG)Y_3}{Y_5} \tag{5.33}$$

Equation 5.24 can now be solved for "c" and the result substituted into equation 5.25 to obtain a quadratic in "d".

The two solutions to this quadratic are given by:

$$d = -\frac{1}{2}\left[X_8 + Y_8 + \frac{X_6 - Y_6}{Y_7 - X_7}\right] + \pm\frac{1}{2}\left\{\left[X_8 + Y_8 + \frac{X_6 - Y_6}{Y_7 - X_7}\right]^2 - 4\left[X_8 Y_8 + \frac{X_6 Y_8 - Y_6 X_8}{Y_7 - X_7}\right]\right\}^{\frac{1}{2}} \qquad (5.34)$$

These (numeric) solutions for "d" can now be substituted into the previous equations to determine two sets of the S-parameters "a", "c", "d", "f", "b^2" and "e^2". It has been observed that one of these sets is always passive or nearly passive and the other set obviously does not correspond to a pair of passive two-ports. The former set is the correct solution. If measurements have been made at a number of frequencies and it is known that the unknown two-ports behave approximately like transmission lines (which was the case for the cryostat lines), a simple iterative algorithm can now be used to find "b" and "e".

It should be noted that equation 5.11 was not used in the above process. The author has observed that if there are measurement or modelling errors, then when the S-parameters estimated by the above procedure are cascaded onto the S-parameters of the two-port calibration standard, the calculated values of s_{11} and s_{22} agree exactly with the measured values M_{13} and M_{23}, but there is a discrepancy between the resulting value of s_{21} and the measured value M_{33}. This is because M_{33} and equation 5.11 have not been used in the algorithm just discussed.

The additional information can be put to good use. Suppose there is a circuit element in the model of one of the terminations whose value is uncertain. This value can then be iteratively adjusted, and the calibration algorithm repeated, to minimise the size of the discrepancy. This ought to result in a more accurate estimate of the value of the parasitic element, and in a better estimate of the S-parameters of the unknown two-ports.

Chapter 6

Measurement Errors

Estimates of the noise parameters of two-ports having a high input reflection coefficient are very sensitive to measurement errors, especially S-parameter and frequency errors. This chapter first examines the random and systematic errors in the measurements used to obtain noise parameter estimates, and then discusses the sensitivity of the methods of estimation to these errors. In order to obtain a reasonable result with a high reflection coefficient device, instrument errors must be minimised and a method of estimation with the lowest possible sensitivity to measurement errors must be chosen. Even then, the error of the estimate can be as large as 20%. For this reason, noise parameter estimates must be checked by measuring a passive device.

6.1 Instrument Errors

To obtain the data required to make noise parameter estimates, measurements are made of received noise power and of various reflection coefficients and S-parameters at a given frequency. For the purposes of this project, S-parameter and reflection coefficient measurements were made using a modified Hewlett Packard 8410 S-parameter test set (M. Chau, 1984), and noise power measurements were made using an HP8970A noise figure meter. There are both random and systematic errors in the measurements made by both these instruments. In addition there is a significant discrepancy in the center frequency of these two instruments.

6.1.1 S-Parameter Measurement Errors

The S-parameter test set used without an error correction program has an accuracy of perhaps 10% of full scale. Most of the error in the basic test set is systematic. The HP85 computer error correction algorithm developed by Chau (M. Chau, 1984) and later corrected by Vaneldik (J.F. Vaneldik, private communication) corrects for linear errors using a model of twelve error vectors. In addition to these linear errors (which are corrected for), the test set suffers from measurement errors due to harmonic skip, display non-circularity, display feed-through, DC offset instability, and susceptibility to interference. The display feed-through error has a maximum value of 1.2%. In order to enhance the accuracy of the test set, a routine was added to the HP85 program set which measures this error and removes it from each measurement. It was found that the DC offset fluctuates for as long as 10 minutes after the test set display intensity is adjusted. Subsequent to this discovery, 15 minutes were allowed for the DC offset to stabilize after any display adjustment. It was also found that the HP8411A Harmonic Convertor (part of the S-parameter test set) was susceptible to magnetic interference, and that two shielded pole motors in 4 in. cooling fans mounted on the rear of the test set were causing baseband modulation of the RF signal. This problem was solved by using a single cooling fan with a DC motor, mounted further away from the harmonic convertor. The error due to display non-circularity is less than 2%. The error due to harmonic skip is ±2° in phase or ±3% in magnitude (Chau, 1984).

6.1.2 Analysis of Frequency Related Errors

The frequency discrepancy between the noise figure meter and the S-parameter test set is due mainly to instability in the measurement frequency of the noise figure meter. The measurement frequency of the S-parameter test set is determined by the EIP-575 source locking counter, which has a frequency drift less than one part in 3×10^{-7} per month. This was the most accurate microwave counter available to us, and was used as the frequency reference for all the work described in this thesis. The measurement frequency of the noise figure meter is specified to be accurate only to ±10 MHz and was found to be in error by 3 MHz and to vary by up to 300 KHz in 10 minutes.

At first glance these frequency errors appear to be unimportant, since they are a small percentage of the measurement frequency. It is perhaps more important to compare the frequency error with the measurement bandwidth, which is 4 MHz. Unfortunately, this comparison does not begin to describe the true effects caused by an error in measurement frequency.

Since the measurement frequency is not used directly in noise parameter estimation it is not immediately obvious how to express the error due to a frequency discrepancy. It will be seen that the effect of a frequency discrepancy can conveniently be expressed as an error in the power measurement. The following analysis also obtains the error due to the noise power spectral density not being constant across the measurement bandwidth of the noise measurement receiver. The error due to non-zero bandwidth has been discussed by Bosma (1967); however, his results are considerably less detailed than the results which follow and correspondingly less accurate. The severity of the errors will be seen to depend on the magnitude of the reflection coefficients in the noise measurement system and the lengths of the interconnecting transmission lines.

The noise power spectral density delivered to a load (such as a noise measurement receiver) as a function of frequency can be expressed as a Taylor's series expanded about the measurement frequency.

$$G(f) = G(f_M) + G'(f_M)(f-f_M) + G''(f_T)\frac{(f-f_M)^2}{2} \tag{6.1}$$

where: G is the power spectral density

f_M is the measurement frequency

f_T is a frequency between f and f_M

Note that f_T has been chosen so that the expression is exact. The last term is sometimes known as the "Lagrangian" form of the remainder of the series. This expression can be integrated with respect to frequency to find the power delivered over a given bandwidth centered at the measurement frequency. The following result is obtained:

$$P_{REC} = G(f_M)(2\delta f) + G''(f_1)\frac{\delta f^3}{3} \qquad (6.2)$$

where: δf is one half the bandwidth
f_1 is a frequency within the measurement bandwidth

This is the power which will actually be measured. On the other hand, the noise power which one desires to measure is the noise power spectral density at the desired frequency, multiplied by the measurement bandwidth. To facilitate the comparison between the desired power and the measured power, the spectral power density in equation 6.2 can be expressed in terms of the spectral power density at the desired frequency. The relative error is obtained by dividing the measured power (given by equation 6.2) by the desired power. The relative error is:

$$\frac{P_{REC}}{G(f_M)(2\delta f)} = 1 + \frac{G'(f_2)}{G(f_C)} f_O + \frac{G''(f_1)}{G(f_C)}\frac{\delta f^2}{6} \qquad (6.3)$$

where: f_C is the desired center frequency
f_2 is a frequency between f_C and f_M
f_O is the offset frequency $f_M - f_C$

This expression contains two error terms, one of which describes the error due to non-zero bandwidth and one of which describes the error due to the frequency offset. If one is simply seeking to determine the maximum error or the behavior of the error function, then f_1 and f_2 can be replaced by f_C. Since these are in fact our objectives, these substitutions will be made in the following sections. We must now find the maxima of the terms in equation 6.3 in terms of the circuit small signal parameters.

Consider a noise generator and a noise measurement receiver connected by a transmission line of length "l", as shown schematically in figure 6.1. The quantities represented by the vertices of the flow graph in figure 6.1 are given by:

$$v_1 = B_G\Psi_{BG} + v_3\Gamma_1 e^{-j\beta l} \qquad (6.4)$$

$$v_2 = A_T\Psi_{AT} + v_1 e^{-j\beta l} \qquad (6.5)$$

$$v_3 = B_T\Psi_{BT} + v_2\Gamma_2 \qquad (6.6)$$

$$v_5 = g v_4 \qquad (6.7)$$

where: $\Gamma_1 = \rho_1 e^{j\phi_1}$

$\Gamma_2 = \rho_2 e^{j\phi_2}$

$\beta = \dfrac{2\pi f}{v_p}$

g is the (unknown) gain from node v_2 to the power meter

l is the length of the transmission line

v_p is the phase velocity on the transmission line

These equations can be solved to obtain the signal measured

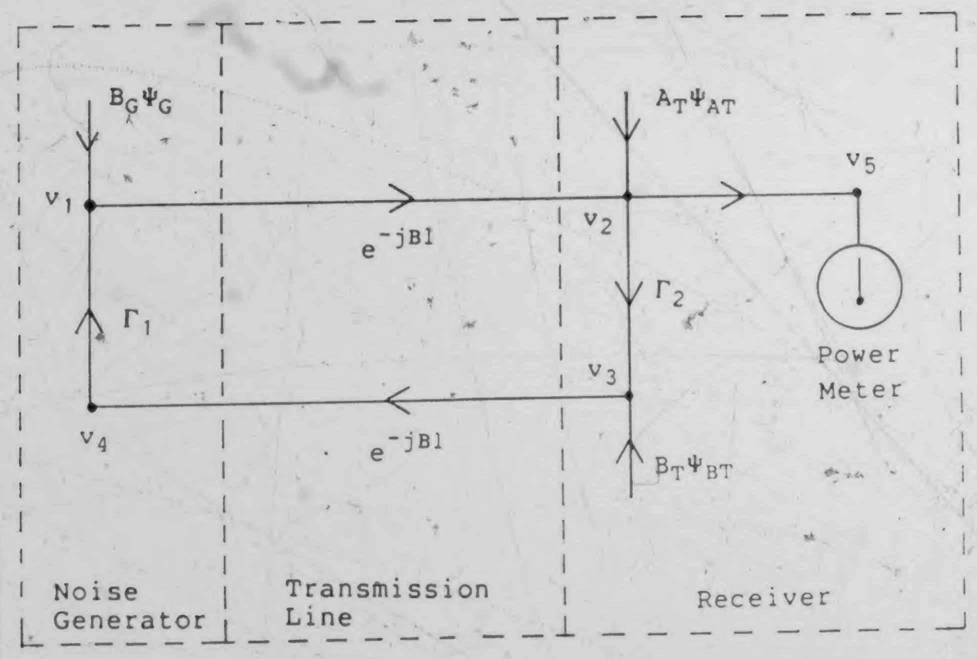
$B_G\Psi_G$
$A_T\Psi_{AT}$
v_5
v_1
v_2
$e^{-j\beta l}$
Γ_2
Γ_1
Power Meter
v_3
v_4
$e^{-j\beta l}$
$B_T\Psi_{BT}$
Noise Generator
Transmission Line
Receiver

Figure 6.1 Flow Diagram for a Noise Generator and Receiver Connected by a Transmission Line

by the power meter as:

$$v_5 = g\,\frac{A_T\Psi_{AT} + B_G\Psi_{BG}e^{-j\beta l} + \Gamma_1 B_T\Psi_{BT}e^{-j2\beta l}}{1 - \Gamma_1\Gamma_2 e^{-j2\beta l}} \tag{6.8}$$

By taking the autocorrelation of v_5, one obtains the noise power measured by the power meter as:

$$P_{BEC}(f) = |g|^2 \times \tag{6.9}$$

$$\frac{B_G^2 + B_T^2\rho_1^2 + A_T^2 + 2A_TB_T\mathrm{Re}\{\alpha_T\Gamma_1 e^{-j2\beta l}\}}{1 + \rho_1^2\rho_2^2 - 2\rho_1\rho_2\cos(2\beta l+\phi)}$$

where: $\phi = \phi_1 + \phi_2$

For many noise measurement systems, one can assume that all the small signal and noise parameters of the circuit elements are constant over the frequencies of interest and that all the frequency variations are accounted for by the length of the transmission line.

It can now be seen that the relative errors obtained in equation 6.3 depend on both the small signal parameters and the noise parameters of the composite receiver and the noise generator. If one attempts to obtain the maxima of the relative errors by analytic methods, the algebra becomes extremely complex. The problem can be simplified by assuming that the correlation coefficient, α_T, is zero. Given these assumptions, the error terms derived in equation 6.3 as a function of frequency are the following:

$$e_1 = \frac{G'(f_2)}{G(f_C)} f_O \tag{6.10}$$

$$= -\frac{4\pi l f_O}{v_p} \frac{2\rho_1\rho_2 \sin(2\beta l+\phi)}{1+\rho_1^2\rho_2^2 - 2\rho_1\rho_2\cos(2\beta l+\phi)}$$

$$e_2 = \frac{G''(f_1)}{G(f_C)} \frac{\delta f^2}{6} \tag{6.11}$$

$$= \frac{\rho_1\rho_2}{3} \left[\frac{4\pi l \delta f}{v_p}\right]^2 \times$$

$$\left[\frac{4\rho_1\rho_2 - (1+\rho_1^2\rho_2^2)\cos(2\beta l+\phi) - 2\rho_1\rho_2\cos^2(2\beta l+\phi)}{1+\rho_1^2\rho_2^2 - 2\rho_1\rho_2\cos(2\beta l+\phi)}\right]$$

If the phase of the reflection coefficients is a strong function of frequency this can be compensated for by adjusting the line length and the reflection coefficient phase in the model. If, however, the magnitude of the reflection coefficients is a strong function of frequency then the error terms will be altogether different from the results given above.

By applying some elementary calculus, it is possible to find the minimum and maximum values of the error terms given in equation 6.10 and equation 6.11. The first term has a maximum excursion of:

$$e_{10} = \pm \frac{4\pi l f_0}{v_p} \frac{2\rho_1\rho_2}{1-\rho_1^2\rho_2^2} \tag{6.12}$$

The second error term achieves a minimum value of:

$$e_{20} = \left[\frac{4\pi l \delta f}{v_p}\right]^2 \frac{\rho_1\rho_2}{3(1-\rho_1\rho_2)^2} \tag{6.13}$$

If the product $\rho_1\rho_2$ exceeds $4-\sqrt{15}$, then the second error term has a maximum value of:

$$e_{22} = \left[\frac{4\pi l \delta f}{v_p}\right]^2 \frac{1+34\rho_1^2\rho_2^2+\rho_1^4\rho_2^4}{48(1-\rho_1^2\rho_2^2)^2} \tag{6.14}$$

It is of interest to note that the power received and the error terms are cyclical functions of frequency and are all functions of the term $\cos(2\beta l+\phi)$. The frequency spacing of the extrema is inversely proportional to the transmission delay of the interconnecting line. A change in the phase of the reflection coefficients simply shifts the frequencies at which the extrema occur.

Figure 6.2 through figure 6.4 present graphs of the error terms for some typical values of circuit parameters. The worst case state (for error) of the PIN diode multiple impedance load has a reflection coefficient with a magnitude of .69 and a phase rotation equivalent to that induced by a 33 cm airline. The worst case state (for error) of the relay multiple impedance load has a reflection coefficient with a magnitude of .92 and a phase rotation equivalent to that induced by a 69 cm airline. The additional lines and fixtures in the cryogenic measurement configuration add a transmission delay equivalent to 33 cm of airline. Therefore, for the purposes of estimating the error when using the PIN diode multiple impedance load, a line length of 66 cm is used, and a line length of 102 cm is used to estimate the error when using the relay multiple impedance load. From figure 6.2 through figure 6.4, the maximum error due to a 1 MHz discrepancy is 32%, and therefore the 3 MHz frequency offset of the HP8970A is unacceptable. It must be remembered that these estimates are arrived at by ignoring the effect of the noise wave generator correlation, and therefore the error might even be larger than these figures indicate.

6.1.3 Power Measurement Errors

The noise power measured by the noise figure meter undergoes a random, time independent fluctuation, which results in a random error in the measured power. The

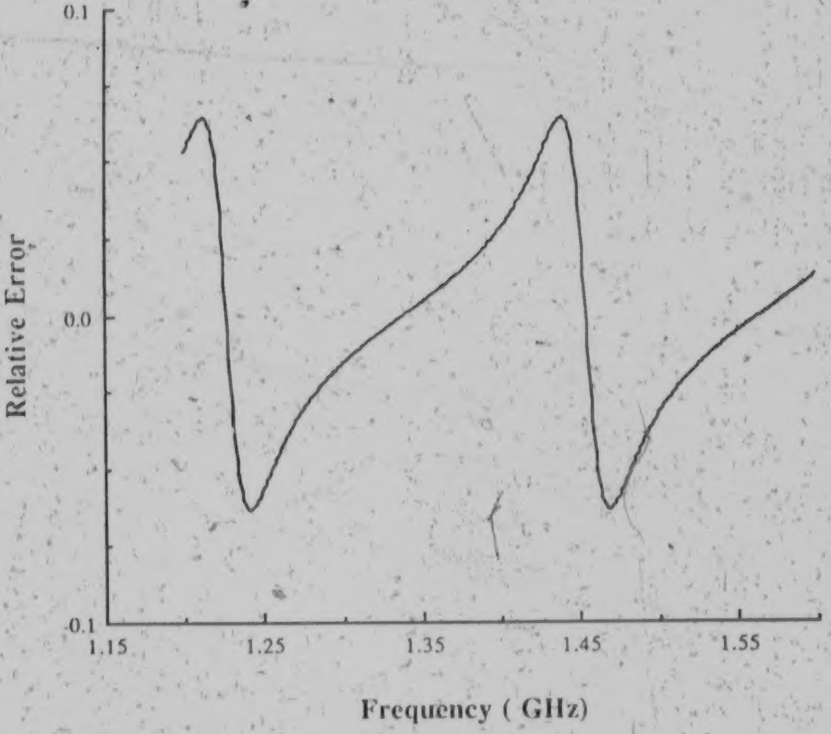

Figure 6.2 Relative Error Due to a 1 MHz Frequency Offset for Cryogenic Noise Measurement with the PIN Diode MIL (ρ_1=0.69, ρ_2=0.95, l=66 cm)

amplitude of the fluctuation depends in a complex manner upon the gains of the various stages of the noise measuring system and the amount of noise added at each stage and is therefore difficult to predict a-priori from circuit characteristics. However, an estimate of the expected error due to statistical fluctuation is easily obtained by making a number of power measurements and calculating the standard deviation. Then, the number of measurements and the integration time can be adjusted so that the uncertainty of the average of the measurements is sufficiently small. In

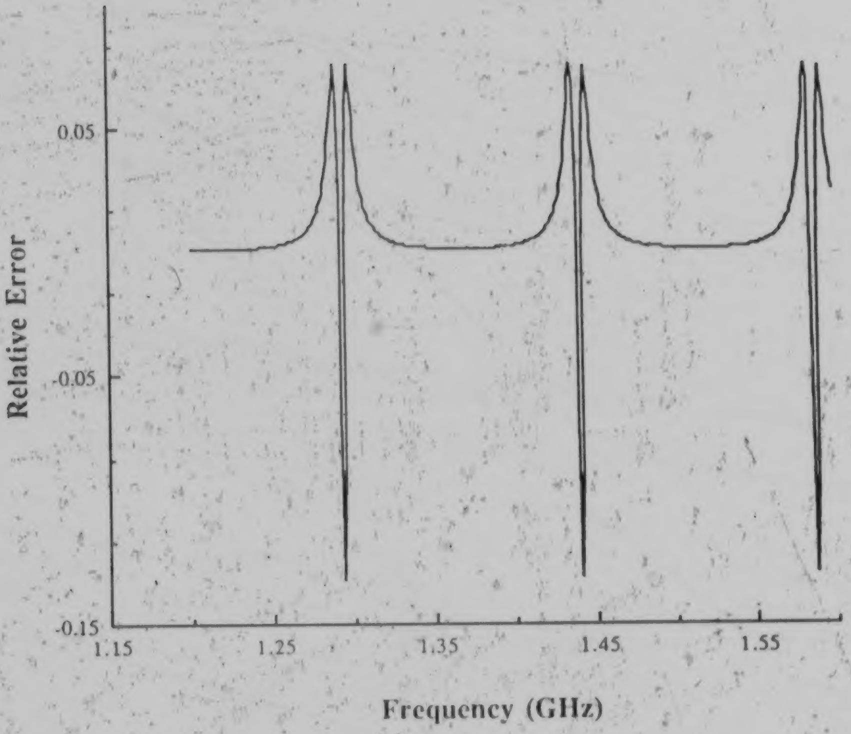

Figure 6.3 Relative Error Due to the 4 MHz Noise Measurement Bandwidth for Cryogenic Noise Measurement with the Relay MIL ($\rho_1=0.92$, $\rho_2=0.95$, $l=102$ cm)

the final measurements the integration time and the number of measurements were adjusted so that the population standard deviation of the power measurements was approximately 0.1%.

The signal and/or noise received by the noise figure meter is amplified and down-converted to 20 MHz in several stages, after which it is detected by a rather complicated detector comprising a specially manufactured diode and a circuit which provides D.C. bias current to the diode. The

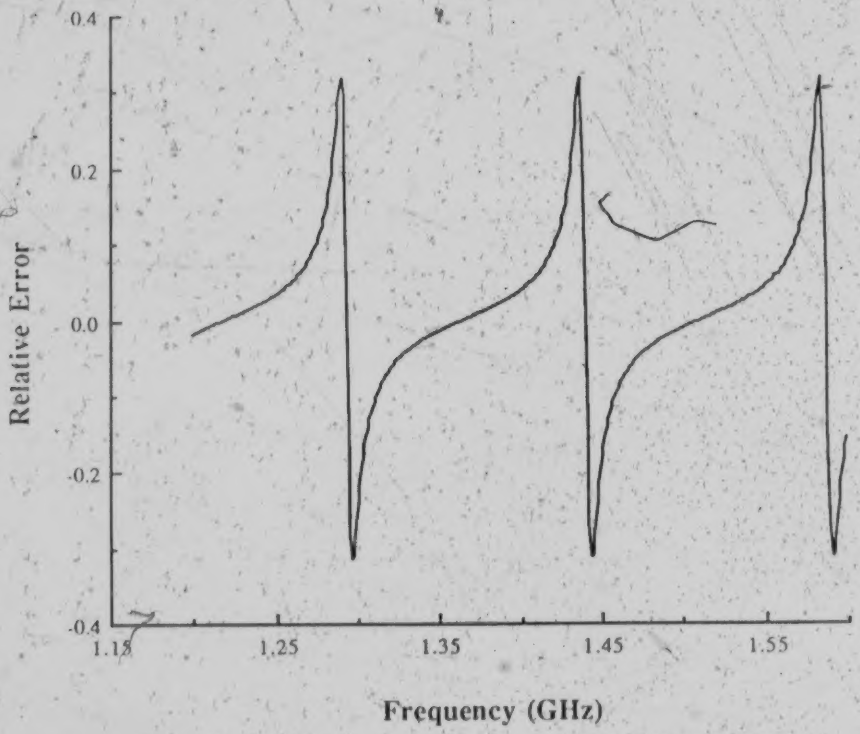

Figure 6.4 Relative Error Due to a 1 MHz Frequency Offset for Cryogenic Noise Measurement with the Relay MIL (ρ_1=0.92, ρ_2=0.95, l=102 cm)

detector output is proportional to voltage, and is measured by an A/D converter which integrates over one power line cycle. A microprocessor in the noise figure meter converts the readings to power, and averages a number of readings. The linearity of the detector depends on the bias current; therefore there is no a-priori reason to consider the detector linearity to be perfect. Using the frequency stabilisation scheme described in chapter 4 to reduce the power level fluctuations due to frequency drift, the detector was found to deviate 1.6% from perfect linearity

25 dB below the maximum power level permitted at the detector.

Chapter 7

Experimental Procedure and Results

This chapter explains how the equipment and techniques described in previous chapters were used to measure a cooled GaAsFET transistor, and presents the estimated noise parameters.

7.1 Room Temperature Experiments

The room temperature experiments were performed to check on the validity of the cryogenic results and to test the proposed measurement procedures. Initial measurements were performed with just the PIN diode multiple impedance load, and repeatedly generated non-physical noise parameter estimates. A sensitivity analysis indicated that the noise parameter estimates made with the PIN diode multiple impedance load alone were very sensitive to S-parameter measurement errors, and that it was necessary to build a load with very large reflection coefficients to reduce this sensitivity. Hence, the relay multiple impedance load was constructed, reducing the maximum sensitivity to about 20. Furthermore, this high sensitivity made it impossible to use simple adaptor models and fixture models. To get good results it was also found that the frequency offset of the noise measurement receiver had to be stabilized.

7.1.1 PIN Diode Multiple Impedance Load Noise Calibration

The PIN diode multiple impedance load was configured as a two-port tuner, with an HP346B noise source connected to port 1. The method described in section 3.4.2.1 was used to present a fixed reflection coefficient to the noise measurement receiver, shown in figure 7.1. The noise temperature at port 2 of the PIN diode multiple impedance load (see figure 3.2), with port 1 connected to a passive termination, was found to be within 5K of the ambient temperature, or 3K of the physical temperature of the load. Based on these results, the PIN diode multiple impedance load was treated as a passive two-port tuner for all the room temperature measurements.

7.1.2 Receiver and Noise Generator Calibration

A simplified diagram of the equipment configuration used for room temperature receiver calibration is shown in figure 7.2. Note that the PIN diode multiple impedance load can assume one of two noise temperatures for each reflection coefficient, depending on the state of the HP346C noise source. The measurement frequencies were chosen to be 1.2 GHz, 1.3 GHz, 1.4 GHz, and 1.5 GHz. The PIN diode multiple impedance load, the relay multiple impedance load, and the HP346C in the hot state were each connected to the noise measurement receiver and noise power measurements were made for all states. The noise parameters and gain bandwidth product of the receiver were estimated using the LRPG

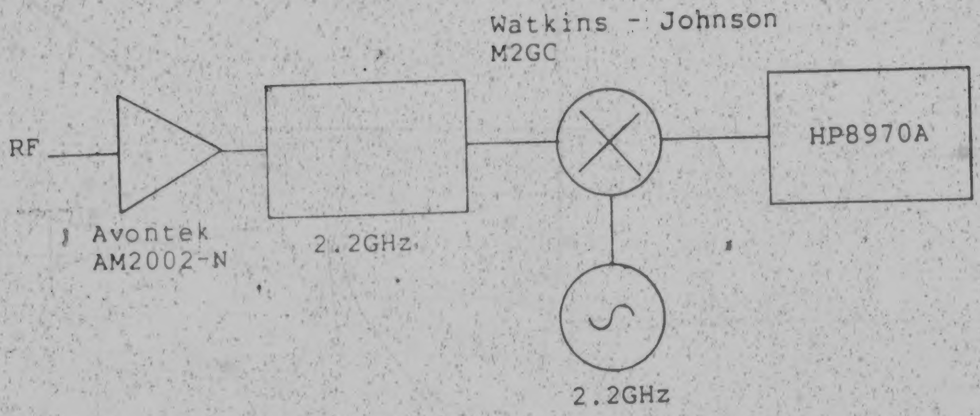

Figure 7.1 The Room Temperature Noise Measurement Receiver Used for Noise Temperature Calibration of the PIN Diode MIL

method, using all but the PIN diode multiple impedance load "hot" measurements. The noise temperature of the PIN diode multiple impedance load in the "hot" state was then estimated using the two-power method described in section 5.1.2.

7.1.3 FET and Passive DUT Noise Measurements

A simplified diagram of the equipment configuration used for room temperature noise measurements is shown in figure 7.3. The fixture used is an earlier version than the one described in chapter 4, and cannot be calibrated to the transistor socket. A Mitsubishi MGF 1412 GaAs FET was chosen

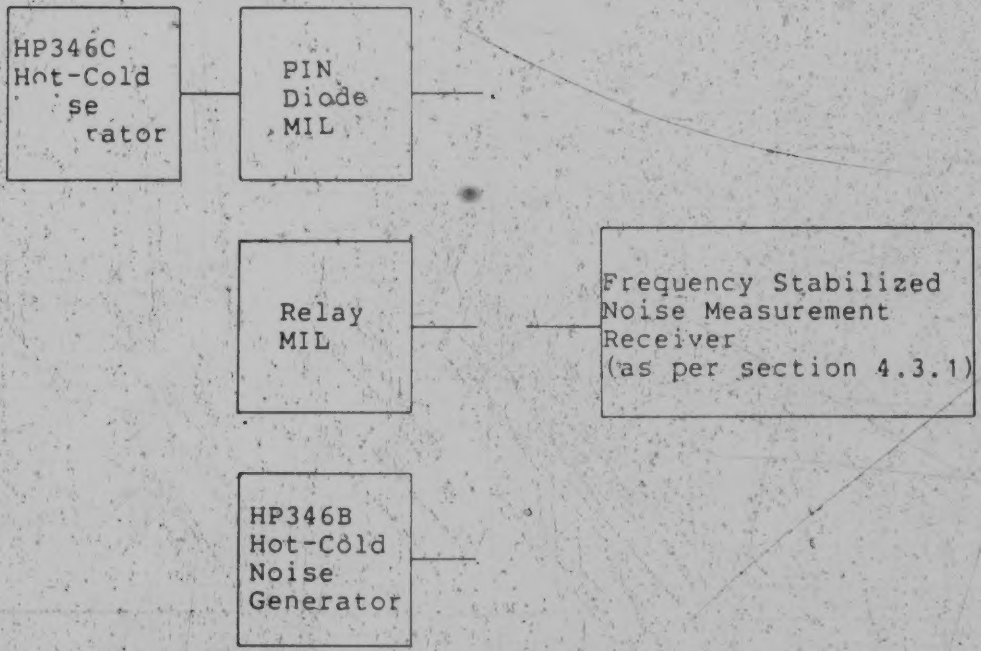
HP346C
Hot-Cold
se
rator
PIN
Diode
MIL
Relay
MIL
Frequency Stabilized
Noise Measurement
Receiver
(as per section 4.3.1)
HP346B
Hot-Cold
Noise
Generator

Figure 7.2 The Room Temperature Receiver Calibration Configuration

as the active DUT, and was biased at 3.00 V drain to source voltage and 15.0 mA drain current. The relay multiple impedance load and the PIN diode multiple impedance load were each connected to the DUTs, and power measurements made for each state. The noise parameters of the RUTs were then estimated using the LRPG method. The receiver noise parameters were then de-embedded from the noise parameters of the RUT (using the equations of section 3.4.3) to obtain the noise parameters of the DUTs. At this point the noise parameters of the passive DUT required no further de-embedding; however, the noise parameters and S-parameters of the fixture, the bias tees, and the attenuator had to be

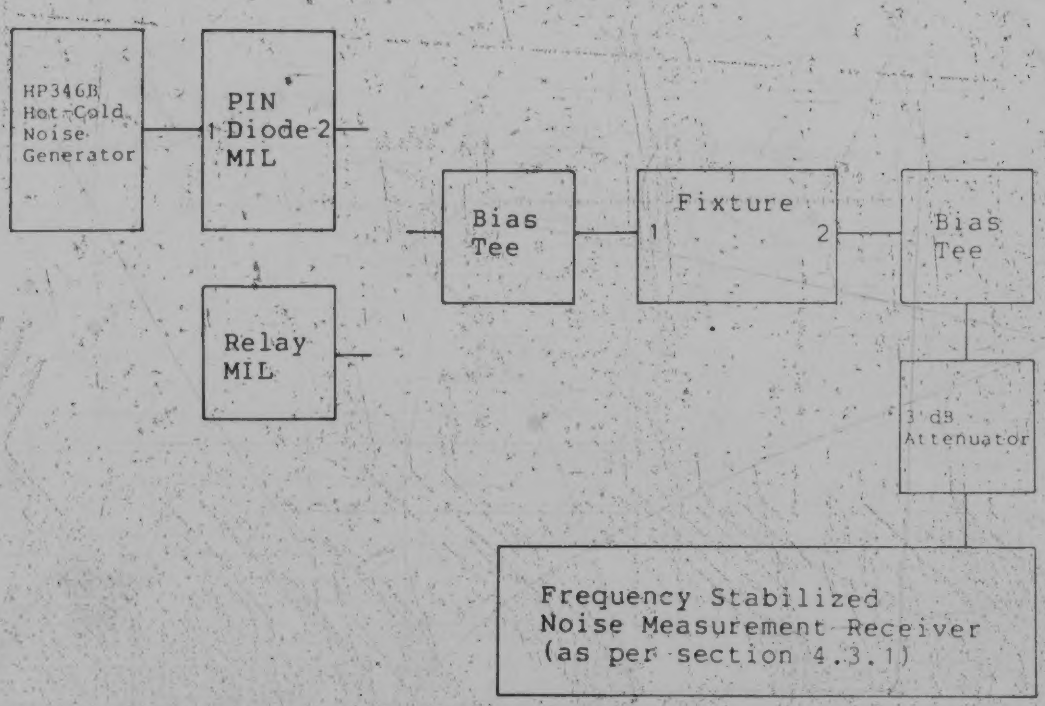
HP346B Hot-Cold Noise Generator
1 PIN Diode 2 MIL
Relay MIL
Bias Tee
Fixture
1
2
Bias Tee
3 dB Attenuator
Frequency Stabilized Noise Measurement Receiver (as per section 4.3.1)

Figure 7.3 The Room Temperature Noise Measurement Configuration

de-embedded to obtain the noise parameters and S-parameters of the FET. Although, the noise parameters of the attenuator and bias-tees were de-embedded without difficulty, it was not possible to de-embed the noise parameters of the fixture. The reason for this is that the fixture used was not constructed in such a manner as to make it possible to measure its S-parameters to the transistor socket, and the fixture itself was unreliable because certain ground plane electrical connections, made with silver epoxy, failed repeatedly. Results are given in table 7.1 through table 7.5.

7.2 The Cryogenic Measurements

Simplified diagrams of the equipment configurations used for cryogenic measurements are shown in figure 7.4 and figure 7.5. The fixture used was described in chapter 4. Relay K7 connects the appropriate multiple impedance load to the fixture. Relay K8 connects the appropriate noise generator to port one of the PIN diode multiple impedance load. Each reflection coefficient state of the PIN diode multiple impedance load can assume one of three noise temperatures. The coldest noise temperature (called the "cold" state) is assumed when relay K8 connects the cryogenic termination to the multiple impedance load. The next highest noise temperature (called the "warm" state) is assumed when relay K8 connects the HP346B noise source to the multiple impedance load, and the noise source is off. The highest noise temperature (called the "hot" state) is assumed when relay K8 connects the HP346B noise source to the multiple impedance load, and the noise source is on. Thus the PIN diode multiple impedance load actually has forty-eight possible states. The noise temperature of each state of the relay multiple impedance load is assumed to be its physical temperature. In figure 7.4 the apparatus can be divided into two two-ports. The first, consisting of all the connections between side one of the fixture socket and port one of the cryostat, will be referred to as the 'input line'. The second, consisting of all the connections between side two of the fixture socket and port two of the cryostat,

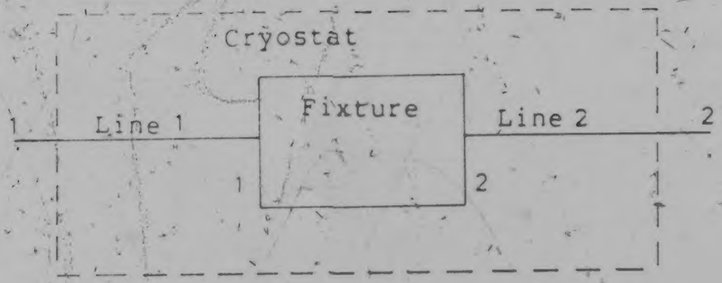
Cryostat
Fixture
1
Line 1
Line 2
2
1
2
1

Figure 7.4 The Cryogenic S-parameter Measurement Configuration

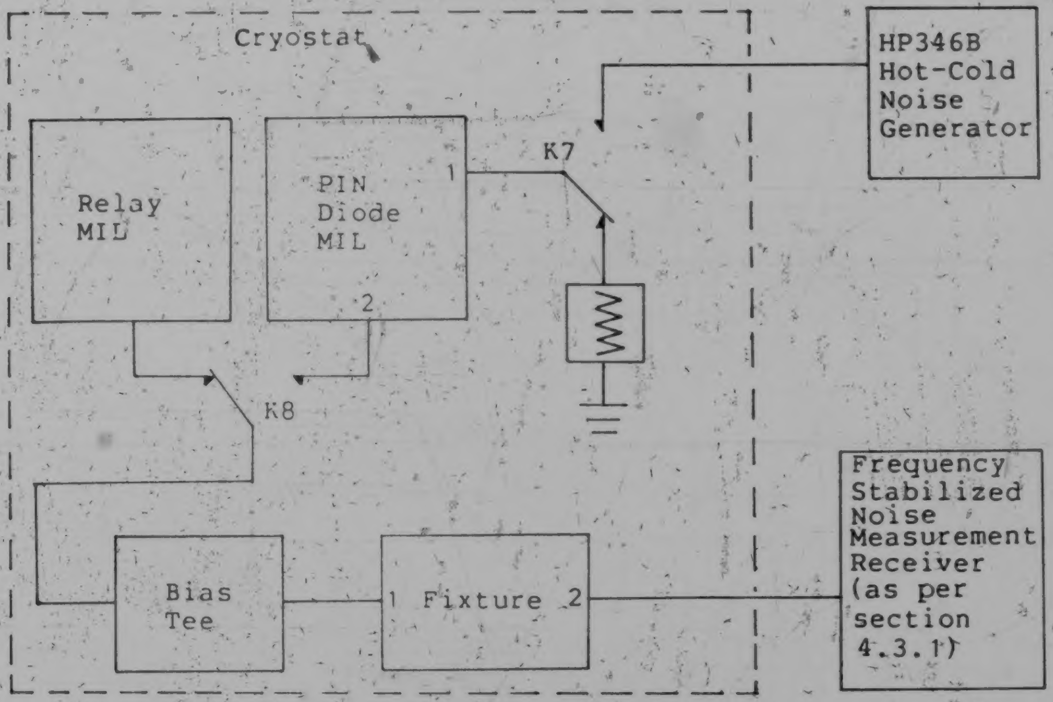
Cryostat
HP346B Hot-Cold Noise Generator
Relay MIL
PIN Diode MIL
1
2
K7
K8
Bias Tee
1
Fixture
2
Frequency Stabilized Noise Measurement Receiver (as per section 4.3.1)

Figure 7.5 The Cryogenic Noise Measurement Configuration

will be referred to as the 'output line'. Note that the output line is present in both measurement configurations.

The measurement frequencies were chosen to be 1.2 GHz, 1.3 GHz, 1.4 GHz, 1.5 GHz, and 1.6 GHz. It should be noted that no results for the GaAsFet are presented at 1.3 GHz; this is because the noise parameter estimate for the passive DUT is so clearly in error at that frequency. In addition, none of the noise parameter estimates for the GaAsFET were physical at this frequency, and it was not possible to complete many of the calculations. Cryogenic S-parameter and noise parameter measurements were made of a passive device and the same Mitsubishi MGF 1412 GaAsFET used for room temperature measurements. The FET was placed in the fixture with the drain connected to side 2 of the fixture and the gate to side 1. The drain-to-source DC bias voltage was held at 3.00 V. The FET measurements were repeated for drain currents of 10 mA, 15 mA , and 20 mA. The passive DUT was a 200 Ohm chip resistor, with gold-plated tabs soldered on each end. When used, this DUT was placed in the fixture socket in series between the two halves of the fixture.

7.2.1 Cryogenic S-parameter Calibrations

The three S-parameter calibration standards were placed in the fixture and S-parameter measurements were made at the cryostat ports. The models in figure 4.21 through figure 4.23 were assumed as models for the S-parameter calibration standards. The S-parameters of the input line and the output line were estimated by the method discussed in section 5.2. The root mean square discrepancy between the measured and predicted value of M_{33} was 0.031. The S-parameters of the passive DUT and of the FET in the cryostat were then measured. Finally, the S-parameters of the input and output lines were de-embedded from these measurements, to obtain the S-parameters of the passive DUT and the FET referred to the fixture socket. The FET S-parameters are given in table 7.6.

The measurement configuration was then changed to that of figure 7.5. The through-line calibration standard was inserted in the fixture, and reflection coefficient measurements were made at port two of the cryostat. The reflection coefficients of the multiple impedance loads at side one of the fixture socket were obtained by de-embedding the S-parameters of the output line and of the through-line from these measurements.

7.2.2 Noise Generator Calibration

For the purposes of noise temperature calibration of the PIN diode multiple impedance load, the receiver in figure 4.20 was used without the bias tee and the attenuator at the input. The noise parameters and gain of this receiver were estimated from a single noise temperature measurement using the method of section 3.4.4. The noise behavior of the output line was assumed to be the same as if the entire line had a physical temperature of 175K. This receiver was then connected to the cryostat, with the through-line in the fixture socket, and noise power measurements were made for each state of the PIN diode and relay multiple impedance loads. The output noise temperature of the PIN diode multiple impedance load at the input side of the fixture socket was then found using the method described in section 5.1.1.

7.2.3 The Passive DUT Noise Measurements

For the purposes of passive DUT noise measurements, the receiver in figure 4.20 was used again without the bias tee and the attenuator at the input. The passive DUT was placed in the fixture in the configuration of figure 7.5, and noise power measurements were made for each state of the PIN diode and relay multiple impedance loads. The physical temperature of the fixture was between 10.7K and 14.5K. Noise parameters of the RUT comprising the passive DUT, the output line and the noise measurement receiver were estimated using the LRPG method described in chapter 3. The estimated noise parameters of the receiver were finally de-embedded from the estimated RUT parameters to obtain the estimated parameters of the passive DUT cascaded with the output line. However, upon attempting to de-embed the output line from these last results, using the procedure in section 3.4.3, the noise parameters were sufficiently non-physical that de-embedding was not possible.

7.2.4 The Cryogenic FET Noise Measurements

For the purposes of FET noise measurements, the receiver in figure 4.20 was used. The attenuator at the input was necessary to prevent oscillations. The FET was placed in the fixture in the configuration of figure 7.5, and noise power measurements were made for each state of the PIN diode and relay multiple impedance loads. for drain bias currents of 10 mA, 15 mA and 20 mA. The physical temperature of the fixture was between 10.7K and 14K. Noise parameters of the RUT comprising the FET, the output line and the noise measurement receiver were estimated using the LRPG method described in chapter 3. The estimated noise parameters of the receiver and output line were then de-embedded from the estimated RUT parameters to obtain the estimated parameters of the FET. These results are given in table 7.7.

7.2.5 Iterative Improvement of the S-parameter Calibration

In an effort to improve the accuracy of the noise parameter estimates, an improved S-parameter calibration was sought. Additional circuit elements were added to the models of the S-parameter calibration standards as shown in figure 4.24 through figure 4.26. The values of these components were iteratively adjusted to minimise the RMS discrepancy between the predicted and actual values of M_{33}. The final RMS discrepancy was 0.012. All the calculations based on the S-parameter calibrations were then repeated, reducing the RMS error of fit from approximately 15K to 10K. The S-parameters and noise parameters of the FET and the passive DUT improved by iteration are given in table 7.8 through table 7.11. In addition, de-embedding the output line from the passive DUT now proved possible. Passive DUT noise parameters, predicted from S-parameters, are presented so that they may be compared to the noise parameters estimated from power measurements as a test of the validity of the noise parameter estimation procedure.

Table 7.1 Room Temperature Passive DUT S-Parameters

Frequency	S_{11}		S_{21}		S_{12}		S_{22}	
(GHz)	Mag.	Ang.	Mag.	Ang.	Mag.	Ang.	Mag.	Ang.
1.200	.65	52	.65	23	.65	23	.50	173
1.300	.77	29	.54	-10	.55	-10	.59	128
1.400	.87	6	.41	-43	.41	-44	.68	84
1.500	.95	-20	.25	-77	.25	-78	.75	40

Table 7.2 Passive DUT Room Temperature Noise Parameter Estimated from S-Parameters

Frequency	T_{MIN}	T_N	Γ_{OPT}	
(GHz)	(K)	(K)	Mag.	Ang.
1.200	105	182	.64	-52
1.300	116	195	.74	-28
1.400	121	207	.85	-4
1.500	140	234	.94	20

Table 7.3 Measured Passive DUT Room Temperature Noise Parameters

Frequency	T_{MIN}	T_N	Γ_{OPT}		RMS Error
(GHz)	(K)	(K)	Mag.	Ang.	(K)
1.200	93	165	.65	-50	6
1.300	99	171	.76	-28	11
1.400	109	186	.86	-4	9
1.500	163	239	.93	20	10

Table 7.4 FET Room Temperature S-Parameters

MGF1412 GaAs FET 3.00 V 15.0 mA in Fixture

Frequency	S_{11}		S_{21}		S_{12}		S_{22}	
(GHz)	Mag.	Ang.	Mag.	Ang.	Mag.	Ang.	Mag.	Ang.
1.200	.97	17	3.84	-162	.028	113	.66	19
1.300	.98	-10	3.80	170	.030	87	.66	-6
1.400	.97	-35	3.80	145	.032	61	.67	-31
1.500	.97	-60	3.78	119	.034	35	.66	-57

Table 7.5 FET Room Temperature Noise Parameters

MGF1412 GaAs FET 3.00 V 15.0 mA in Fixture

Frequency (GHz)	T_{MIN} (K)	T_N (K)	Γ_{OPT} Mag.	Γ_{OPT} Ang.	RMS Error (K)
1.200	24	62	.80	-26	15
1.400	20	34	.89	25	10
1.500	28	74	.78	49	18

Table 7.6 FET Cryogenic S-Parameters Before Iteration

MGF1412 GaAsFET 3.00 V 10 mA

Frequency	S_{11}		S_{21}		S_{12}		S_{22}	
(GHz)	Mag.	Ang.	Mag.	Ang.	Mag.	Ang.	Mag.	Ang.
1.200	.98	-25	4.01	156	.026	68	.64	-22
1.400	.99	-31	4.18	34	.032	-52	.63	98
1.500	.98	-32	3.96	-28	.032	-114	.64	-25
1.600	.98	-34	4.04	-88	.034	-174	.66	-142

MGF1412 GaAsFET 3.00 V 15 mA

Frequency	S_{11}		S_{21}		S_{12}		S_{22}	
(GHz)	Mag.	Ang.	Mag.	Ang.	Mag.	Ang.	Mag.	Ang.
1.200	.98	-27	4.44	156	.025	68	.61	-23
1.400	.99	-33	4.64	34	.030	-52	.60	98
1.500	.98	-33	4.40	-29	.030	-115	.61	-25
1.600	.98	-36	4.50	-89	.033	-174	.63	-143

MGF1412 GaAsFET 3.00 V 20 mA

Frequency	S_{11}		S_{21}		S_{12}		S_{22}	
(GHz)	Mag.	Ang.	Mag.	Ang.	Mag.	Ang.	Mag.	Ang.
1.200	.98	-27	4.70	155	.024	68	.59	-23
1.400	.99	-34	4.90	33	.029	-53	.58	98
1.500	.98	-34	4.64	-29	.029	-115	.59	-25
1.600	.98	-37	4.76	-90	.032	-175	.61	-143

Table 7.7 FET Cryogenic Noise Parameters Before Iteration

MGF1412 GaAsFET 3.00 V 10 mA

Frequency (GHz)	T_{MIN} (K)	T_N (K)	Γ_{OPT}		RMS Error (K)
			Mag.	Ang.	
1.200	10	20	.87	18	15
1.400	9	29	.81	22	12
1.500	13	30	.82	23	13
1.600	11	21	.85	24	11

MGF1412 GaAsFET 3.00 V 15 mA

Frequency (GHz)	T_{MIN} (K)	T_N (K)	Γ_{OPT}		RMS Error (K)
			Mag.	Ang.	
1.200	11	21	.85	19	15
1.400	9	30	.80	22	12
1.500	13	30	.81	24	13
1.600	11	22	.84	25	11

MGF1412 GaAsFET 3.00 V 15 mA

Frequency (GHz)	T_{MIN} (K)	T_N (K)	Γ_{OPT}		RMS Error (K)
			Mag.	Ang.	
1.200	11	22	.85	19	15
1.400	9	31	.79	23	12
1.500	14	31	.81	24	13
1.600	12	25	.83	26	11

Table 7.8 Passive DUT Cryogenic S-parameters Improved by Iteration

Frequency (GHz)	s_{11}		s_{21}		s_{12}		s_{22}	
	Mag.	Ang.	Mag.	Ang.	Mag.	Ang.	Mag.	Ang.
1.200	.71	-8	.29	-9	.29	-9	.64	-10
1.300	.70	-9	.28	-69	.28	-69	.65	-125
1.400	.69	-11	.30	-129	.30	-129	.65	115
1.500	.71	-11	.28	171	.28	171	.64	-9
1.600	.69	-12	.29	110	.29	110	.66	-125

Table 7.9 Passive DUT Cryogenic Noise Parameters Estimated From S-parameters Improved by Iteration

Frequency	T_{AT}	T_{BT}	α_T	
(GHz)	(K)	(K)	Mag.	Ang.
1.200	53	52	.999	-172
1.300	55	53	.996	-171
1.400	48	49	1.001	-169
1.500	54	53	.998	-169
1.600	51	50	.998	-168

Table 7.10 Measured Passive DUT Cryogenic Noise Parameters Improved by Iteration

Frequency	T_{AT}	T_{BT}	α_T		RMS Error
(GHz)	(K)	(K)	Mag.	Ang.	(K)
1.200	49	54	.998	-157	16.67
1.300	-110	-27	1.195	-4	15.76
1.400	14	50	1.100	-150	15.76
1.500	69	67	.979	-172	15.78
1.600	21	34	1.115	-143	18.35

Table 7.11 FET Cryogenic Noise Parameters Improved by Iteration

MGF1412 GaAs FET 3.00 V 10 mA

Frequency (GHz)	T_{MIN} (K)	T_N (K)	Γ_{OPT} Mag.	Γ_{OPT} Ang.	RMS Error (K)
1.200	14	19	.85	21	8
1.400	5	18	.85	26	5
1.500	13	28	.79	28	14
1.600	11	15	.87	30	14

MGF1412 GaAs FET 3.00 V 15 mA

Frequency (GHz)	T_{MIN} (K)	T_N (K)	Γ_{OPT} Mag.	Γ_{OPT} Ang.	RMS Error (K)
1.200	13	18	.85	22	9
1.400	5	19	.84	27	5
1.500	13	29	.78	28	14
1.600	11	16	.86	31	14

MGF1412 GaAs FET 3.00 V 20 mA

Frequency (GHz)	T_{MIN} (K)	T_N (K)	Γ_{OPT} Mag.	Γ_{OPT} Ang.	RMS Error (K)
1.200	14	19	.85	23	9
1.400	6	22	.83	28	5
1.500	13	30	.77	29	13
1.600	13	17	.85	32	14

Table 7.12 FET Cryogenic S-Parameters Improved by Iteration

MGF1412 GaAs FET 3.00 V 10 mA

Frequency	s_{11}		s_{21}		s_{12}		s_{22}	
(GHz)	Mag.	Ang.	Mag.	Ang.	Mag.	Ang.	Mag.	Ang.
1.200	.99	-30	4.42	153	.029	65	.70	-21
1.300	.97	-31	4.43	150	.031	65	.69	-24
1.400	1.00	-37	4.73	148	.037	62	.68	-28
1.500	.99	-37	4.44	146	.035	60	.69	-27
1.600	.98	-41	4.67	143	.039	57	.68	-32

MGF1412 GaAs FET 3.00 V 15 mA

Frequency	s_{11}		s_{21}		s_{12}		s_{22}	
(GHz)	Mag.	Ang.	Mag.	Ang.	Mag.	Ang.	Mag.	Ang.
1.200	.98	-31	4.89	152	.027	64	.67	-22
1.300	.97	-33	4.92	150	.030	65	.66	-24
1.400	1.01	-39	5.25	148	.034	62	.65	-29
1.500	.99	-39	4.94	145	.034	59	.66	-27
1.600	.97	-43	5.19	142	.038	57	.65	-33

MGF1412 GaAs FET 3.00 V 20 mA

Frequency	s_{11}		s_{21}		s_{12}		s_{22}	
(GHz)	Mag.	Ang.	Mag.	Ang.	Mag.	Ang.	Mag.	Ang.
1.200	.98	-32	5.17	151	.026	64	.65	-22
1.300	.97	-34	5.20	149	.029	64	.64	-25
1.400	1.01	-40	5.54	147	.033	61	.62	-29
1.500	.99	-40	5.20	145	.033	59	.64	-28
1.600	.97	-44	5.49	141	.037	56	.63	-33

Chapter 8

The APL Programs

The experimental work described in this thesis generated a large volume of data which needed to be reduced by various methods of curve fitting, cascading, de-embedding, circuit element modeling and numerical sensitivity analysis. Many of these calculations were sufficiently lengthy that they could not reliably be done by hand. In general, each calculation had to be repeated at each measurement frequency and for each state of the noise generator. The number of generator states and measurement frequencies varied from experiment to experiment. The circuit analysis programs COMPACT and TOUCHSTONE were available; it was decided not to use these programs because they did not support calculations for multiple circuit states and did not allow the user to write new noise parameter estimation subroutines.

A software package called IMPCAP (for Interactive Multiple Parameter Circuit Analysis Program) was written by this author in APL[7] and was used for all the modelling and noise parameter estimation performed for this thesis. The purpose of this chapter is to present the details of this software package, including the syntax and data structure which have been developed. Appendix 2 contains a brief summary of each program, and a complete listing (about three hundred pages) can be obtained from the author. Although the program has been written in APL, it is hoped that this information would be useful if such a program were to be written in another computer language.

---

[7] VS APL Release 3, © International Business Machines Corporation 1975,1976,1978 modified for the Michigan Terminal System at the University of Alberta

8.1 The APL Language

APL is a programming language based on a number of unusual concepts. Program and variable names are made up of characters from an alphabet which is extended beyond the usual Roman characters. A single file is used to hold both the programs and the data. APL has on the order of sixty predefined functions, each represented by a special symbol. With a few minor exceptions, these functions are defined for array as well as scalar operations. For those not familiar with APL, a brief description is given in chapter 2.

8.2 The IMPCAP Workspace

The IMPCAP workspace contains some two hundred functions which comprise approximately fifty kilobytes of source code. The "subroutine" nesting can be deeper than ten levels in extreme instances. As a result, a high degree of organization and good documentation is required to maintain system integrity.

In the IMPCAP workspace each circuit element is represented by an array of rank 3 or more, henceforth referred to as the "standard form". The standard form tabulates the circuit parameters against frequency and contains flags which indicate which sets of circuit parameters are tabulated and what type of circuit element is represented. The standard form consists of a number of sub-arrays, each of which contains data referring to a particular type of circuit parameter. This scheme is inefficient in utilizing computer memory because space must be allotted for each possible type of circuit parameter, even if that circuit parameter is not specified for a particular circuit element. In addition this scheme is very difficult to modify, making programming more time consuming. The CPU time used to transfer data in and out of this format is greater than that used to transfer data to an array with a single axis (a vector). For these reasons the structure of the standard form will not be described in detail. A much better scheme, which has been tried in another application, but which has not yet been implemented for IMPCAP, is to store the data in a vector, with pointers to indicate how the elements of the vector are allocated.

When an IMPCAP function handles a standard form variable, it first passes that variable to a common subroutine which transfers the data to smaller (secondary) arrays each of which contain a particular type of circuit parameter. The name of each of these secondary arrays is fixed from program to program, and this simplifies the programmers job enormously. These secondary arrays all have a similar structure, and this also simplifies programming. The first array axis indexes the real and imaginary parts of the data, and is of length one if the data is real. The second axis indexes the frequency and the third axis indexes the various parameters. If it is desired to store data corresponding to different circuit states in one array, the fourth and higher axes are used to index the data corresponding to the different circuit states. For example, if some circuit element is varied, the fourth axis can be used to index the data corresponding to the different states of that element. If a second circuit element is also varied independently, the fifth axis can be used to index the data corresponding to the states of the second element, and so on.

The standard form can represent one of three types of circuit elements, and contains different sets of circuit parameters for each type. The standard for for the three types of circuit elements are described below.

1. A one-port. The standard form representing a one-port contains two sets of one-port small signal parameters, a set of one-port noise parameters, the small signal gain and an auxiliary field useful for indicating error, uncertainty or noise temperature. The primary small signal parameter and noise temperature refer to the conditions at the terminals of the one-port. The available gain, and the additional noise temperature and reflection coefficient allow one to store (and manipulate) the gain, excess noise temperature and generator reflection coefficient of a cascade.
2. A two-port. The standard form representing a two-port

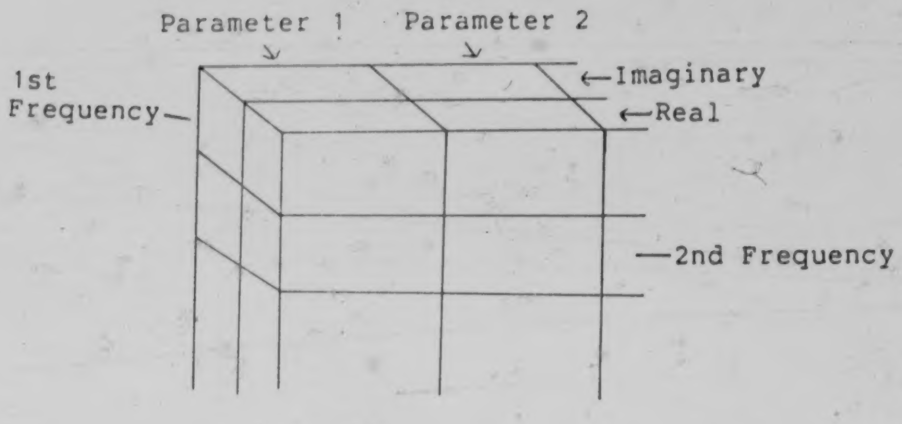

Figure 8.1 The Array Structure for Complex Data

contains one set of small signal parameters and one set of two-port noise parameters. Both sets of parameters refer to the conditions at the terminals of the two-port.

3. A "receiver". This is actually a two-port with one port inaccessible, hence the small signal parameters are those of a one-port, but the noise parameters are those of a two-port. The standard form representing a receiver contains two sets of one-port small signal parameters, one set of two-port noise parameters, the small signal gain and an auxiliary field. This arrangement allows one to store the input reflection coefficient, noise parameters and power gain of a receiver, as well as a noise measurement of some sort and the generator reflection coefficient with which that measurement was made.

The IMPCAP workspace is a closed within open design. Since the manipulations involved in the circuit modeling, sensitivity analysis and noise parameter estimation required for this thesis were unpredictable as to nature and sequence, the functions which implement these things were written as an open workspace. However, data entry into the standard form is repetitive (leading to more frequent user error) and predictable, so this part of IMPCAP was written in closed form.

The functions in the workspace are divided into four classes. The first class is that of the functions intended to be executed directly by the user. These are the main IMPCAP functions. Data is expected in standard form, and this data is checked for errors. The next class is that of the specific subroutines. These functions are executed only by one or by a limited number of main IMPCAP functions or other specific subroutines. Yet another class is the class of general subroutines. These are executed by many of the main IMPCAP functions and by the specific subroutines. The last class of functions consists of those that function as system variables. The system variables have been replaced by niladic functions so that they cannot be easily changed, and so that changes which are made can be documented. None of the subroutines expect data in standard form, and most do not check the data for errors, since this is the programmers responsibility.

IMPCAP functions and variables are named so as to allow the user to distinguish between classes of objects, and to avoid inadvertent conflicts between object names. Names starting with A through Z are reserved for variables and functions generated by the user, and for local variables. Names starting with $\underline{A}$ through $\underline{Z}$ are used for IMPCAP functions intended to to be executed directly by the user (the "main IMPCAP functions"), and for global variables used to transfer data to IMPCAP subroutines. Names starting with Δ and $\underline{\Delta}$ are reserved for IMPCAP subroutines and IMPCAP system variables. The IMPCAP subroutines are subdivided into the three classes by further naming conventions which are not discussed here.

Workspace integrity is maintained by a number of devices. All the main IMPCAP functions are written so as to be independent of all the other main IMPCAP functions and all but two of the global variables. This is easily verified by erasing all the global variables and executing the function under test. If any "new" variables appear, these are used in the function under test and have not been declared. Thus there is no way a main IMPCAP function can be affected by modifying any other global variable or any other main IMPCAP function. The general subroutines and the system variable subroutines are short, well documented and changed infrequently. In addition there is an IMPCAP function which will insert a line with the time, date and IMPCAP version as the second line in a function. This program is used religiously after every change to an IMPCAP function, and in this way version control is maintained.

8.2.1 Some Details

Since this version of APL has no special internal representation for complex numbers, some convention must be used to represent complex numbers, and functions are required to perform complex arithmetic. The public workspace 46 COMPLEX contains an extensive library of functions for complex arithmetic, and uses a convention whereby a complex variable is represented by an array whose first axis is of length two and indexes the real and imaginary parts of the array. This convention was used for all the complex variables in the IMPCAP workspace, and many of the functions in 46 COMPLEX are used as general subroutines. Real data in the IMPCAP workspace is represented by a similar array, with the first axis of length one. Most of the general subroutines are written in such a way as to accept arrays with any number of additional axis of any length, and to perform manipulations on all the array elements simultaneously. In this way, looping to handle successive frequencies and successive circuit element states is completely avoided.

Every main IMPCAP function begins by calling a general subroutine which transfers the data from each standard form argument into five 46 COMPLEX type variables (one for each parameter set) and generates additional variables indicating the type of circuit parameters, the frequencies tabulated, and some identifying information. If both arguments of the function are in standard form, they must represent the same set of frequencies and be of the same rank. After calling a data transfer subroutine, every main IMPCAP function then calls a general subroutine which transforms each of the sets of circuit parameters to the type required, and checks that all the required data is available. Any data returned by a main IMPCAP function is assembled into standard form by a general subroutine. Because the same four subroutines are used for all the data transfer operations, consistency is easy to maintain, and modifications are easily implemented.

The problem of parameter conversion is complicated by the large number of two-port small signal and noise parameter sets, and by the fact that one would prefer not to have to write conversion subroutines between each pair. This problem was solved by using a chart, generated by a niladic function, indicating which sequences of conversion subroutines lead to a particular parameter type. The main conversion subroutine is given the data to be converted (in 46 COMPLEX form), flags indicating which parameter sets are required, and uses the chart to choose the appropriate sequence of subroutines to obtained the desired parameter set. If there is no sequence leading to the desired parameter set, an error message is returned. This scheme performs parameter type checking as well as parameter conversion, and allows one to start with very few conversion routines, adding more routines at will.

A summary of the main IMPCAP functions is given in appendix 2.

Conclusions

A noise generator having an electronically controlled reflection coefficient and operating at both room temperature and cryogenic temperatures was built. The use of this noise generator for room temperature and cryogenic noise parameter measurements was demonstrated. When measuring devices which have a high input reflection coefficient, the accuracy of the method was not very high. However, the major sources of error were identified and progress was made in reducing these errors.

The original noise parameter estimates were very sensitive to S-parameter measurement errors. This problem was alleviated by increasing the accuracy of the S-parameter test set, and by adding noise generator states that have high reflection coefficients. The added reflection coefficients reduced the condition number of the least squares estimate and the sensitivity of the estimated noise parameters to measurement errors.

A number of new measurement techniques were developed. A method was developed of holding the noise temperature of the noise measurement receiver constant; this makes it easier to determine the noise contribution of the receiver. Another method was developed whereby the noise parameters of a composite noise measurement receiver can be determined from one noise temperature measurement of the composite receiver and one two-port S-parameter measurement of the unilateral element which is the front end of the composite receiever. The unilateral element is only assumed to be passive and unilateral; no other conditions need be met. A new S-parameter calibration method was introduced which allowed the use of simple, lossless, broadband calibration standards to calibrate the S-parameters of the fixture and the associated transmission lines to the fixture socket. Because the standards were lossless, their behavior was easy to predict at cryogenic temperatures.

Material presented in this thesis shows that a frequency discrepancy between the measurement frequency for small signal measurements and noise measurements can be treated as an error in the power measurements. The error is first found as a function of the frequency discrepancy, the noise measurement bandwidth, and the first and second derivatives of the power spectral density with respect to frequency. Formulae are presented which predict the error for the common situation where the noise generator and receiver have reflection coefficients whose magnitude is not a function of frequency. These results demonstrate that measurement errors increase as the magnitude of the reflection coefficients of receiver and generator increases and as the rate of phase rotation of these reflection coefficients with frequency increases. This thesis describes a system which reduces the frequency discrepancy by at least a factor of ten.

The author introduced the use of the singular value decomposition and the condition number to estimate the uncertainty of the least squares of noise parameters. These concepts proved a useful conceptual tool in redesigning the experimental apparatus to reduce the sensitivity of the noise parameter estimates to measurement errors. However, the rank-reduced fitting procedures have met with limited success, possibly due to the lack of alternative accurate experimental data.

The author has introduced a new notation which simplifies the circuit analysis of linear noisy networks. This new notation was used to derive new equations for cascading and de-embedding linear noisy two-ports, and to perform the circuit analysis for a new method of receiver noise parameter calibration (that using a unilateral element) mentioned above.

A program was written and tested that performs circuit analysis of noisy linear networks for a large number of circuit states and frequencies simultaneously. This program was invaluable in the modelling of the noise measurement system and in the estimation of noise parameters. Because the source code was available, new noise parameter estimation algorithms were easily implemented. Some aspects of this program are discussed in the thesis.

Recommendations

The task of measuring low noise GaAs FET parameters at L-band is very difficult because of the extremely high gate (input) reflection coefficient of these devices in this region. This task should become simpler as frequency increases because the input reflection coefficient of these devices falls with increasing frequency. Noise parameter measurements of low noise HEMTs will be more difficult because these devices have even higher input reflection coefficients than GaAs FETs.

In the course of these measurements, great demands were placed upon the accuracy of the S-parameter measurements. For noise parameter measurements of devices such as the MGF1412 GaAs FET or HEMTs, it is crucial to use an S-parameter test set designed for automated high speed measurements, such as the HP8510, and an accurate set of S-parameter calibration standards. Improved results could also be obtained by developing better models of the S-parameter calibration standards used to calibrate to the fixture socket. Particularly, the short calibration standard is offset from the center of the fixture socket; this offset has proved very difficult to measure. The offset might be determined by iterative adjustment to reduce the discrepancy between the calculated and measured values of the unused S-parameter as discussed in the thesis.

It is important to reduce the sensitivity of the estimated noise parameters to measurement errors. When measuring two-ports having high input reflection coefficients, this can be accomplished primarily by using a noise generator having both large and small reflection coefficients with the same phase angles as Γ_{OPT} and Γ_{IN}^* of the DUT cascaded with the noise measurement receiver. Unless the noise parameters of the DUT and the noise measurement receiver are known in advance, the noise generator must have an even distribution of reflection coefficients on the reflection coefficient plane within the unity reflection coefficient circle.

The accuracy of the estimated noise parameters could also be improved by increasing the accuracy of the noise power measurements. It is extremely important to keep transmission lines between the DUT input and the noise generator as short as possible. The change of the noise generator reflection coefficient with frequency, in magnitude and in angle, should also be minimised. The accuracy of the noise power measurements could also be improved by decreasing the noise measurement bandwidth.

The use of passive DUTs having a range of reflection coefficients has proved extremely useful in determining the accuracy of these noise measurements. The passive DUT used for the cryogenic noise measurements was a series 200 Ohm resistor; this was not a good choice because the magnitude of Γ_{OPT} for any series resistor is 1, and small measurement errors may easily result in non-physical noise parameter estimates ($|\Gamma_{OPT}| \geq 1$). A better passive DUT for cryogenic noise measurements should have a magnitude of Γ_{OPT} approximately equal to 0.9.

When investigating new methods of noise parameter estimations it is necessary to have access to the source code of a circuit analysis program so that new algorithms can be implemented at will. The IMPCAP program described in this thesis has proved invaluble for this purpose. The data structure used for storage (as opposed to calculation) by this program should be modified to be simpler and use less memory.

References

Adamian, V., Uhlir, A., 1973, "A Novel Procedure for Receiver Noise Characterization," *IEEE Trans. Inst. Meas.* **IM-22**, pp. 181-182

Adamian, V., Uhlir, A., 1982, "Input Reflection and Noise Figure Dependence on Source Reflection: Determination using Noise Generator," ELECTRO-82, Boston, MA.

Adamian, V., Uhlir, A., 1984, "Simplified Noise Evaluation of Microwave Receivers," *IEEE Trans. Inst. Meas.* **IM-33**, pp. 136-140

Adler, R.B., Haus, H.A., 1958, "Network Realization of Optimum Amplifier Noise Performance," *IRE Trans. Circuit Theory* **46**, pp. 156-161

Albinsson, B., 1987, "Noise Parameter Transformations of Interconnected Two-port Networks," *IEE Proceedings* **134**,pp. 125-129

Anastassiou, A., Strutt, M.J.O., 1974, "Effect of Source Lead Inductance on the Noise Figure of a GaAs FET," *Proc. IEEE* **62**, pp. 406-408

Baechtold, W., Strutt, M.J.O., 1968, "Noise in Microwave Transistors," *IEEE Trans. Microwave Theory Tech.* **MTT-16**, pp. 578-585

Bard, Y., 1974, Nonlinear Parameter Estimation, Academic Press

Beatty, R.W., 1973, Applications of Waveguide and Circuit Theory to the Development of Accurate Microwave Methods and Standards, NBS Monograph 137, National Bureau of Standards, U.S. Department of Commerce

Ben-Israel, A., 1966, "On Error Bounds for Generalized Inverses," *SIAM J. Numer. Anal.* **3** pp. 585-592

Bosma, H., 1967, "On the Theory of Linear Noisy Systems," *Phillips Research Report Supplements*,

Brady, M.M., 1964, "The Influence of Mismatch Error in Noise Performance Measurements," *Proc. IEEE (Corresp.)* **52**, pp. 1075-1076

Brewitt-Taylor, C.R., Robson, P.N., Sitch, J.E., 1978, "New Estimate of the Minimum Noise Figure of a MESFET," *Electronics Letters* **Vol. 14, No. 25**, pp. 130-131

Brookes, T.M., 1984, "The Noise Properties of High Electron Mobility Transistors," *Electronics Division Internal Report* **EDIR 257**, National Radio Astronomy Observatory, Charlottesville, VA.

Calandra, E.F., Martines, G., Sannino, M., 1984, "Characterization of GaAs FET's in Terms of Noise, Gain and Scattering Parameters Through a Noise Parameter Test Set," *IEEE Trans. Microwave Theory Tech.* **MTT-32**, pp. 231-237

Cappy, A., 1988, "Noise Modeling and Measurement Techniques," *IEEE Trans. Microwave Theory Tech.* **MTT-36**, pp. 1-10

Carson, A.B., 1968, Communication Systems-An Introduction to Signals and Noise in Electrical Communication, New York: McGraw Hill

Caruso, G., Sannino, M., 1977, "Analysis of Frequency Conversion Techniques in Measurements of Microwave Transistor Noise Temperatures," *IEEE Trans. Microwave Theory Tech.* **MTT-25**, pp. 870-873

Caruso, G., Sannino, M., 1978, "Computer-Aided Determination of Microwave Two-Port Noise Parameters," *IEEE Trans. Microwave Theory Tech.* **MTT-26**, pp. 639-642

Caruso, G., Sannino, M., 1979, "Determination of Microwave Two-Port Noise Parameters Through Computer-Aided Frequency Conversion Techniques," *IEEE Trans. Microwave Theory Tech.* **MTT-27**, pp. 779-783

Churchill, R.V., Brown J.W. and Verhay, R.F., 1974, Complex Variables and Applications, Third Edition, New York: McGraw Hill

Chau,M., 1984, "Microprocessor-Controlled ANA System for De-embedding FET Parameters," MSc. Thesis, University of Alberta

Coombs, C.F., (ed.), 1979, Printed Circuits Handbook, 2nd Ed., New York: McGraw Hill

Cooper, J.F., Gupta, M.S., 1977, "Microwave Characterization of GaAs MESFET and the Verification of Device Model," *IEEE J. Solid State Circuits* SC-12, pp. 325-329

Eisele, K.M., 1964, "Refrigerated Microwave Noise Sources," *IEEE Trans. Inst. Meas.* IM-13, pp. 336-342

Engberg, J., 1974, "Simultaneous Input Power Match and Noise Optimization Using Feedback," *Proc. Fourth European Microwave Conference, Montreux*, pp. 385-389

Engberg, J., 1985, "Noise Parameters of Embedded Noisy Two-Port Networks," *IEE Proceedings* 132, pp. 17-22

Engen, G.F., 1970, "A New Method of Characterizing Amplifier Noise Performance," *IEEE Trans. Inst. Meas.* IM-19, pp. 344-349

Engen, G.F., 1973, "Mismatch Considerations in Evaluating Amplifier Noise Performance," *IEEE Trans. Instr. Meas.* IM-22, pp. 274-278

Fanelli, N., 1983, "A New Measurement Method of the Noise Parameters of Two-Port Devices," *IEEE MTT-S International Microwave Symposium Digest*, pp. 366-368

Friis, H.T., 1944, "Noise Figures of Radio Receivers," *Proc. IRE* 32, pp. 419-422

Fukui, H., 1966, "The Noise Performance of Microwave Transistors," *IEEE Trans. Electron Devices* ED-13, pp. 329-341

Fukui, H., 1966, "Available Power Gain, Noise Figure and Noise Measure of Two-Ports and Their Graphical Representations," *IEEE Trans. Circuit Theory* CT-13, pp. 137-142

Fukui, H., 1979, "Design of Microwave GaAs MESFETS for Broad Band Low Noise Amplifiers," *IEEE Trans. Microwave Theory Tech.* **MTT-27**, pp. 643-650

Fukui, H., 1981, "Addendum to 'Design of Microwave GaAs MESFETs for Broad Band Low-Noise Amplifiers'," *IEEE Trans. Microwave Theory Tech.* **MTT-29**, p 119

Gonzalez, G., 1984, Microwave Transistor Amplifiers, Analysis and Design, Prentice Hall, Englewood Cliffs, New Jersey

Gunston, M.A.R., 1972, Microwave Transmission-Line Impedance Data, Van Nostrand Rheinhold:London

Gupta, K.C., Garg, R., Chadha, R., 1981, Computer-Aided Design of Microwave Circuits, Artech House, Dedham, Massachusetts

Gupta, M.S., 1970, "Determination of the Noise Parameters of a Linear Two-Port," *Electron. Lett.* 6, pp. 543-544

Gupta, M.S., 1983, "Impossibility of Linear Two Port Measurement with a Single Temperature Noise Source," *IEEE Trans Inst. Meas.* **IM-32**, pp. 443-445

Gupta, M.S., Greiling, P.T., 1988, "Microwave Noise Characterization of GaAs MESFET's: Determination of Extrinsic Noise Parameters," *IEEE Trans. Microwave Theory Tech.* **MTT-36**, pp. 745-751

Harper, C.A., (ed.), *1970, Handbook of Materials and* Processes for Electronics, New York: McGraw Hill

Harris, I.W., 1966, "Dependence of Receiver Noise-Temperature Measurement on Source Impedance," *Electronics Letters* **Vol. 2, No. 4**, pp. 130-131

Hartmann, K., 1976, "Noise Characterization of Linear Circuits," *IEEE Trans. Circuits and Systems* **CAS-23**, pp. 581-590

Haus, H.A., Adler, R.B., 1957, "An Extension of the Noise Figure Definition," *Proc. IRE* **45**, pp. 690-691

Haus, H.A., Adler, R.B., 1958, "Canonical Form of Linear Noise Networks," *IRE Trans. Circuit Theory* **CT-46**, pp. 161-167

Haus, H.A., Adler, R.B., 1959, Circuit Theory of Linear Noisy Networks, Technology Press of the Massachusetts Institute of Technology and John Wiley and Sons, Inc.

Hecken, R.P., 1981, "Analysis of Linear Noisy Two Ports Using Scattering Waves," *IEEE Trans Microwave Theory Tech.* **MTT-29**, pp. 997-1004

Hillbrand, H., Russer, P.H., 1976, "An Efficient Method of Computer Aided Noise Analysis of Linear Amplifier Networks," *IEEE Trans Circuits and Systems* **CAS-23**, pp. 235-238

Hirano, K., Kanema, S., 1968, "Matrix Representations of Noise Figures and Noise Figure Charts in Terms of Power Wave Variables," *IEEE Trans. Microwave Theory Tech.* **MTT-16**, pp. 692-699

Howe, H., 1974, Stripline Circuit Design, Artech House

Huber, W.R., 1970, "Two Port Equivalent Noise Generators," *Proc. IEEE* **58**, pp. 807-809

IRE Subcommittee 7.9 on Noise, 1960, "IRE Standards on Methods of Measuring Noise in Linear Two-Ports, 1959 (59 IRE 20.S1)," *Proc. IRE* **48**, pp. 60-68

IRE Subcommittee 7.9 on Noise, 1960, "Representation of Noise in Linear Two Ports," *Proc. IRE* **48**, pp. 69-74

IRE Subcommittee 7.9 on Noise, 1963, "Description of the Noise Performance of Amplifiers and Receiving Systems," *Proc. IEEE* **51**, pp. 436-442

IRE Subcommittee 7.9 on Noise, 1963, "IRE Standards on Electron Tubes: Definition of Terms, 1962 (62 IRE 7. S2)," *Proc. IEEE* **51**, pp. 434-435

Iverson, S., 1975, "The Effect of Feedback on Noise Figure," *Proc. IEEE* **63**, pp. 540-542

Iverson, S., 1975, "Comments on 'Effect of Source Lead Inductance on the Noise Figure of a GaAs FET'," *Proc. IEEE* **63**, pp. 983-984

Johnson, J.B., 1928, "Thermal Agitation of Electricity in Conductors," *Phys. Rev.* **32**, pp. 97-109

Kato, Y., Komiyama, K., Yokoshima, I., 1988, "A Method for Evaluating the Noise Temperature of Microwave Thermal Noise Sources by Introducing an Auxiliary Transmission Line," *IEEE Trans. Microwave Theory Tech.* **MTT-36**, pp. 145-147

Kato, Y., Yokoshima, I., 1987 "A 4-Ghz Band Low-Noise Measurement System," *IEEE Trans Inst. Meas.* **IM-36**, pp. 60-66

Kenney, J.M., 1968, "The Simultaneous Measurement of Gain and Noise Using Only Noise Generators," *IEEE Trans. Microwave Theory Tech.* **MTT-16**, pp. 603-607

Kittel, C., 1969, Thermal Physics, New York: John Wiley and Sons

Kodaira, S., Weinreb, S., Granlund, J., 1984, "Design of a Low Noise, Balanced 2-4 GHz GaAsFET Amplifier," *Electronics Division Internal Report* **EDIR 241**, National Radio Astronomy Observatory, Charlottesville, VA.

Kotyczka, W., Leupp., A., Strutt, M.J.O., 1970, "Computer-Aided Determination of Two-Port Noise Parameters (CADON)," *Proc. IEEE* **58**, pp. 1850-1851

Krazewski, A., Stuchly, A., Stuchly, M., 1983, "ANA Calibration Method for Measurements of Dielectric Properties," *Trans. Inst. Meas.* **IM-32**, pp. 385-386

Lane, R.Q., 1969, "The Determination of Device Noise Parameters," *Proc. IEEE* **57**, pp. 1461-1462

Lane, R.Q., 1978, "A Microwave Noise and Gain Parameter Test Set," *ISSCC Dig. Tech. Papers*, pp. 172-173,274

Lane, R.Q., 1982, "A .5-18 GHz Semi-Automatic Noise Parameter Measurement Technique," ARFTG Paper

Lange, J., 1967, "Noise Characterization of Linear Twoports in Terms of Invariant Parameters," *IEEE J. Solid State Circuits* **SC-2**, pp. 37-40

Larock, V.D., Meys, R.P., 1982, "Automatic Noise Temperature Measurement Through Frequency Variation," *IEEE Trans. Microwave Theory Tech.* **MTT-30**, pp. 1286-1288

Leake, B.W., 1982, "A Programable Load for Power and Noise Characterization," IEEE MTT-S Int. Microwave Symp., Dallas, Tx.

Linvill, Gibbons, 1961, Transistors and Active Circuits, New York: McGraw Hill

Mamola, G., Sannino, M., 1975, "Source Mismatch Effects on Measurements of Linear Two-Port Noise Temperatures," *IEEE Trans. Instr. Meas.* **IM-24**, pp. 239-242

Martines, G., Sannino, M., 1982, "Determination of Microwave Transistor Noise and Gain Parameters Through Noise Figure Measurements Only," *IEEE Trans. Microwave Theory Tech.* **MTT-30**, pp. 1255-1259

Martines, G., Sannino, M., 1985, "Simultaneous Determination of Transistor Noise, Gain and Scattering Parameters for Amplifier Design Through Noise Figure Measurements Only," *IEEE Trans. Inst. Meas.* **IM-34**, pp. 88-91

Martines, G., Sannino, M., 1987, "A Method for Measurement of Losses in the Noise-Matching Microwave Network While Measuring Transistor Noise Parameters," *IEEE Trans. Microwave Theory Tech.* **MTT-35**, pp. 71-75

Merlo, D., Houghton, E.W., Halford, G.J., 1965, "Effect of Some Component Tolerances and Measuring Errors on Noise Measurements," *Electronics Letters* 1, pp. 250-251

Meys, R.P., 1978, "A Wave Approach to the Noise Properties of Linear Microwave Devices," *IEEE Trans Microwave Theory Tech.* **MTT-26**, pp. 34-37

Meys, R.P., 1982, "A Microprocessor Controlled Automatic Noise-Temperature Meter," *IEEE Trans. Instr. Meas.* **IM-31**, pp. 6-8

Miller, C.K.S., Daywitt, W.C., Arthur, M.G., 1967, "Noise Standards, Measurements, and Receiver Noise Definitions," *Proc. IEEE* **55**, pp. 865-877

Mishima, K., Sawayama, Y., 1982, "Comments on 'Simultaneous Determination of Device Noise and Gain Parameters Through Noise Measurements Only'," *Proc. IEEE* **70**, pp. 100-101

Mitama, M., Katoh, H., 1979, "An Improved Computational Method for Noise Parameter Measurement," *IEEE Trans. Microwave Theory Tech.* **MTT-27**, pp. 612-615

Mukaihata, T., 1968, "Applications and Analysis of Noise Generation in N Cascaded Mismatched Two-Port Networks," *IEEE Trans. Microwave Theory Tech.* **MTT-16**, pp. 699-708

Niclas, K.B., 1982 "Noise in Broad Band GaAs MESFET Amplifiers with Parallel Feedback," *IEEE Trans Microwave Theory Tech.* **MTT-30**, pp. 63-70

Nyquist, H., 1928, "Thermal Agitation of Electric Charge in Conductors," *Phys. Rev.* **32**, pp. 110-113

Otoshi, T.Y., 1968, "The Effect of Mismatched Components on Microwave Noise Temperature Calibrations," *IEEE Trans. Microwave Theory Tech.* **MTT-16**, pp. 675-686

Papoulis, A., 1965, Probability, Random Variables and Stochastic Processes, New York: McGraw Hill

Penfield, P., 1962, "Wave Representation of Amplifier Noise," *IRE Trans. Circuit Theory* **CT-9**, pp. 84-86

Podell, A.F., 1981, "A Functional GaAs FET Model," *IEEE Trans. Electron Devices* **ED-28**, pp. 511-517

Pospieszalski, M., 1984, "Low-Noise 8.0-8.8 GHz Cooled GaAsFET Amplifier," *Electronics Division Internal Report* **EDIR 254**, National Radio Astronomy Observatory, Charlottesville, VA.

Pospieszalski, M., 1986, "On the Noise Parameters of Isolator and Receiver with Isolator at the Input," *IEEE Trans. Microwave Theory Tech.* **MTT-34**, pp. 451-453

Pospieszalski, M., 1986, "On the Measurement of Noise Parameters of Microwave Two-Ports," *IEEE Trans. Microwave Theory Tech.* **MTT-34**, pp. 456-458

Pospieszalski, M., 1988, "Comments on 'A Method for Measurement of Losses in the Noise-Matching Microwave Network while Measuring Transistor Noise Parameters'," *IEEE Trans. Microwave Theory Tech.* **MTT-36**, pp. 170-172

Pospieszalski, M., Martines, G., Sannino, M., 1986, "Comments on 'Simultaneous Determination of Transistor Noise, Gain and Scattering Parameters for Amplifier Design through Noise Measurements Only'," *IEEE Trans. Inst. Meas.* **IM-35**, p 228

Pospieszalski, M., Wiatr, W., 1986, "Comments on 'Design of Microwave GaAs MESFET's for Broadband, Low Noise Amplifier'," *Microwave Theory and Techniques* **MTT-34**, p 194

Pospieszalski, M., Weinreb, S., Norrod, R.D., Harris, R., 1988, "FET's and HEMT's at Cryogenic Temperatures - Their Properties and Use in Low-Noise Amplifiers," *IEEE Trans. Microwave Theory Tech.* **MTT-36**, pp. 552-560

Pucel, R.A., Masse, D.J., Krumin, C.F., 1976, "Noise Performance of Gallium Arsenide Field Effect Transistors,"

Rogers Corporation, 1982, Bulletin RT2.8.1, Box 700, Chandler, Arizona *IEEE J. Solid State Circuits* SC-11, pp. 243-255

Rothe, H., Dahlke, W., 1956, "Theory of Noisy Fourpoles," *Proc. IRE* **44**, pp. 811-818

Sannino, M., 1979, "On the Determination of Device Noise and Gain Parameters," *Proc. IEEE* **67**, pp. 1364-1366

Sannino, M., 1980, "Simultaneous Determination of Device Noise and Gain Parameters Through Noise Measurements Only," *Proc. IEEE* **68**, pp. 1343-1345

Sannino, M., 1982, "Comments on "Simultaneous Determination of Device Noise and Gain Parameters Through Noise Measurements Only"(Reply)," *Proc. IEEE* **70**, pp. 100-101

Sawayama, Y., Mishima, K., 1981, "Evaluation Method of Device Noise Figure and Gain Through Noise Measurements," *Proc. IEEE* **69**, pp. 1578-1579

Sierra, M., 1982, "15 GHz Cooled GaAsFET Amplifier - Design Background Information," *Electronics Division Internal Report* **EDIR 229**, National Radio Astronomy Observatory, Charlottesville, VA.

Statz, H., Haus, H.A., Podell, R.A., 1981, "Noise Characteristics of Gallium Arsenide Field Effect Transistors," *IEEE Trans. Electron Devices* **ED-21**, pp. 511-517

Soares, R. (Ed.), 1988 GaAs MESFET Circuit Design, Artech House, Norwood, Massachusetts

Strid, E.W., 1981, "Measurement of Losses in Noise Matching Networks," *IEEE Trans. Microwave Theory Tech.* **MTT-29**, pp. 247-252

Twiss, R.Q., 1955, "Nyquists and Thevenins Theorems Generalized for Nonreciprocal Linear Networks," *J. App. Phys.* **26**, pp. 599-602

Valk, E.C., Walker, G., Vaneldik, J.F. and Routledge, D., 1987, "A Simple Method of Removing Receiver Noise From Microwave Measurements," *J. Instn Electronic & Radio Engineers*, **57**, pp. 297-300

Valk, E.C., Routledge, D., Vaneldik, J.F. and Landecker, T. L., 1988, "De-embedding Two-Port Noise Parameters Using A Noise Wave Model," *Trans. Instr. Meas.* **IM-37**, pp. 195-200

Van der Ziel, A., 1962, "On the Noise Figure of Negative Conductance Amplifiers," *IRE Trans. Circuit Theory* **CT-9**, pp. 83-84

Wait, D.F., Nemoto, T., 1968, "Measurement of the Noise Temperature of a Mismatched Noise Source," *IEEE Trans. Microwave Theory Tech.* **MTT-16**, pp. 670-675

Wait, D.F., 1968, "Thermal Noise from a Passive Linear Multiport," *IEEE Trans. Microwave Theory Tech.* **MTT-16**, pp. 687-691

Weinreb, S., 1980, "Low-Noise Cooled GaAsFET Amplifiers," *Electronics Division Internal Report* **EDIR 202**, National Radio Astronomy Observatory, Charlottesville, VA.

Weinreb, S., 1980, "Tests of Cooled 5 GHz Parametric and GaAs FET Amplifiers," *Electronics Division Internal Report* **EDIR 203**, National Radio Astronomy Observatory, Charlottesville, VA.

Weinreb, S., 1982, "Noise Parameters of 1.5 GHz. GaAsFET Amplifiers," *Electronics Division Internal Report* **EDIR 231**, National Radio Astronomy Observatory, Charlottesville, VA.

Weinreb, S., Fenstermacher, D.L., Harris, R.W., 1982, "Ultra Low Noise 1.2 to 1.7 GHz. Cooled GaAs FET Amplifiers," *IEEE Trans. Microwave Theory Tech.* **MTT-30**, pp. 849-853

Weinreb, S., Williams, D.R., Lum, W., 1980, "L Band Cryogenically Cooled GaAs FET Amplifier," Microwave Journal, October

Wells, J.S., Daywitt, W.C., Miller, C.K.S., 1964, "Measurement of Effective Temperatures of Microwave Noise Sources," *IEEE Trans. Inst. Meas.* IM-13, pp. 17-28

White, J.F., 1981, Microwave Semiconductor Engineering, Van Nostrand Rheinhold:New York

Wiatr, W., 1980, "A Method of Estimating Noise Parameters of Linear Microwave Two-ports," Ph.D. Dissertation, Warsaw Tech. Universty, Warsaw, Poland (in Polish)

Woods, D., 1966, "Effect of Some Component Tolerances and Measuring Errors on Noise Measurement," *Electronics Letters* 2, pp. 47-48

Appendix 1 - A Brief Description of APL

The following is a brief description of APL, which introduces some concepts and terms specific to APL. A more complete description of APL may be found in Gilman and Rose (1976).

APL is an interactive, interpretive language. The APL alphabet consists of the capitalized Roman letters, the underlined, capitalized Roman letters, the Roman numerals, the Greek capital delta and the underlined Greek capital delta. In addition, the APL interpreter recognizes approximately sixty special symbols which represent built in functions such as addition, subtraction, random number, matrix inverse and least squares fit. An APL workspace is a file which contains all the programs, which are called functions, and variables which can be used when that workspace is active (loaded). Each object (function or variable) has a name which is made up from the APL alphabet. Function names and variable names are not distinguished in any way, consequently no function and variable can have the same name.

An APL variable may contain either string, logical or numeric values, and can be a simple variable or an array with any number of dimensions. An APL variable exists as soon as some value is assigned to it; there is no facility to declare variable type or size. If an APL variable is declared in the first line of a function, that variable is said to be "local" to that function, in which case the definition of that variable when the function is executing is independent of, and separate from, its definition otherwise. If an APL variable is defined when no function is executing, it is said to be "global".

An array can be visualized as a cell structure with a number of axes. Each cell is a generalized cube with the same number of axes as the array, containing one element of the array. The number of cells along each array axis is referred to as the length of that axis. The shape of an array is the vector of the lengths of all the axes, its rank is the number of its axes. An element of an array is referred to by its index along each axis. Arrays of rank 0 and arrays having axes of length 0 are allowed; these arrays contain no elements.

Any function can be referenced by any other function; recursion is allowed. Each function may have no arguments (niladic), a right argument (monadic) or a right and a left argument (dyadic). A function may or may not return a value. Since data passed to a function via its arguments is limited to two variables, and data returned by a function is limited to one variable, additional data is often passed via global variables. If a function is intended to be used directly by the user, it is poor design to pass data to the function via global variables because it is not immediately obvious to the user that this linkage exists. Thus, the user may change a variable, and this may affect his results in some way he does not realize.

A software package in APL can be written as a 'closed' or an 'open' workspace, or a combination. In an 'open' workspace, the user input is interpreted directly by the APL interpreter, and any valid APL expression will be executed. The software package consists of a number of functions and variables which, when used appropriately, produce the desired result. User errors may cause an error message to be generated by the interpreter or by one of the functions in the workspace. Since interpreter error messages are necessarily of a general nature, they are usually less helpful than error messages generated by functions written specifically for the workspace. User errors may even damage the system variables in the workspace and cause future results to be invalid. This type of workspace is more flexible but less user friendly.

In a closed workspace, the user input is passed directly to an APL function which performs error checking, and then generates the appropriate actions. With a considerable amount of work, this type of work space can be made very user friendly. A closed workspace is better suited to the novice user, and to well defined applications.

Appendix 2 - A Summary of the Main IMPCAP Functions

This appendix lists each of the IMPCAP functions, followed by a short description. The main IMPCAP functions can be divided into several groups. The first group are the functions used for documentation:

1. CHANGES: This function modifies the the target function (whose name is given as the right hand argument) so that the second line is a comment containing the current time, date and IMPCAP version in a standard format. The revision time and date of IMPCAP is then updated.
2. DISLOG: This function displays the workspace activity log, which is located in the variable ΔLOG.
3. EDLOG: This function converts the workspace activity log, located in the variable ΔLOG, to a function LOG, so that the activity log can be edited using the function editor, or executed.
4. HDRS: This function displays the name, IMPCAP version, revision time and date of each function in the workspace, sorted by date. This allows one to determine which functions have recently been modified.
5. L: This function accepts keyboard input as a string, appends the string to the activity log, ΔLOG, and executes the string. Input which generates an APL interpreter error is appended with '***FAILED' in the activity log.
6. RESTΔLOG: This function converts the function LOG back to the variable ΔLOG.

7. REVDATE: This function displays the revision time and date and the IMPCAP version number.

The second group consists of the functions used for data input and output from standard form variables.

1. DATA: This function is used to enter data into standard form variables, and is actually a small interpreter which recognizes nine commands.
2. DISP: This function displays data in polar form tabulated by frequency.
3. DISR: This function displays data in rectangular form tabulated by frequency.
4. FRQ: This function displays the sytem variable ΔFTAB, which lists the tabulation frequencies used for data input and circuit element modeling.
5. FTAB: This function sets the vector ΔFTAB (a system variable) which is a list of the frequencies used for data entry and circuit element modeling.
6. INIT: This function generates an "empty" standard form variable using ΔFTAB
7. SMITH: This function plots the real and imaginary components of the scattering parameters using variable scale factors and plot size. One scale factor is used to adjust the vertical scale factor and the other is used to adjust the scale of the horizontal axis relative to the vertical axis to compensate for the different aspect ratios of the type used on different terminals.
8. SMTH: This function is an abbreviated form of SMITH with

the scale factors and plot size fixed. This function is designed to be used on an Anderson Jacobson AJ510 terminal.

9. STATUS: This functions displays the shape, frequencies of tabulation and type of circuit parameters of a standard form variable.

The third group are functions designed to change the shape of a standard form variable.

1. LIKE: This function modifies a standard form argument of rank 3 by adding extra axes (the data is replicated) so that the shape of the result matches that of the other argument.
2. JOIN4: This function concatenates two arrays along the fourth axis. Both arrays must have at least four axes and the same shape, excepting the fourth axis.
3. JOIN5: This function concatenates two arrays along the fifth axis. Both arrays must have at least four axes and the same shape, excepting the fifth axis.
4. SELECT: This function selects data from a standard form variable by choosing a subset of indices along an axis or by choosing one index and deleting that axis.
5. XTEND: This function adds an extra axis to and/or lengthens an existing axis of a standard form variable.

Another group of functions models circuit elements. Each of these functions use the variable ΔFTAB for the list of frequencies.

1. MATCH: This function generates the scattering parameters

of an ideal 50 Ohm termination .

2. OPEN: This function generates the scattering parameters of an ideal open circuit.
3. PASSNP: This function calculates the noise parameters of a passive one or two-port given its S-parameters and physical temperature.
4. SHORT: This function generates the scattering parameters of an ideal short circuit
5. RLCPA: This function generates the impedances of a parallel RLC circuit.
6. RLCSE: This function generates the impedances of a series RLC circuit.
7. TRL: This function generates the scattering parameters of a transmission line of specified characteristic impedance, physical length, dielectric constant and attenuation.
8. TRM: This function generates the scattering parameters of a lossless 50 Ohm transmission line of specified length.
9. STPWSL: This function generates the scattering parameters of a step change in width of a stripline using the model found in Gupta (1981).

Yet another group of functions is used to model the effect of circuit interconnections.

1. CAS: This function calculates the small signal and noise parameters and the applicable gain of a two-port cascaded with a one-port, two-port or a receiver.

DECAS This function removes a cascaded two-port from a one-port, two port or receiver.

2. DERCVR: This function removes a receiver from a receiver - two-port cascade using the method of section 3.4.3.
3. FLIP: This function reverses the orientation of a two-port represented by an array standard form variable.
4. PWR
5. SHUNTEL: This function calculates the two-port S-parameters of an impedance connected in shunt and can be used to model a parrellal branch transmission line.
6. SEREL: This function calculates the two-port S-parameters of an impedance connected in series and can be used to model a series branch transmission line.

Another group of functions is used for general analysis and comparison of data.

1. ABS: This function takes the absolute value of all the data in a standard form variable. Data pairs which represent complex numbers are treated as such.
2. AVG: This function averages all the data "along" a specified axis in a standard form variable. The specified axis disappears.
3. COMB: This function combines the data in two standard form variables into one, if the two variables do not contain data of similar types.
4. COMP: This function compares the data in two standard form variables by subtraction.

5. CONV: This function converts the data in a standard form variable into a specified parameter set.
6. MAXABS: This functions finds the maximum absolute value of the data along a specified axis in a standard form variable. The specified axis disappears. Data pairs which represent complex numbers are treated as such.
7. RMS: This functions calculates the root mean square of the data along a specified axis in a standard form variable. The specified axis disappears. Data pairs which represent complex numbers are treated as such.

Another group of functions is used for sensitivity analysis:

1. MAXSENSΔGAMMA: This function calculates the maximum sensitivity of the rsult of some calculation to the one-port small signal parameter in a standard form argument.
2. SENSΔNMEAS: This function calculates the maximum sensitivity of the rsult of some calculation to the noise measurement in a standard form argument.
3. SENSΔNTEMP: This function calculates the maximum sensitivity of the rsult of some calculation to the noise temperature in a standard form argument.

Yet another group of functions manipulates noise measurements and estimates noise parameters from measurement data:

1. CALNSΔP: This function estimates the noise temperature of a one-port from one power measurement, receiver noise

parameters and receiver gain.

2. CALNS2ΔP: This function estimates the noise temperature of a one-port from two power measurements, receiver noise parameters and receiver gain.
3. NPFIT4T: This function estimates noise parameters using the linearization and least-squares method described by Caruso and Sannino (1978) (the conventional method) The input is assumed to be a four dimensional array, with the fourth axis indexing the measurements of excess noise temperature and reflection coefficient of the input termination.
4. NPFIT5PΔP: This function estimates noise parameters using a linearization and least-squares method, minimizing the error in noise power. The input is assumed to be a four dimensional array, with the fourth axis indexing the measurements of noise power and noise temperature and reflection coefficient of the input termination.
5. NPFIT5PΔT: This function estimates noise parameters using a linearization and least-squares method, minimizing the error in excess noise temperature (the LRPG method). The input is assumed to be a four dimensional array, with the fourth axis indexing the measurements of noise power and noise temperature and reflection coefficient of the input termination.
6. TEFROMY: This function calculates excess noise temperature given a y-factor measurement and the hot and

cold noise generator temperatures.

7. YFAC: This function calculates a Y-factor (power ratio) given two power measurements.